Galling wear detection and measurement in sheet metal forming

Brendan Voss

April 2018

A thesis submitted for the degree of
Doctor of Philosophy
of
the Australian National University

I declare that this thesis is my own original work except where due reference is made. All substantive contribution by others to the work presented, including jointly authored publications, are clearly acknowledged.

Brendan Voss

Brendan Voss

April 2018

Acknowledgments

A number of individuals have provided support to me during my PhD candidature and I would like to express my sincerest gratitude and appreciation to all of them.

My supervisory panel, Michael Pereira, Bernie Rolfe, and Mick Cardew-Hall. Thank you all for your supervision, helpful feedback, and support. And to my primary supervisor – Matt Doolan, thank you for giving me the opportunity to pursue a PhD, for having an open door whenever I needed advice, and for always being able to point me in the right direction.

Anthony Sexton and everyone at the Royal Australian Mint, thank you for your support and for giving me access to equipment that was crucial for completing this thesis.

Dave Tyson-Smith, thank you for being happy to help whenever I needed anything from the workshop.

Thank you to the Ford Motor Company in Geelong and Thailand for opening your doors to me and answering my questions, that access and assistance is very much appreciated.

To my office mates and colleagues during my time at ANU – Cam Summerville, Vi Kie Soo, Dave Adams, Brendan Maloney, Tegan McAnulty, Yimeng Jiang, and Chris Stokes-Griffin. Thank you all for always being available for a chat, providing help and guidance, and generally making work a nice place to be.

To my family - Mum, Dad, Kath, and Meg. I cannot thank you all enough. I would not have been able to get this far without your ongoing love and support. Your care and encouragement has helped me through not only my PhD but also my entire education.

Finally, to my girlfriend, Luisa Kreft, thank you for your love and support, and most of all your patience. Your belief and understanding has given me the drive to finish this thesis.

This research is supported by an Australian Government Research Training Program (RTP) Scholarship and an Australian Research Council Linkage Project (LP1201000239).

Abstract

Galling wear of sheet metal stamping tooling is an expensive issue for sheet metal forming industries. Forming of high strength steels, particularly in the automotive industry, has led to accelerated tool wear rates. These wear rates lead to product quality and die maintenance issues, making galling wear an expensive issue for automotive manufacturers and the sheet metal forming industries in general.

Process monitoring allows for the continuous monitoring of tooling condition so that wear development can be detected. The aim of this investigation was to develop an in-depth understanding of the relationship between punch force variation and wear for implementation in future process monitoring regimes.

To achieve this aim, the effect of wear and other friction influencing factors on punch force signatures were investigated. This required the development of an accurate method for quantifying galling wear severity so that the relationship between galling wear progression and punch force signature variation could be quantified. Finally, the specific effects of wear and friction conditions on the punch force signatures were examined.

An initial investigation using a statistical pattern recognition technique was conducted on stamping force data to determine if the presence of galling wear on press tooling effected punch force variation. Galling wear on tooling, changes in lubrication type, and changes in blank holder pressure were all found to effect variation in punch force signatures shape. A new galling wear severity measurement methodology was developed based on wavelet analysis of 2D surface roughness profiles that accurately provided an indication of the location and severity of galling wear damage. Using the new method for quantifying galling wear severity in the relationship between punch force variation and galling wear progression was investigated, and a strong linear relationship was found. Finally, two prominent

forms of punch force signature shape variation were linked to friction conditions driven by wear, lubrication, and blank holder pressure.

This work describes and quantifies the relationship between galling wear and punch force signature variation. A new methodology for accurate measurement of galling wear severity is presented. Finally, specific forms of punch force signature variation are linked to different friction conditions. These results are critical for future implementation of punch force based galling wear process monitoring and a significant reduction in costs for the metal forming industries.

List of Publications

Journal Papers

- **Voss, B.**, Pereira M., Rolfe, B., Doolan, M., (2017). A new methodology for measuring galling wear severity in high strength steels. *Wear*, 390-391, pp.334-345.

Conference Papers

- **Voss, B.**, Pereira, M., Doolan, M., (2014). Automated identification of tool wear in sheet metal stamping. *Proc. International Deep Drawing Research Group 2014 Conference (IDDRG 2014)*, Paris, France, pp.399–404.
- Pereira, M., Ubhayaratne, I., **Voss, B.**, Simon, S., Doolan, M., Xiang, Y., Rolfe, B., (2015). Extending light-weighting and mass-production of ultra high strength steels via condition-based maintenance. *SAE Tech. Pap.*
- **Voss, B.**, Pereira, M., Rolfe, B., Doolan, M., (2017). Using stamping punch force variation for the identification of changes in lubrication and wear mechanism. *J. Phys. Conf. Ser.* 896, 12028.

Additional publications unrelated to this thesis

- Adams, D., Summerville, C., **Voss, B.**, Jeswiet, J., Doolan, M., (2016). Correlating variations in the dynamic resistance signature to weld strength in resistance spot welding using principal component analysis. *J. Manuf. Sci. Eng.* 139, pp.44502–44504.

Table of Contents

Acknowledgments iv

Abstract vi

List of Publications viii

Table of Contents ix

Introduction 1

1.1 Background 1

1.1.1 Sheet metal forming 1

1.1.2 Galling wear 3

1.1.3 Condition monitoring 4

1.2 Motivation and problem statement 5

1.3 The presented work 5

1.4 Research objectives 7

1.5 Thesis summary 7

Literature Review 10

2.1 Introduction 10

2.2 Process variation and monitoring 10

2.2.1 Stamping process variation and important signals 12

2.2.2 Using stamping force or load to identify process issues 15

2.2.3 Punch force analysis techniques 17

2.3 Factors affecting forming forces 19

2.3.1 Punch and forming force 19

2.3.2 Lubrication 21

2.3.3 Galling wear 23
2.4 Galling wear assessment and measurement 25
2.4.1 Visual assessment 26
2.4.2 Mass and volume 27
2.4.3 3D profilometry 27
2.4.4 2D profilometry 28
2.5 Summary 29
Methodologies 31
3.1 Introduction 31
3.2 Experimental approach and justification 31
3.3 Channel forming processes 32
3.3.1 Semi-industrial stamping press 33
3.3.2 Semi-industrial stamping press data collection 35
3.3.3 Laboratory stamping press 36
3.3.4 Laboratory stamping press data collection 38
3.4 Visual assessment 38
3.5 Metrology 39
3.5.1 Surface characterisation 39
3.5.2 3D and 2D profilometry 40
3.6 Signal analysis 41
3.6.1 Principal Component Analysis 41
3.7 Summary 42
Punch force signature variation 44
4.1 Introduction 44
4.2 Base case punch force signatures 45
4.3 Wear and other friction conditions 47
4.3.1 Comparisons experimental setup 47
4.3.2 Wear comparison 49

4.3.3 Other friction conditions comparison 53
4.4 Wear and friction condition comparisons discussion 56
4.5 Summary 58
Galling wear severity quantification 60
5.1 Introduction 60
5.2 Galling wear features 61
5.3 Surface characterisation using frequency analysis 62
5.4 Discrete Wavelet Transform methodology 66
5.4.1 Surface profile collection 66
5.4.2 Mother wavelet selection 67
5.4.3 Selection of detail coefficient level 69
5.4.4 Detail coefficient calculation and wear severity quantification 70
5.4.5 DWT wear severity parameter 71
5.5 Case study: Galling initiation 72
5.5.1 Experimental method 73
5.5.1.1 Surface characterisation 73
5.5.2 Galling initiation case study visual assessment 74
5.5.3 Mother wavelet and detail coefficient level selection 77
5.5.4 Results and analysis 78
5.5.4.1 DWT detail coefficients 78
5.5.4.2 Wear parameters 82
5.5.5 Galling initiation case study discussion 84
5.6 Case study: galling progression 86
5.6.1 Experimental method 87
5.6.1.1 Channel forming operation 87
5.6.1.2 Surface characterisation 88
5.6.1.3 Galling progression case study visual assessment 88
5.6.2 Mother wavelet and detail coefficient level selection 90

5.6.3 Results and analysis 92
5.6.3.1 DWT detail coefficients 92
5.6.3.2 Wear parameters 96
5.6.4 Galling progression case study discussion 98
5.7 Summary 100
Progression of galling wear 102
6.1 Introduction 102
6.2 Wear progression experimental setup 103
6.3 Wear progression results 103
6.4 Principal Component Analysis 106
6.4.1 Extended trial 1 106
6.4.2 Extended trial 2 108
6.5 Principal Component and wear progression comparison 109
6.6 Wear progression discussion 113
6.7 Summary 116
Wear and lubrication mechanism effects on punch force 118
7.1 Introduction 118
7.2 Experimental design 120
7.3 Results 121
7.3.1 PCA results 121
7.3.2 Punch force signature magnitude 124
7.3.3 Lubrication effect on punch force signature progression 126
7.3.4 Wear effect on punch force signature progression 127
7.4 Discussion 132
7.5 Summary 135
Discussion 137
8.1 Introduction 137
8.2 Summary of key findings 137

8.3 Forms of punch force signature shape variation ____ 140
8.3.1 Punch force signature magnitude ____ 140
8.3.2 Punch force signature progression ____ 142
8.4 Limitations and assumptions ____ 144
Conclusions and recommendations ____ 147
9.1 Conclusion ____ 147
9.2 Summary of contributions ____ 147
9.3 Significance and place in the field ____ 150
9.4 Recommendations for future work ____ 151
References ____ 153
Appendix A. Wavelet functions ____ 164

CHAPTER ONE

Introduction

This thesis examines the relationship between stamping press tool wear and punch force signatures. Variation in punch force signatures was analysed and compared to galling wear severity and its influencing factors. In order to accurately quantify galling wear in semi-industrial trials a new method for quantifying galling wear severity was also developed.

This work is significant because it provides critical insights for future implementation of effective galling wear process monitoring using punch force signals. In addition, the work provides a new methodology for accurate measurement of galling wear severity.

This chapter will provide background information and highlight the motivation for the presented research. A summary of the work conducted is provided, and the specific research objectives are presented. This is followed by the thesis structure and chapter summary.

1.1 Background

1.1.1 Sheet metal forming

Sheet metal stamping processes are the primary manufacturing techniques utilised in the automotive industry. Stamping is used to form automotive body panels and components, for both the underlying structure and the majority of the external panels in most vehicles, an example of these components can be seen in Figure 1.1.

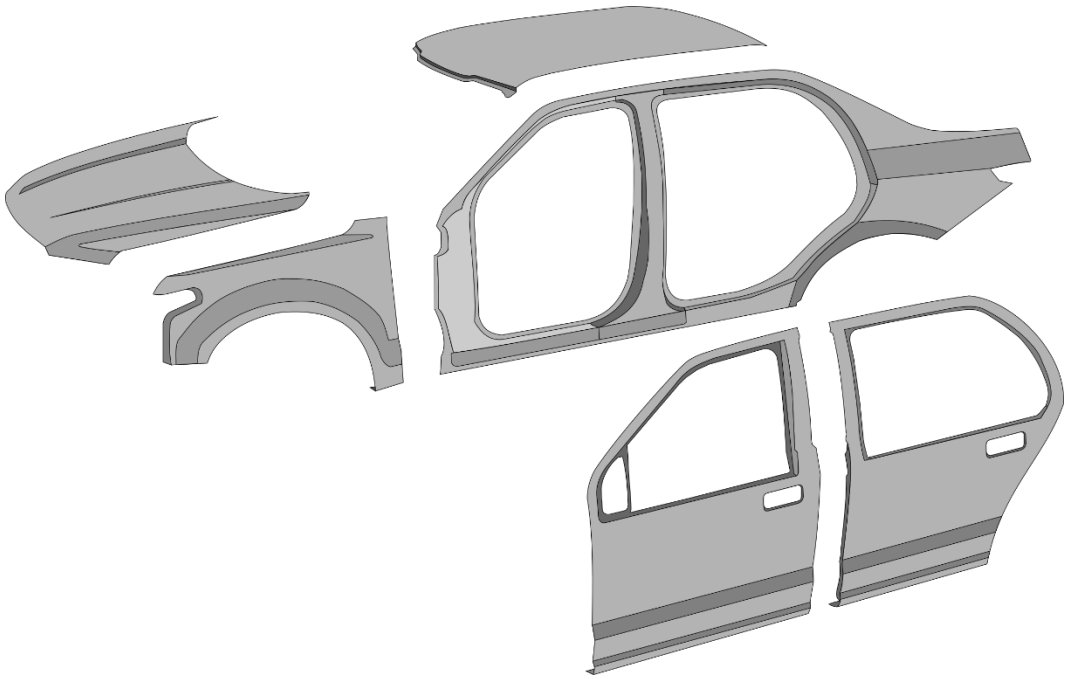

Figure 1.1: Example of stamped sheet metal automotive components.

The process involves forming pieces of sheet metal, known as blanks, between a die and punch tooling combination. As the punch is moved into the die cavity, the blank material conforms to the punch and is drawn into the die cavity. This produces a part with shape and depth from the blank sheet. As the blank material is drawn into the die cavity it goes through a process of bending and unbending over the die cavity edges while under tension. This tension is provided by the blank holder that clamps the flanges of the blank onto the die.

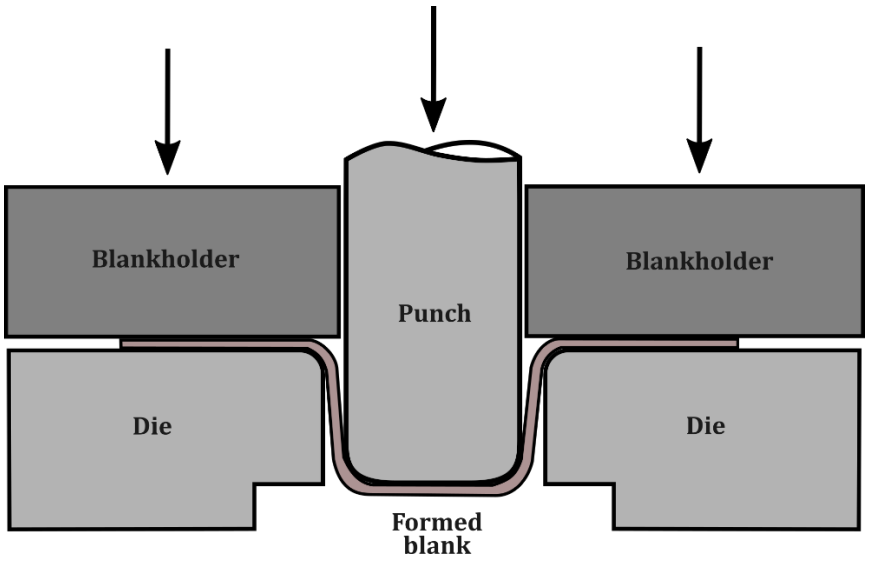

Figure 1.2: Deep drawing operation with arrows indicating applied blank holder force and punch force.

Punch force is the force that acts to deform and draw the blank material into the die and precipitate forming. As is seen in Figure 1.2 the direction of the punch movement is perpendicular to the blank surface. So, the punch force is a result of the restraining frictional force applied to the blank by the blank holder, in addition the force required to plastic deform the blank material (Dieter, 1961). Punch force and forming load process signals are rich in process information, and the signals are widely recorded on industry presses.

1.1.2 Galling wear

The forces required to form high strength steels used in the automotive industry result in high levels of friction and contact pressure on tooling, in particular the die cavity radius (Pereira et al., 2008). These conditions coupled with the repetitive sliding contact on the tooling result in the cumulative adhesive and abrasive mechanisms of galling wear (Schedin, 1994). Galling wear is the common type of tool wear observed in sheet metal stamping of automotive body components. Galling damage affects the surface quality of product, which has the possibility to effect tolerances and lowers the standard of paint finishes. The cost of galling is significant when considering both damage to formed product and tool maintenance and replacement costs.

The presence of galling on stamping dies in the automotive industry significantly reduces tool life, as the resultant galling or scratch damage on the formed part increases scrap rates (Hou et al., 2009). Wear damage on parts can affect the dimensional tolerances and paint finish, and so damaged parts must be scraped or refinished. As a result, continuing to form with galled dies is economically unfeasible. Production tooling and dies are very expensive, with estimates of a single production die set for large parts costing upwards of 1 million USD (Bubna and Humbert, 2016), this means that the replacement of extensively worn dies is a costly proposition. Refinishing of worn die surfaces causes production downtime, which if unscheduled can also prove costly in industry given the current predominant trend of lean production (Smith, 2001).

1.1.3 Condition monitoring

Galling prevention techniques include expensive die coatings or treatments, and continued application of expensive high-performance lubricants. Modeling and prediction of galling is another component of galling prevention, however, available models of wear mechanisms seen in sheet metal forming only provide approximations of wear rates (Williams, 1999).

While progress into the fields of wear modelling and galling prevention technology continues, galling will remain an economic burden to the industry. An on-line wear monitoring system can provide an ongoing solution that will continue to be relevant in conjunction with the advancement of other possible solutions. Monitoring for wear will prevent the production of sub-standard quality parts and minimise progression of die damage. Monitoring systems also have the potential to provide forecasting of die condition, so that maintenance can be scheduled in a timely manner.

Effective on-line galling wear monitoring systems require understanding of how process variation is linked to signal variation, in addition to effective analysis techniques for capturing and characterising these relationships. In the field of sheet metal stamping, punch force or load signals have been linked to a series of press and final part issues. Investigation of punch force or forming load variation and their links to various stamping process issues have been undertaken throughout the literature. Punch force or forming load signature features have been linked to part failure (Doolan et al., 2003), poor blank and tooling alignment (Breitling et al., 1997), and press condition (Jin and Shi, 1999). While links to wear have been proposed (Breitling et al., 1997), variation of punch force has only been firmly linked to large changes in process condition, like those mentioned above, and no work has investigated the link to wear and its progression. One important component in investigating such a link is an accurate measure of galling wear severity that is applicable to use in stamping operations, where dies are difficult to access, and large numbers of parts are produced. Visual assessment of galling severity is the current standard (ASTM Standard G98-02, 2009), and quantitative methods vary throughout the literature. Traditional surface roughness or texture parameters are often used in conjunction with visual assessment when assessing severity (Andreasen et al., 1998; Christiansen and De Chiffre, 1997; Swanson et al., 1988; van der Heide et

al., 2001). However, no evidence has been provided to demonstrate that any of these traditional surface parameters correlate with galling severity as perceived by visual assessment. With one exception (Vermeiden and Hobleke, 2003), there are no targeted measures of galling wear severity, and no available measures are particularly suited to the localised nature of galling wear features. The large contact area of sheet metal forming operations adds to the complexity of galling severity measurement, as multiple initiation sites may progress through different stages of severity.

1.2 Motivation and problem statement

As discussed in Section 1.1.2 galling is a significant challenge for the automotive industry. It is also an issue that stands to become more prevalent with the continued use of higher strength steels that are needed to improve crash performance and fuel efficiency. On-line wear monitoring systems will play an important role in addressing the issue of galling wear on production dies, however, such systems cannot be effective without an in-depth knowledge of the relationship between galling wear and a range of process signals. Punch force is widely recorded on industrial presses, and is also information rich, making it a suitable candidate for galling monitoring systems. Therefore, it is necessary to develop an understanding of the relationship between punch force variation and galling wear development. In order to investigate the relationship between forming signals and wear an accurate measure of galling wear severity on formed parts is also required.

1.3 The presented work

In this work an investigation of the relationship between variation of sheet metal stamping punch force signatures and galling wear of tooling has been conducted. The effect of galling wear progression and other friction influencing factors are assessed, and the associated variation in punch force is isolated and quantified, providing an in-depth assessment of the relationship. This knowledge is a necessary

foundation for future work into the development of effective galling process monitoring systems.

An initial set of experiments were conducted to establish if galling wear has an observable effect on punch force signature variation. A distinct observable difference was noted in punch force signatures collected under different die wear levels. The effect of different friction conditions due to lubrication and blank holder force changes were also investigated. The results of these initial experiments justified the further investigation into the link between punch force signature variation and galling wear development and progression.

Through the process of investigating the link between galling wear and punch force, a comprehensive review of galling wear measurement techniques was undertaken in order to ensure that any relationship could be quantified accurately. This review found that the standard for assessment of galling wear was qualitative visual assessment and that other techniques used to measure galling wear varied vastly in the literature. Galling wear assessment is a space without a standard quantitative measure and a reliance on subjective and qualitative visual assessment. In addition to this, no currently available measurement technique had been demonstrated to provide a measure of galling wear severity that tracks with perceived galling damage severity through visual assessment. In response to this lack of appropriate techniques, a targeted measure of galling wear severity that tracked with visually perceived galling severity was developed using 2D profilometry. This new technique also utilised the counter surface of the tooling, or part, making it suitable for the extended wear trials performed as part of the investigation into the link between galling wear and punch force signals.

The severity of galling wear in a series of extended deep drawing trials was then measured using the new method and results were compared to Principal Component Analysis (PCA) of punch force signatures from the trials. This comparison linked the dominant forms of punch force signature variation and galling wear progression. This demonstrated that punch force signature variation, captured using PCA, can be used as a tool for monitoring wear in sheet metal forming.

Finally, dominant forms of punch force signature variation were investigated with regard to specific friction influencing factors including lubrication, blank holder

force, and mid-stroke wear development. This final investigation provides additional insights into the factors effecting the shape of punch force signatures and the relationship of those signature shapes to friction in the deep drawing process.

1.4 Research objectives

The goal of this thesis was to investigate the link between punch force signature shape variation and galling wear development. This has led to the specific research objectives:

- Determine if variation in wear and other friction influencing factors have a demonstrable effect on punch force signatures (Chapter 4).
- Develop an accurate method for quantifying galling wear severity that can be applied to channel forming experiments conducted in this work (Chapter 5).
- Examine if the onset and progression of galling wear has a quantifiable relationship with punch force signature shape variation (Chapter 6).
- Investigate how specific wear events and changes in friction influencing factors affect the punch force signature (Chapter 7).

By meeting these objectives, this thesis will provide key insights and a step towards the development of on-line wear condition monitoring systems for production sheet metal stamping operations. This has the potential to provide significant productivity and economic improvements for the automotive manufacturing industry.

1.5 Thesis summary

A summary of the thesis and individual chapters will be provided in this section.

Chapter two provides a review of the current state of the relevant literature. Galling wear, contact conditions, and lubrication in sheet metal stamping are discussed. An overview of process monitoring and monitoring of stamping is provided. An emphasis on the relationship between punch force or load signal variation and process issues is given. This provides justification for the use of punch force and highlights the gap that this thesis aims to fill through relating punch force to wear

development. Finally, an assessment of the galling wear measurement techniques is provided, highlighting the lack of accurate measures of galling wear severity and justifying the research objective of developing such a measure.

Chapter three outlines the details of common experimental methods utilised through-out the remainder of the work. Details of semi-industrial channel forming trials, data collection and analysis, visual galling wear assessment, and metrology are all presented.

In **Chapter four** the effects of changes in galling wear severity on punch force signature variation is assessed using Principal Component Analysis (PCA). Friction influencing factors, including lubrication and blank holder force, are also assessed in order to determine if characteristic forms of signature shape variation can be linked to changes in different conditions. This initial investigation into the effects of wear and friction on punch force signatures establishes that wear of forming tools has an observable effect on punch force signatures. This sets the foundation for further investigation of punch force signature variation with galling wear progression, and as a consequence establishes the need for an accurate measure of galling wear severity.

In **Chapter five** a new measure of galling wear severity is developed. The requirements of the galling wear targeted measures are addressed, and the localised nature of galling wear and typical 2D features are assessed. Based on this assessment a new methodology utilising Discrete Wavelet Transform is outlined, including mother wavelet and detail level selection and cumulating in the definition of a new galling wear severity measure, W_{DWT}. Finally, two case studies are conducted to establish the performance of the new methodology when compared to ranked visual assessment of wear severity. The first case study focuses on early galling initiation and the second case study focuses on extended galling wear progression. Accurate measurement of galling severity in both initiation and progression cases are important for real world application and investigating the link between galling wear and punch force signature variation. These case studies demonstrate the application of the Discrete Wavelet Transform (DWT) galling wear severity measure methodology and highlight its accuracy in both situations.

In **Chapter six**, punch force signatures for a series of extended wear progression trials are analysed using PCA and compared with measured wear severity to

demonstrate the link between punch force signature variation and galling wear progression.

In **Chapter seven**, the dominant forms of punch force signature shape variation are assessed with regard to specific friction influencing factors such as lubrication change, blank holder force, and mid-stroke wear development. Additional experiments are conducted in order to assess the effects of mid-stroke friction changes, which were identified as a potential driving factor of punch force variation. These experiments focus on mid-stroke friction changes due to lubrication and wear mechanism transitions. The magnitude of punch force signatures is linked to friction level, regardless of the dominant cause, whether it be wear, lubrication, or blank holder force. In the absences of variation of other factors, slope of the punch force signature plateau is linked to lubrication mechanism change, suggesting mid-stroke wear mechanism changes may also drive this form of signature variation. Visual assessment supports the link but quantitative measure results using W_{DWT} are inconclusive.

In **Chapter eight** the results of Chapters four, five, six, and seven are discussed with regard to the motivation of the thesis. The key forms of punch force variation isolated in the trials conducted and their relationship to galling wear and friction are discussed. Finally, the limitations and assumptions of the work are addressed.

Chapter nine concludes the thesis with a summary of results and contributions of the work. Recommendations for future work based on the findings of this thesis are also proposed.

CHAPTER TWO

Literature Review

2.1 Introduction

This Chapter presents a review of the relevant literature. Firstly, an overview of process monitoring of manufacturing processes and sheet metal stamping in particular is provided. Then a detailed assessment of the current state of literature related to the understanding of the relationship between sheet metal stamping process signals and process variation is given. An overview of the theory behind punch and forming force in deep drawing operations is provided, emphasising how friction is a significant influencing factor. The various process conditions that effect friction, including lubrication and galling wear, are discussed. Finally, a critical assessment of currently available wear severity measurement and assessment techniques is provided. This critique of the literature will demonstrate the novelty of the objectives and work conducted in this thesis.

2.2 Process variation and monitoring

Manufacturing equipment reliability is crucial for maintaining product quality and reducing production cost. Well-timed equipment maintenance ensures reliability and will consequently help to maintain product quality and tolerances (National Research Council, 1991, pp. 54–57). Equipment that is poorly maintained will produce products that do not meet quality and tolerance specification, and may be damaged during operation which can require extended and costly repairs in large and complex equipment (Smith and Hawkins, 2004, pp. 1–14). Maintenance downtime can also be costly, and so industry must find a balance between

maintaining equipment and minimising downtime, therefore process monitoring is crucial for maintaining this balance (Lee, 1995; National Research Council, 1991).

Process monitoring is the ongoing checking of a manufacturing process during operation to ensure functionality and product quality (Stavropoulos et al., 2013). In its broadest and most basic form, process monitoring can be periodic manual inspection of the manufacturing equipment or products by an operator to check that the process is functioning correctly. Advances in manufacturing including automation and computer integration has allowed for automated on-line process monitoring across the breadth of the manufacturing space (Inasaki and Tönshoff, 2008). While this space is expansive, on-line automated systems involve the capture of various process signals, either from plant equipment or products. These signals are then processed to provide an indication of the current state of the system (Eppinger et al., 1995).

Sheet metal stamping techniques play a crucial role in numerous industries, most notably automotive, but also aerospace, consumer electrical and whitegoods, making sheet metal stamping a multibillion USD market (Grand View Research, 2017). As such, research and development into on-line process monitoring for sheet metal stamping is of significant importance and has been an ongoing focus in the literature (Doege et al., 2008; Du, 2006; Ravindran and Su, 2012).

Wear of stamping press tooling equipment is an ever-present issue in industries such as automotive, and is often responsible for costly down-time or part quality issues (Pereira et al., 2010). As discussed in Section 1.1.3, wear modelling and prediction is extremely complex (Williams, 1999) and so automated on-line process monitoring provides a useful tool for minimising the costs associated with tooling wear.

Process or machine control regimes are often inextricably linked to process monitoring, in many instances recording a process parameter and making real-time adjustments in order to maintain some pre-determined desirable trajectory (Lim et al., 2008). Such systems are unable to maintain part quality in the event of unexpected issues during production (Lim et al., 2012), and often do not provide insight into on-line issues.

A more effective method of monitoring the system is through developing an understanding of variation in process signals (Doolan et al., 2001). Through appropriate selection of process signals and developing thorough understanding of how that signal varies with process changes or issues provides a robust foundation for process monitoring and control regimes.

2.2.1 Stamping process variation and important signals

Sheet metal stamping processes have numerous process variables or signals that correspond to physical attributes and quantities from the sheet metal workpiece or the press machine. These process variables or signals can have a relationship with or provide an indication of process conditions, such as press set up, press condition, material properties, and part quality (Doege et al., 2008; Ravindran and Su, 2012). Stamping process variables or signals can be acquired from distinct regions in the production line: from the raw blank material, from the lubrication application step, from the forming process, and final part inspection (Doege et al., 2008), see Figure 2.1.

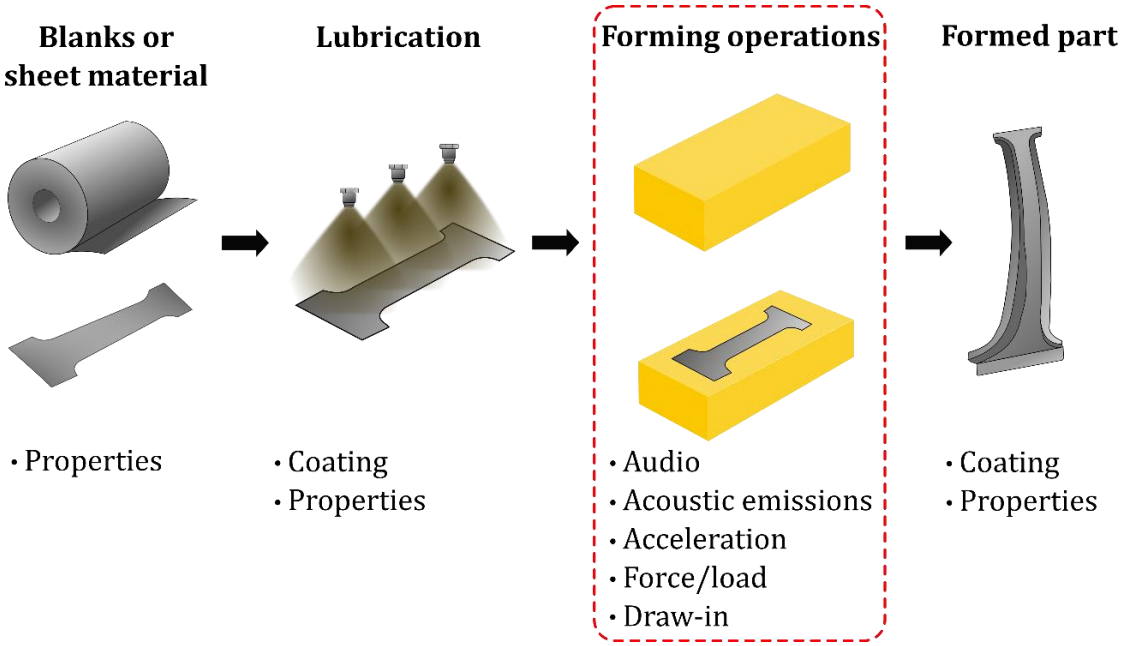

Figure 2.1: Sheet metal forming production stages and acquirable signals.

Signals from the different stages are limited in what information they can provide. Signals collected from the material feeding stage are limited to material properties, while signals from the lubrication step are limited to lubricant properties and coating information. Information or signals from final inspection of formed parts provide valuable details about part quality and localised lubrication and die issues, however, these details lag behind production. This lag may result in the exacerbation of issues (Shui et al., 2015), and the details available from formed parts do not relate to many other press condition issues. Signals from the forming process are the most varied and have the potential to contain extensive information about press, tooling, and part condition. The variation of numerous signals acquired from the forming process have been investigated in the literature, including force or load, material flow, acceleration, acoustic signals, and audio signals (Doege et al., 2002; Doolan et al., 2003; Hao et al., 2000; Ubhayaratne et al., 2015; Zhang et al., 2002).

Acceleration signals acquired from stationary lower die mounts give an indication of the vibration in the tooling during the stroke. The features of these acceleration signals have been linked to blank thickness variation, slug pick up, and blank misfeed (Ge et al., 2002; Zhang et al., 2002). The acceleration vibration signal was found to be largely featureless until that blank begins to deform. However, analysis of the signal after deformation showed distinct responses in the frequency domain with variation of the issues previously mentioned (Ge et al., 2002; Zhang et al., 2002). These results indicate that the acceleration signal does not provide information about initial loading, which may be useful when assessing friction related factors such as wear and lubrication.

Quantifying material flow and draw-in of flanges requires in-die sensors. Numerous sensors located in multiple regions may be required to acquire a comprehensive picture of material flow. Doege et al. (2003) and Doege et al. (2002) measured material displacement in the flanges of a deep drawn rectangular part using in-die optical sensors. Safe working control limits were determined for the onset of wrinkling and cracks. Implementation of these in-die sensor systems is difficult and needs to be reimplemented for each new die set, and the acceptable draw-in values are specific to each part. “Draw-in” as a process signal also only provides information about part quality and alignment issues and can be used to infer loading indirectly - making draw-in less attractive than other signals for process monitoring.

Audio signals acquired from near the press tooling have been linked to wear development of die wear after signal separation. Ubhayaratne et al. (2017) captured and processed audio signals with semi-blind signal separation to isolate the stamping operation and found that specific frequency bands contained wear related information. This frequency range fell slightly outside of the human audible range, and wear development was found to increase the magnitude of the frequency response. Relevant signal separation is required to isolate issue related frequencies with audio signals, and whether individual process issues can be linked to distinct forms of signal variation remains to be determined.

Skåre et al. (1998) found that acoustic emission signals acquired for sensors located on the dies are influenced by galling wear and other friction changing factors. However, separating out the features of signals and linking those features to specific events was challenging. Similar to audio signals, separation and isolation of relevant components is an issue with acoustic emissions. Skåre and Krantz (2003) also assessed acoustic emission signals in addition to punch force and tool temperature in a channel forming process. A distinct acoustic emission increase was observed when stick-slip phenomenon between part and tooling began occurring. Increases in the acoustic emission signal and punch force signature were noted with this stick-slip event, with the magnitude of increase in acoustic emission signal being more significant. However, the punch force signature did increase in magnitude, and significant noise (a distinct feature) was present for the entire stroke, indicating that punch force contains useful information that merits further investigation. Acoustic emission signals, punch force and tool temperature were highlighted as important when developing understanding of tool wear in sheet metal forming (Skåre and Krantz, 2003).

Press force or load signals are the most commonly used signals in stamping process monitoring. These signals can be recorded at a number of locations on the press, including on the tooling, connection rods, or press frame by providing an indication of the load being applied to tooling and the blank. Hydraulic overload protection is a basic form of force based process monitoring that is implemented on most modern mechanical presses (Wagener, 1997). This involves the monitoring of pressure in the press main cylinder to infer tonnage or sensor-based load monitoring to ensure that the operation is within normal limits and to protect the press and die from

damage. Overload protection systems primarily act to stop operation when threshold load values are exceeded. Ceasing operation is generally achieved through release of cylinder pressure and stops expensive damage to the press or dies (Overly, 2001). This thresholding does not provide any insight into the state of the process, however, overload protection system sensors signals can be recorded, either as an inferred load from cylinder pressure (Wagener, 1997) or as a direct force signal if load cells are fitted, making load or force signals readily available from most presses. **As well as being readily available, variation of force and load signals has been shown to be closely linked to part and press conditions. Stamping force signal features extracted through various means have been linked to a wide range of issues** (Doolan et al., 2003; Jin and Shi, 1999; Koh et al., 1995, 1996). These issues vary the shape of the characteristic ramp-up to maximum force/load or changing signal features as the sheet is deformed.

2.2.2 Using stamping force or load to identify process issues

While overload protection is a common implementation of stamping force monitoring, stamping force or load signals have been linked to other various process issues. Generally, these faults that have been examined in the literature can be categorised as sudden faults or failures and escalating faults or degradation.

Sudden faults or failures are issues that can occur on a stroke without forewarning, that result in a significant/observable difference in process signals, similar to overload. Such faults have been detected using analysis of stamping force signals and include issues such as part splits and failure (Doolan et al., 2003; Koh et al., 1995) (Figure 2.2a & b), blank misfeeds (Bassiuny et al., 2007; M. Ge et al., 2004; Ming Ge et al., 2004; Ming et al., 2008; Xu and Ge, 2004), blank thickness change (Bassiuny et al., 2007; Breitling et al., 1997; M. Ge et al., 2004; Ming Ge et al., 2004; Jin and Shi, 1999; Koh et al., 1996; Ming et al., 2008; Xu and Ge, 2004) (Figure 2.2c), cushion pressure changes (Koh et al., 1996), and large pieces of debris adhering to tooling (slug) (M. Ge et al., 2004; Ming Ge et al., 2004; Koh et al., 1995; Ming et al., 2008; Xu and Ge, 2004). All of these sudden faults have been detected through analysis of stamping force signals, and this demonstrates the richness of the signals for process monitoring purposes. However, these sudden issues and the

corresponding significant changes in force signals do not closely resemble the gradual progressive changes that are expected for wear development on tooling.

Escalating faults or degradation are issues that develop gradually and become more severe with continued operation. Worn press components (gib, bearings, clutch, and brake) (Jin and Shi, 1999; Koh et al., 1996) and loose tie rods (Jin and Shi, 1999; Koh et al., 1995, 1996) are examples of escalating faults that have been found to have an observable effect on stamping force or load signals (Figure 2.2d). **Tool wear is another escalating fault that might be detectable through monitoring shifts in the force signature but has not been investigated** (Breitling et al., 1997)**.** The work that has identified signal features associated with escalating faults did not monitor progression of the faults, rather binary assessments were conducted, where example signals with the issues at advanced stages were compared to normal unaffected signals. Not only is there a clear gap in the literature regarding the link between tool wear and stamping force signals and the monitoring of tool wear using stamping force signals, but there is also a gap in progressively tracking escalating faults and degradation in stamping. This highlights the need for two research objectives of this work, firstly **to determine if variation in tooling wear and other friction factors have a demonstrable effect on stamping force signals**. And secondly, to investigate the ongoing effect of wear progression, an escalating fault, on stamping force signals by **determining if the onset and progression of galling wear on tooling has a quantifiable relationship with punch force variation**.

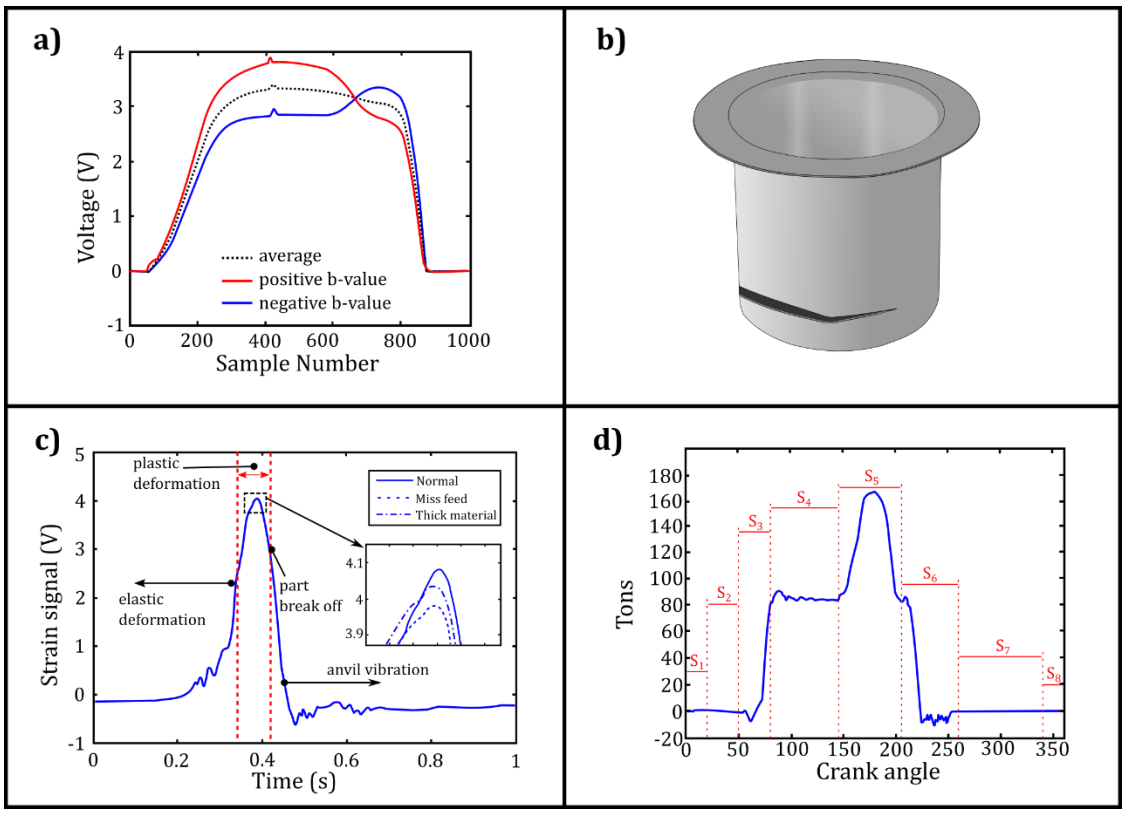

Figure 2.2: Punch force and load signal variation assessment. a) Punch force signature forms of variation allowing for identification of fractured parts, adapted from (Doolan et al., 2003). b) Example of a fractured deep drawn cup part. c) Load signal assessment from blanking operation showing process steps and variation for process issues, adapted from (Bassiuny et al., 2007). d) Stamping load signature segmented into regions of interest ($S_{1\text{-}8}$) for issue related features such as press component wear, adapted from (Koh et al., 1996).

2.2.3 Punch force analysis techniques

Process monitoring of stamping operations generally involves 2 distinct stages of data analysis, information processing and diagnosis/decision making (Ding et al., 2006; Rolfe et al., 2003). The diagnosis/decision making stage of the analysis takes the processed stamping signals and uses modelling to predict the state of the process based off the input signal. Machine learning techniques are often used in this stage with training to provide accurate state prediction. Hidden Markov Models (M. Ge et al., 2004; Ming et al., 2008; Xu and Ge, 2004), Support Vector Machines (Ming Ge et al., 2004; Ming et al., 2008), learning vector quantization networks (Bassiuny et al., 2007), and autoregressive models (Bassiuny et al., 2007; M. Ge et al., 2004) are all machine learning techniques that have been utilised for state prediction and monitoring of stamping processes using force signals. Clustering (Rolfe et al., 2003; Zhou and Jin, 2005), regression (Jin and Ding, 2004), and control limits (Jin and Shi, 2001) have also been used for state prediction. The techniques

utilised in the diagnosis/decision making stage are designed for decision making and state prediction, however, to be implemented effectively the relevant input signal types or signal features are generally identified before application (Kotsiantis et al., 2006).

The information processing stage of analysis involves taking raw stamping force signals and processing them to provide more useful information for the following stage. The purpose of the applied techniques should be to highlight issue relevant features in the signal. Various techniques have been applied to stamping force signals involving data reduction, compression, segmentation (Figure 2.2d). However, feature extraction and isolation are important tools for identifying variation and features related to process issues (Inasaki and Tönshoff, 2008). Wavelet analysis (Jin and Shi, 2001, 1999; Koh et al., 1995; Li and Bassiuny, 2008; Ming et al., 2008; Xu and Ge, 2004) and Principal Component Analysis (PCA) (Doolan et al., 2003; Jin and Ding, 2004; Jin and Shi, 2000; Rolfe et al., 2003; Zhou and Jin, 2005) are commonly used techniques for feature extraction of stamping force signals.

Wavelet analysis allows for the decomposition of the signal using a series of wavelet functions, which makes wavelet analysis techniques well suited for uncovering transient characteristics in signals (Li and Bassiuny, 2008). These features make wavelet analysis techniques ideal for isolating changes in the stamping force signal that are associated with sudden faults or failures.

PCA is a pattern recognition technique that captures the variation information in a data set of same length signals in the form of a series of Principal Components (PCs), and allowing for assessment of signals in terms of those PCs (Rolfe et al., 2003; Zhou and Jin, 2005). If these PCs can be interpreted in terms of the original signal then they can be very effective for understanding process performance and variation (Woodall et al., 2004). Doolan et al. (2003) demonstrated a method for interpreting and displaying stamping force signal PCs (Figure 2.2a) and describing individual force signals in 'b-space'. **As PCA captures variation in the force signals it makes the technique appropriate for characterising gradual changes in signal shape that come with escalating faults or degradation, such as tool wear.**

2.3 Factors affecting forming forces

Press force or load signals provide a close or direct measure of the forming or punch force that is required to form the blank material. Punch force is a function of force required to deform the blank and of the force required to overcome the restraining force provided by the blank holder. This restraining force is due to the friction between the blank material and the tooling, and is affected by a number of factors including tool condition, lubrication, and press conditions (Kim and Kardes, 2012). As a result, punch force is directly related to friction and the factors that influence friction. This section will discuss punch force and how various process parameters effect friction and punch force progression.

2.3.1 Punch and forming force

In order to enable successful forming, deep drawing, as with other forming operations, requires a specific typical punch force progression with punch displacement. However, different tooling geometries, material properties, and friction conditions will alter the magnitude and progression of the force (Billur, 2012). Punch force is the function of force required to plastically deform the blank and of the force required to overcome the friction between blank and blank holder surfaces, once deformation has begun contact with the die, radius also contributes. The dominant factor contributing to the punch force is the friction component (Emmens, 1997).

A number of distinct contact regions have been described in deep drawing operations, however, three distinct contact regions influence the friction and forming in deep drawing (Schey, 1983). These regions are both sides of the blank where contact with the blank holder and die is made (regions 1 and 2 in Figure 2.3) and on the punch radius (region 3 in Figure 2.3). The first two contact regions on the flange of the blank reduce in size over the course of the stroke, influencing pressure distribution and lubrication. After deformation of the blank is initiated the third contact region is established between the blank and the die radius, see region 3 in Figure 2.3. The die radius contact region experiences high pressures as the

restraining tension in the blank and punch movement bends and unbends the blank material over the radius (Westeneng, 2001), increasing potential for wear.

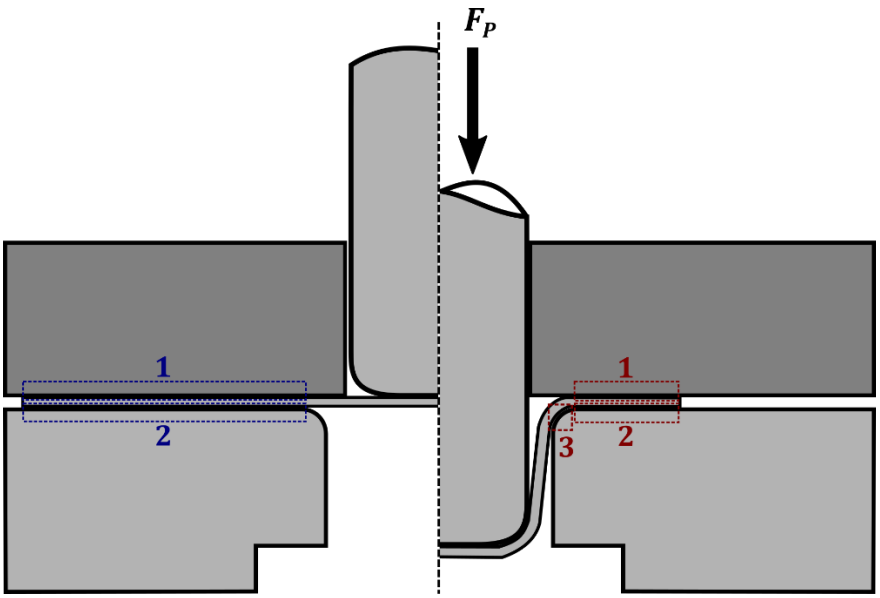

Figure 2.3: Deep drawing operation contact regions that effect friction that influences the required punch force F_P. Prior to forming (left), and after forming (right). 1. Blank – blank holder interface. 2. Blank – die interface. 3. Blank – die radius interface. Adapted from (Westeneng, 2001).

Friction in these contact regions is influenced by a number of factors relating to the blank material, tooling, lubricant, and press conditions (Kim and Kardes, 2012), see Figure 2.4. The material properties such as Ultimate Tensile Strength (UTS) and surface roughness of blank and tooling all contribute to friction. With surface roughness playing a significant role in the friction of contact. Press conditions such as speed and blank holder force are closely linked to friction in the press and are generally optimised for the required part. Temperature is another press condition that contributes to friction in terms of altering materials properties of the tooling and blank, but temperature is also dependent upon friction in the system. Effective lubrication can help to control temperatures to some extent. Lubrication is another significant factor when considering friction in the deep drawing process, with the type and properties of the lubricant influencing the frictional behaviour during the process. However, the lubrication mechanism also plays an important role, with various regimes seen in deep drawing that can drastically alter the level of friction during forming. Finally, tool wear can significantly affect the level of friction during forming, varying the surface roughness and contact conditions, and also changing

lubricant distribution. Given the effect that all these factors have on the level of friction during forming, they will all also influence the required punch force.

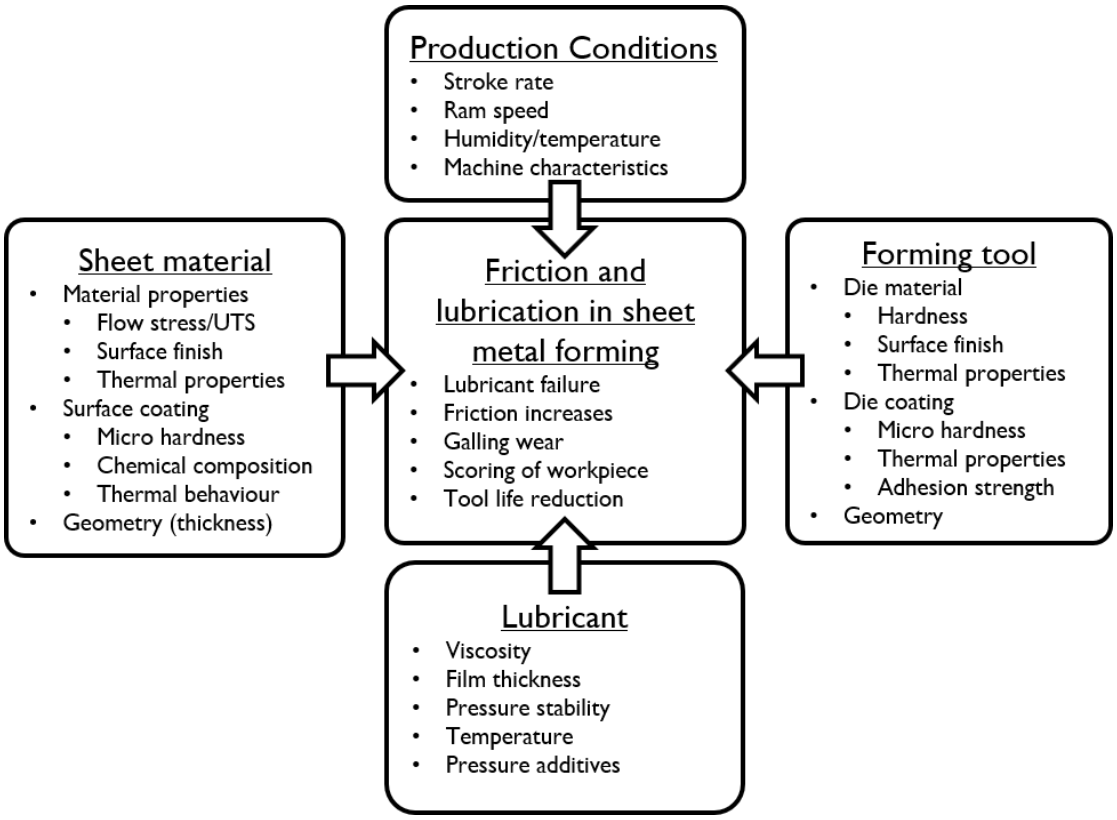

Figure 2.4: Factors affecting friction and lubrication in sheet metal forming, which in turn will influence punch force or load signals from the press (Kim and Kardes, 2012).

2.3.2 Lubrication

In deep drawing it is possible to have different lubrication mechanisms, which influence the friction within the system. The four general mechanism by which lubrication can be described are full hydrodynamic lubrication, mixed lubrication, boundary lubrication, and dry or no lubrication (Schey, 1983; Wilson, 1997). These lubrication mechanisms and conditions are characterised by the lubrication film thickness and distribution on the contacting surfaces, and each regime has a specific range of coefficient friction values that are dictated by the distribution of the lubricant.

The relationship between friction and lubricant film thickness is described by the Stribeck curve, as a function of lubricant viscosity (η), sliding velocity (v) and normal pressure (p), as shown in Figure 2.5.

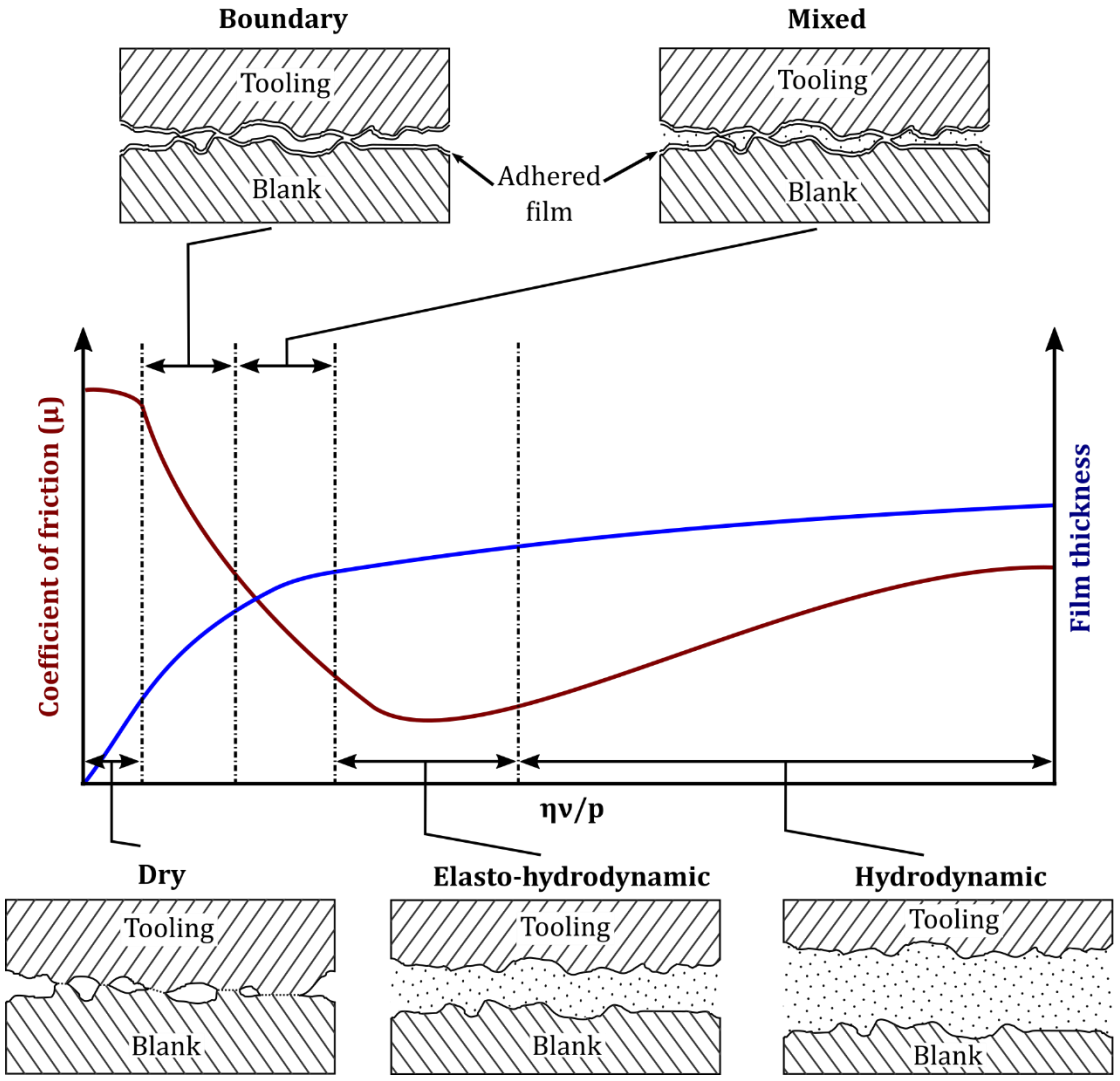

Figure 2.5: Stribeck curve describing lubrication regimes, coefficients of friction, and film thickness as a function of lubricant viscosity (η), sliding velocity (v), and normal pressure (p). Adapted from (Kim and Kardes, 2012; Wilson, 1978).

Full hydrodynamic lubrication describes the condition where a thick layer of liquid lubrication between the two surfaces is present. This category can be broken down into two further subcategories based on the thickness of lubricant film, thick and thin film (Wilson, 1978). Thick film hydrodynamic lubrication sees lubricant films much thicker than the base roughness of the two surfaces, such that friction stress is dominated by the viscous shear of the lubricant layer, making the effects of surface roughness negligible (Bhushan, 2013, pp. 400–403). Thin film hydrodynamic or elastohydrodynamic lubrication is characterised by a full lubrication film with thickness on the scale of the surface roughness of the two surfaces. In this subcategory the lubricant film carries the load between the two surfaces, but surface roughness can no longer be ignored, with asperity to asperity contact possible.

These regimes have been likened to and used for modelling of lubrication solid lubricants (Wilson, 1978). The hydrodynamic regimes can occur in the blank holder flange contact regions (Boljanovic, 2004, pp. 82–83).

Boundary lubrication describes the condition where thin films of lubricant or compounds within the lubricant adhere to the two metals surfaces, acting as a boundary between the two surfaces. However, contact of asperities take the load of contact, and the adhered film reduces the chance of asperity adhesion and lowers the friction of contact (Wilson, 1991).

In mixed layer lubrication the asperity peaks experience boundary lubrication or direct contact, taking a portion of the contact load, while lubricant pools in the asperity troughs, supporting the remainder normal pressure exerted on the surfaces (Bhushan, 2013, pp. 400–403). This regime sits between boundary and hydrodynamic lubrication and as a result, friction is moderate.

Finally, dry contact conditions describe the situation where the two solid surfaces in contact have no lubrication at the interface. Asperities on the two surfaces make direct contact, leading to high levels of friction and chances of adhesion (Kim and Kardes, 2012; Nine, 1978).

In deep drawing the initial pressure applied by the blank holder squeezes lubricant from the blank (Moore, 1975, pp. 113–114; Wilson, 1978), leaving a residual film between the contacting surfaces. This residual film is redistributed as the blank is drawn into the die cavity, with high contact pressures at the die radius and slight thickening of the blank flange playing a role (Wilson, 1978). These conditions lead to varying levels of friction in deep drawing with fluid lubrication that will have an influence on punch force. Solid lubricants are unlikely to see significant change in film thickness during the forming process (Wilson, 1978), and so the friction conditions are likely to remain stable when forming using solid lubrication regimes.

2.3.3 Galling wear

Galling wear in sheet metal stamping is a localised multistage sliding wear mechanism, where material transfer occurs at initiation sites and accumulates with progressive contact. The accumulated material ploughs the opposing surface and

eventually the continual accumulation of galled material can result in fracture (Gåård et al., 2008; Schedin, 1994; Schedin and Lehtinen, 1993). Galling wear damage is characterised by macroscopic localised roughening of the surface, and the creation of protrusions above the original surface due to plastic flow of the material and material transfer (ASTM Standard G40-15, 2015). Galling is the wear mechanism often seen in sheet metal stamping (Kirkhorn et al., 2013) where the tooling experiences repeated sliding contact under high loads with sheet metal blanks. Galling damage on high strength steels commonly used in automotive sheet metal forming operations exhibit transitions from abrasive or ploughing scratch damage through to severe adhesive wear damage with continued sliding contact with worn tooling (Gåård et al., 2008), see Figure 2.6.

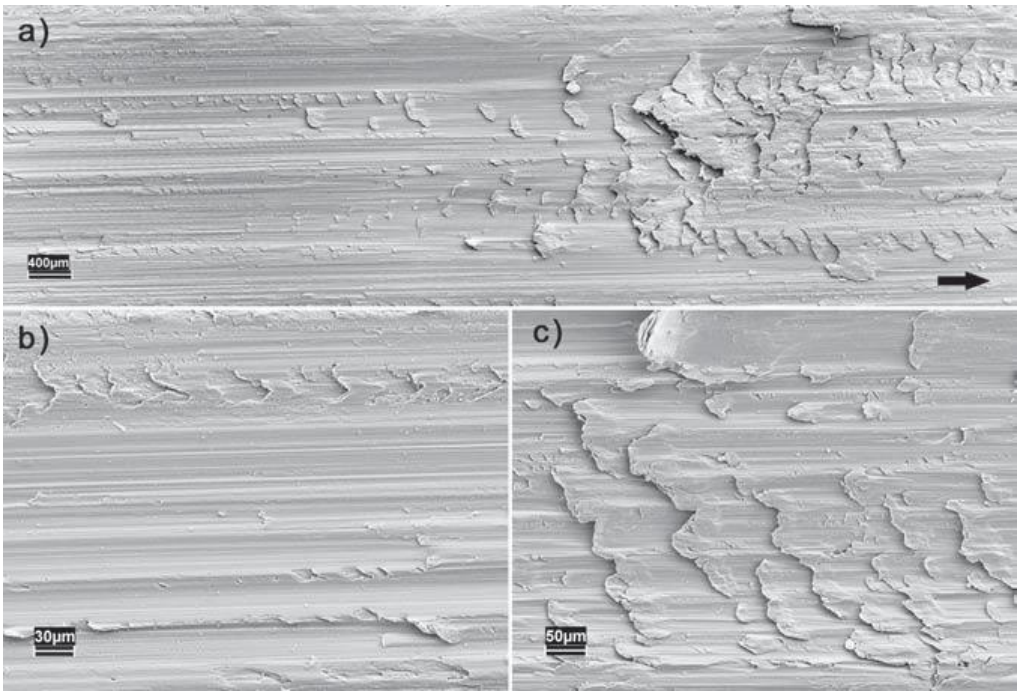

Figure 2.6: Surface damage typical of galling wear on high strength steel sheet material (Gåård et al., 2008). a) transition from abrasive or ploughing scratch damage to adhesive damage with increased sliding distance; the arrow indicates the tool sliding direction. b) Typical appearance of abrasive or ploughing scratch damage. c) Typical appearance of severe adhesive wear damage.

In sheet metal stamping the contact conditions and the disparity in surface roughness and hardness between the blank material and press tooling accelerates the development of galling wear. As a result, the ploughing and adhesion that comes with galling increases the friction between the two surfaces in sliding contact. Akagak and Rigney (1991) found that in low friction ploughing or mild abrasion

occurred in the early stages of wear prior to the advent of adhesion and transfer. After ploughing and abrasion, adhesion and material transfer initiated and cumulated into severe wear and high unstable levels of friction. This indicates that **as galling wear progresses on the tooling in a deep drawing operation a corresponding increase in friction can be expected**. Multiple galling wear sites might also be expected with the large contact areas seen in deep drawing, which would also contribute to friction increases. This cumulates in progressive increases in friction that **will have an effect on the punch force in deep drawing operations**.

2.4 Galling wear assessment and measurement

Measurement and characterisation of this galling wear in real deep drawing situations is a crucial component in investigating the link between process signals and wear. The techniques and parameters that have been used for quantifying and characterising galling wear are often not targeted at the localised features that contribute to and are caused by galling wear. Furthermore, these traditional techniques are not well suited for the implementation in large scale industrial style stamping wear trials that are necessary for developing wear monitoring systems.

Galling wear in sheet metal stamping is difficult to characterise and measure because of the multistage progression of the mechanism on both contacting surfaces and the lack of targeted measures. Wear damage features that precede galling observed in sheet metal forming progress through a number of stages including: asperity smoothing and plastic deformation, abrasive damage of various scales and finally progressing to galling damage (Andreasen et al., 1998; Gåård et al., 2008; Karlsson et al., 2012). These distinct surface features can be observed on both the tooling and formed parts (Gåård et al., 2009). Characterisation is further complicated in sheet metal stamping of irregularly shaped parts, where varying contact conditions can lead to localised wear that develops at different rates. The presence of wear damage can make formed parts unfit for purpose, both functionally and aesthetically, which highlights the requirement of automatic galling wear monitoring for sheet metal stamping.

2.4.1 Visual assessment

Qualitative visual assessment is often used to determine the severity of wear on tooling and parts, and remains the most ubiquitous and effective method for characterising and identifying the severity of galling wear. The effectiveness of visual assessment has led to its use in numerous wear studies, often in addition to other quantitative measures (Andreasen et al., 1998; Christiansen and De Chiffre, 1997; Galakhar et al., 2011; Groche et al., 2011; Karlsson et al., 2012; Olsson et al., 2010; Podgornik et al., 2004; Pujante et al., 2013; Shaffer and Rogers, 2007; Skåre and Krantz, 2003; Swanson et al., 1988; Ubhayaratne et al., 2017; van der Heide et al., 2001; Wang et al., 2013). Due to the difficulty of assessing tooling during forming operations visual assessment of formed parts is a primary method used in industrial applications for determining if tool maintenance is required (Smith, 2001). Visual assessment is widely used for determining the presence and severity of galling wear in sheet metal stamping and is used as a standard in galling test methodologies (ASTM Standard G196-08, 2016; ASTM Standard G98-02, 2009). The ASTM G98 galling test, for example, is widely used for the assessment and ranking of galling resistance of material couples. **This standard utilises subjective visual characterisation of galling and provides a qualitative assessment of galling resistance** (ASTM Standard G98-02, 2009). A number of issues effecting the accuracy of ASTM G98 have been discussed (Hummel, 2011), but **the subjective nature of visual assessment and the need for clear and quantitative characterisation have been highlighted** (Siefert and Babu, 2014). It is difficult to achieve repeatable results and collect a quantifiable output using visual assessment of galling wear severity. Given this, **it is important to identify a quantifiable measure of galling wear equivalent to visual assessment**.

Numerical rankings of galling wear severity have been used to provide a quantitative output for visual assessment (Andreasen et al., 1998; Budinski and Budinski, 2015; Olsson et al., 2010). However, in these instances the assessment has been made on magnified regions where the wear state is consistent throughout. Numerical ranking schemes are less suitable for industrial style trials as they are difficult to apply to larger contact regions with multiple localised instances of wear, and are time consuming when assessing numerous parts. Despite these issues, numerical rankings are an appropriate standard for comparing galling wear

measures in small scale experimental conditions as they provide the closest quantifiable measure of wear severity.

2.4.2 Mass and volume

Mass and volume loss measurements of tooling are common methods for quantifying wear (Fildes et al., 2013; Galakhar et al., 2011; Pujante et al., 2013; Shaffer and Rogers, 2007; Taşan et al., 2005). These methods are convenient for the purposes of modelling given the role of wear volume that is represented in the Archard wear equation (Archard, 1953), which has seen extensive usage in tool wear related studies. Mass and volume loss measurements give a direct assessment of the tooling and are simple to implement in laboratory wear test conditions. However, it is possible that the techniques can give inconsistent results as wear damage can occur without loss of mass, for example with plastic deformation (Kennedy and Hashmi, 1998). Therefore, measuring mass and volume loss gives an incomplete picture of the wear process. Additionally, mass and volume measurements of wear are not suitable for progressive measurement in industrial style trials, where wear assessment is desired from part to part. It is also not possible to obtain mass measurements of large and heavy sheet metal stamping tooling that are accurate enough to identify small localised changes in wear.

2.4.3 3D profilometry

3D profilometry of formed parts or tooling allows for assigning standardised texture parameter values, and provides insightful information about the state of the wear conditions. Christiansen and De Chiffre (1997) assessed adhesive and abrasive wear using bearing curve parameters S_{pk}, S_k, and S_{vk} and worked towards the characterisation of the prominent mechanism observed. Table 2.1 shows a summary of hypotheses of how the different mechanisms seen in galling wear effects S_{pk} and S_{vk} values. However, galling wear in sheet metal forming may exhibit the effects of both of these mechanisms at multiple locations, in which case the characteristic effects on S_{pk} and S_{vk} may cancel out. While 3D surface analysis has the potential to

provide a complete quantitative characterisation of galling wear, a definitive selection of parameters for galling wear quantification has not been identified.

Table 2.1: Galling related wear mechanisms and effects with hypothesised effects on surface topography and 3D bearing curve parameters (Christiansen and De Chiffre, 1997).

Wear mechanism		**Effect**	
Adhesive	Adhesive wear	Asperities' tops break off the tool	Decreased S_{pk} No influence on S_{vk}
	Pickup	Deposits of workpiece material are added to the tool surface peaks	Increased S_{pk} No influence on S_{vk}
Abrasive	Abrasive wear	Tool material is removed, leaving a scratch	Increased S_{pk} Increased S_{vk}
	Ploughing	A furrow and a bulge are formed on the tool	No influence on S_{pk} Increased S_{vk}

2.4.4 2D profilometry

2D profilometry can also be applied to part or tooling surfaces and several standardised 2D roughness parameters are available to give information about the wear conditions. 2D profilometry has been used for the qualitative assessment of galling tracks (Karlsson et al., 2012) and also for collection of quantitative data using roughness parameters such as R_a, R_z, R_y, R_p, and R_v (Andreasen et al., 1998; Christiansen and De Chiffre, 1997; Swanson et al., 1988; van der Heide et al., 2001). One issue with utilising conventional parameters, particularly the average roughness R_a, is that they can return similar values for drastically different surface topographies (Bhushan, 2013). 2D profilometry has also been used to measure wear track depth and estimate wear volume as a means of quantifying wear (Yost, 1983), however, these measures are most suitable for single wear track experiments. Fast Fourier Transform (FFT) has been applied to 2D surface profiles of galled parts in order to give a Galling Severity Index (*GSI*) (Vermeiden and Hobleke, 2003). This *GSI* approach assesses the 2D profiles in terms of wavelengths and takes a mean value of magnitudes within a given wavelength range, which is then normalised using a mean magnitude value for an unworn reference 2D profile. The issue with this

approach is that isolating the specific wavelengths at which wear features are active is difficult as all spatial information of the profile is lost during the FFT. Additionally, taking the mean value for a range of wavelengths also has the potential for reducing or losing wear information. Despite the shortcomings of 2D roughness parameters, 2D profiles taken from parts have a distinct advantage over other methods of measuring wear. Part 2D profiles are fast to acquire, are unobtrusive in terms of press tooling, and measure the product, which is ultimately the subject of interest for industry. While 2D roughness profiles are an appropriate medium for measuring galling wear there is a gap in the literature for targeted measures of galling wear that are appropriate for sheet metal stamping processes. This coupled with visual assessment being the current standard for assessing galling wear suggests that a new galling wear severity measure is required that targets the features of galling wear, is applicable to sheet metal stamping processes, and provides an accurate correlation to visual assessment.

2.5 Summary

This Chapter provided a review of the literature relevant for the investigation of links between punch force signature variation and galling wear. In Section 2.2 process monitoring was reviewed with a particular focus on variation of forming punch force and load and how that variation has been related to process issues. The ability to detect significant single process issues using forming punch force and load was shown, however, no significant work had been conducted relating progression of issues, such as die wear, to signal variation. These findings suggest that **the effects of galling wear events and progression on the variation of punch force signatures should be investigated**.

Section 2.3 discussed the factors that influence forming forces, with friction between the blank and tooling playing a significant role. The review of the literature shows that galling wear increases friction, suggesting that wear progression will drive variation in the punch force signatures during a trial. However, a number of other factors influence the friction between the blank and the tooling, including blank holder force and lubrication. This suggests that **progression and changes of these other factors should be investigated in conjunction with galling wear to**

determine if they influence punch force signature variation in a different manner.

In Section 2.4 a critical assessment of galling wear severity measurement techniques was conducted. It was concluded that the techniques that have been used to measure galling wear in the literature do not target galling wear features specifically. In addition, no currently used measures have been shown to correlate with visual assessment. This assessment suggests that **a new galling wear severity measure is required that targets the features of galling wear so as to provide an accurate correlation to visual assessment**. Given the requirements of applications to deep drawing of large parts and technical limitations, any such severity measure should be based on 2D profiles.

This review of the literature directly supports the research objectives of this thesis:

- Determine if variation in wear and other friction influencing factors have a demonstrable effect on punch force signatures (Chapter 4).
- Develop an accurate method for quantifying galling wear severity that can be applied to channel forming experiments conducted in this work (Chapter 5).
- Examine if the onset and progression of galling wear has a quantifiable relationship with punch force signature shape variation (Chapter 6).
- Investigate how specific wear events and changes in friction influencing factors affect the punch force signature (Chapter 7).

CHAPTER THREE

Methodologies

3.1 Introduction

The presented literature review and research objectives of this thesis have highlighted the need for new methods of galling wear severity quantification and for galling wear monitoring techniques. In order to achieve the research objectives of this thesis a number of sheet metal stamping galling wear and lubrication experiments were undertaken. The galling wear on parts formed in these trials was characterised for further analysis detailed in the following chapters. This Chapter will outline the common experimental methods and techniques utilised throughout the thesis, including the channel forming deep drawing process, worn surface characterisation, and signal analysis techniques.

3.2 Experimental approach and justification

The goal of this thesis is to investigate and develop methods for real time detection and monitoring of galling wear on tooling in sheet metal forming. A review of the literature has revealed an additional requirement of establishing a targeted repeatable and quantitative method for measuring galling wear severity that reflects the accuracy of visual assessment.

In order to achieve these aims, a series of stamping trials were conducted in near industrial conditions. A requirement was to assess the press tool condition at regular intervals so as to have a regular measure of wear for monitoring purposes.

Industrial stamping has been replicated using a semi-industrial stamping process that allows for high volume production and wear conditions similar to those experienced in industry. The semi-industrial process also allowed for capture of press signals and parts that are simple to assess and also mimic geometries common in industry.

The assessment of wear state and severity in the stamping process was focused on the part surface. Assessment of part or die 'counter surface' is common due to difficulty associated with assessing the die and correlation with industry practice (Andreasen et al., 1998). Assessing the part surface also allowed for easy regular assessment of the tool condition, as direct assessment of the tooling at regular intervals required time consuming stoppages, which further distanced the trial from the continuous nature of industrial conditions. Part assessment was conducted visually, as is currently standard, in addition to characterisation and measurement using variable focus microscopy. These visual assessments and profilometry were used to characterise the quantity and severity of die wear in the semi-industrial stamping process.

Punch force has been identified as an appropriate tool wear monitoring signal for stamping, with signal variation being a target for relevant tool condition information. In order to capture this signal variation the signal analysis technique Principal Component Analysis (PCA) was utilised. As discussed in Section 2.2.3, PCA has a precedence for use in sheet metal stamping condition monitoring using punch force and is capable of isolating distinct forms of signal variation, which in turn can be linked to specific process events or conditions (Doolan et al., 2003; Jin and Ding, 2004; Jin and Shi, 2000; Rolfe et al., 2003; Zhou and Jin, 2005).

3.3 Channel forming processes

In this thesis two channel forming press setups have been utilised to collect parts and press signals. These two setups are referred to as semi-industrial stamping press and laboratory stamping press and are discussed here in this section.

3.3.1 Semi-industrial stamping press

Semi-industrial channel forming trials conducted using a single action mechanical press reported by Pereira et al. (2010), Figure 3.1, equipped with an automated sheet feeder and straightener. Press geometry and material selection were designed to represent a wear prone automotive deep drawing operation. The main geometry and press process variables are summarised in Table 3.1. The tooling geometry features two symmetrical removable die radius inserts, that are designed for easy removal. The high contact pressures on these die inserts result in wear damage being localised on the inserts and counter surface of the channel part sidewalls. Blank material was 1.8 mm thick high strength low alloy grade steel (HSLA300 or HSLA400), that conformed to AS/NZS 1594 specifications. The mechanical properties of HLSA300 and HSLA400 blank material in the direction of forming (transverse to the rolled direction of the sheet) are shown in Table 3.2.

Die corner radius inserts used in the trials had nominal radii of either 5 mm or 7.5 mm. The specific details of these inserts, regarding material, finish, and coatings is specified for each trial. Other press tooling, the punch and blank holder components were manufactured from hardened AISI D2 tool steel which was plasma-nitrided and PVD coated with TiCN to prevent the onset of wear.

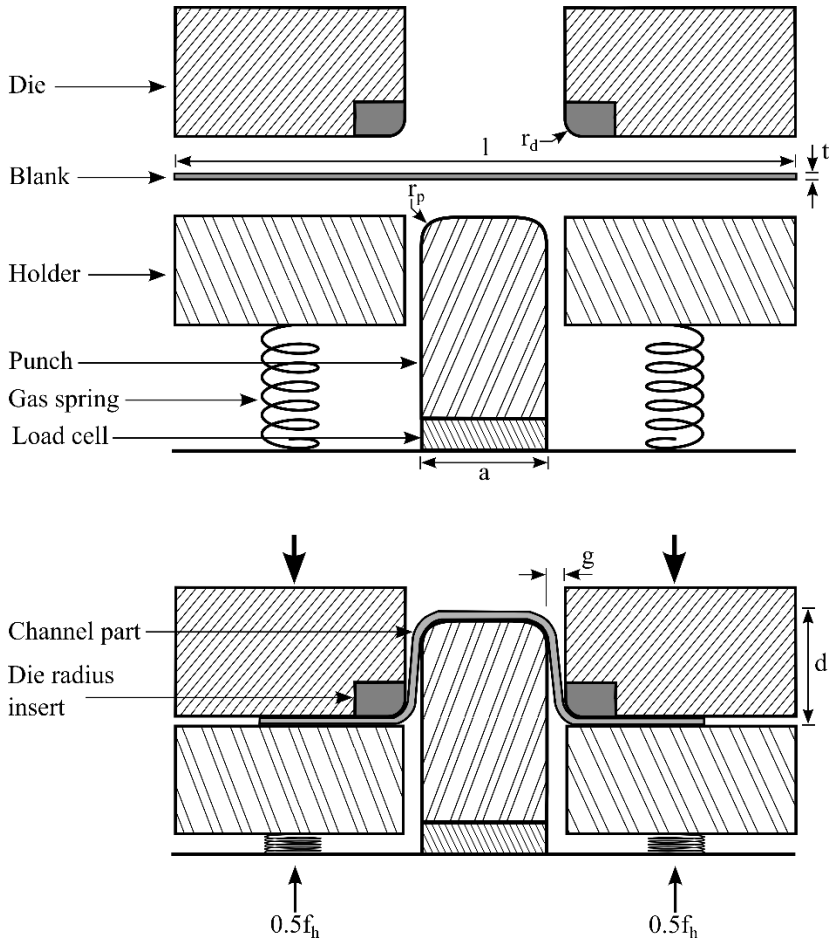

Figure 3.1: Semi-industrial stamping press channel forming operation schematic.

Table 3.1: Details of semi-industrial stamping press channel forming trials.

Channel forming operation process variables	
Punch width, a	30 mm
Draw depth, d	40 mm
Die-to-punch gap, g	2.3 mm
Blank length, l	150 mm
Blank holder force, f_h	17.5 kN / 28kN
Die radius, r_d	5 mm or 7.5 mm
Punch corner radius, r_p	5 mm
Blank thickness, t	1.8 mm
Blank width	26 mm
Press rate	32 min^{-1}

Table 3.2: Mechanical properties of HLSA blank material.

HLSA300 mechanical properties	
Yield strength (MPa)	321
Tensile strength (MPa)	485
Uniform elongation (%)	19.2
HLSA400 mechanical properties	
Yield strength (MPa)	447
Tensile strength (MPa)	525
Uniform elongation (%)	16.8

The press operated with a ram speed of approximately 300 mm/s at the beginning of the forming operation and decelerated to 0 mm/s at the end of the stroke. The blank holder force applied by the gas springs was an average of 17.5/28kN depending on the stated low/high blank holder force conditions.

Unless where otherwise stated, a light film of anti-corrosive oil, Ferrocote 366 K2 50, was applied to blank material. Lubrication was applied to blank material using an automated oil roller system prior to entering press tooling. A number of other lubricants were utilised in the semi-industrial trials, the details of these are summarised in Table 3.3.

Table 3.3: Lubricant details.

Lubricant	Details
Mill oil	Quaker Ferrocote 366 K2 anti-corrosive mill oil
Unlubricated	Die and blank cleaned with ethanol and no lubricant applied
Drawing lubricant	Fuchs Renoform MP631
Ionic liquid	Ionic liquid (P6,6,6,1,4BEHP) 3% by weight in mineral oil (Somers et al., 2013)
Mineral oil	Grade II mineral oil (Somers et al., 2013)
Dry PTFE coating	WD-40 Anti-friction Dry PTFE lubricant
PTFE sheet	PTFE coated fibreglass fabric

3.3.2 Semi-industrial stamping press data collection

The punch force signal was recorded over the course of each stroke using a Kistler piezoelectric load washer (9041A) located at the base of the stationary punch. The

load washer signal was recorded at 1000Hz using a National Instruments DAQ system and National Instruments Signal Express software. This sampling frequency provides approximately 300 individual punch force values per stroke that make up each punch force signature. These punch force signatures were subsequently isolated for further post processing and analysis in Mathworks MATLAB.

3.3.3 Laboratory stamping press

Laboratory channel forming trials were conducted using the electro-hydraulic action of an Erichsen Universal Sheet Metal Testing Machine (Model 145-60), shown in Figure 3.2. The geometry and main process conditions are summarised in Table 3.4. As with the semi-industrial stamping press this channel forming process is designed to allow for close replication of conditions seen in the forming of automotive sheet metal components. The tooling geometry features two symmetrical removable die radius inserts (Die I and Die II) that are designed for easy removal. These inserts had a nominal radius of 5 mm and were made of polished AISI D2 tool steel. The high contact pressures on these die inserts resulted in wear damage being localised on the inserts and counter surface of the channel part sidewalls. Blank material for all laboratory stamping trials was 2 mm thick, uncoated dual phase sheet steel (DP600). Further details of the experimental setup can be found in (Pereira et al., 2009).

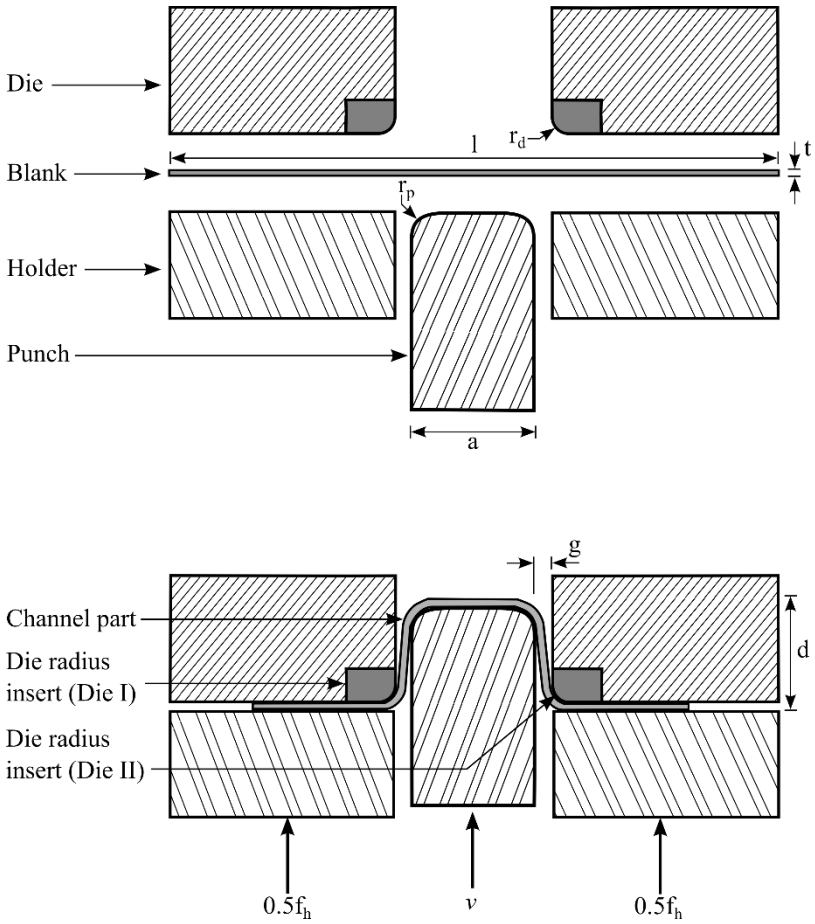

Figure 3.2: Schematic of the laboratory stamping press channel forming process.

Table 3.4: Laboratory stamping press channel forming operation process variables.

Channel forming operation process variables	
Punch width, a	40 mm
Draw depth, d	50 mm
Die-to-punch gap, g	2.1 mm
Blank length, l	150 mm
Blank holder force, f_h	20 kN
Die radius, r_d	5 mm
Punch corner radius, r_p	5 mm
Blank thickness, t	2 mm
Blank width	19.5 mm
Tool-to-sheet clearance	0.1 mm
Punch speed, *v*	1.5 mm/s
Die material	AISI D2 tool steel
Blank material	Uncoated DP600
Die hardness	60 HRC

3.3.4 Laboratory stamping press data collection

Punch force, blank holder force, and punch stroke displacement were all recorded by the Erichsen Universal Sheet Metal Testing Machine during trials. However, this data was not utilised in this thesis as the focus of the laboratory trial was the assessment of wear damage without correlating to press signals (Section 5.5).

3.4 Visual assessment

Visual assessment of wear damage severity on part sidewalls was conducted under a systematic regime that allows for the ease of ranking assignment. This regime involves the subdivision of the assessment region (see Figure 3.3) into smaller sections, for which individual severity rankings are assigned.

Photographs of both sidewalls of parts formed in the channel forming process were taken for ease of visual assessment for galling wear damage. The photographs were subdivided into sections, the size and quantity of which will be described for each case.

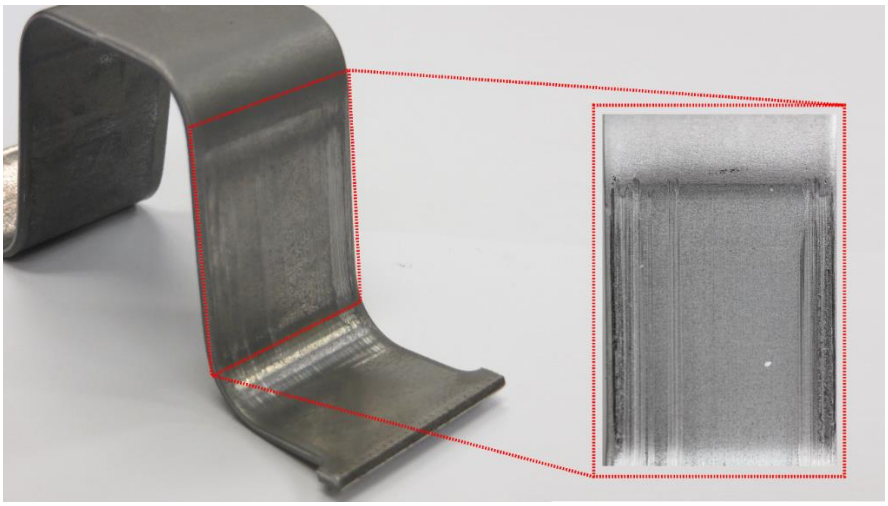

Figure 3.3: Part sidewall visual assessment

3.5 Metrology

3.5.1 Surface characterisation

3D focus-variation scanning microscopy was used to collect 3D surface scans of regions on the channel part sidewalls. These 3D surface scans were then used for the collection of 2D surface profile data and 3D texture data. The 3D focus-variation scanning microscope used was a Alicona Infinite Focus. Unless where otherwise stated, surface scans were undertaken at x20 magnification corresponding to a vertical resolution of 100nm and lateral resolution of 3µm. The scan sampling spacing for both horizontal and vertical axis was set to 1µm.

Figure 3.4: 3D focus variation scanning microscope Alicona Infinite Focus.

A custom channel part holding jig was designed and constructed to hold the scanned part side walls parallel to the scanning stage. The jig was mounted to the scanning stage such that scans could be located in the same regions of the part sidewall for consistent comparisons from part to part.

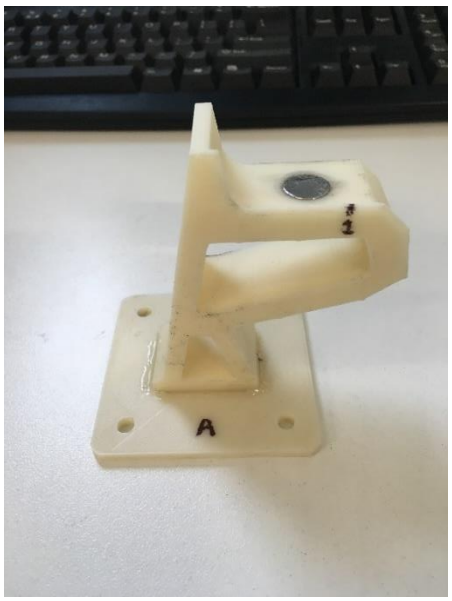

Figure 3.4: Custom channel part holding jig.

3.5.2 3D and 2D profilometry

The 3D focus-variation scanning microscopy described in Section 3.5.1 were used for both 3D and 2D profilometry of the part surface. Scans conducted for the purposes of 2D profile collection were all oriented perpendicular to contact siding direction so as to capture galling features along the entire width of the sidewall. 2D surface profiles subsequently isolated from the 3D surface scans and were restricted to the region starting and finishing 1 mm from either edge of the sidewall, this ensured that edge effects were ignored when characterising the surface. 3D profilometry was conducted using 3D surface scans, the specific locations and orientations of these scans and 3D profilometry regions were case dependent and will be described accordingly. Example 2D and 3D profilometry of a channel part sidewall is depicted in Figure 3.5.

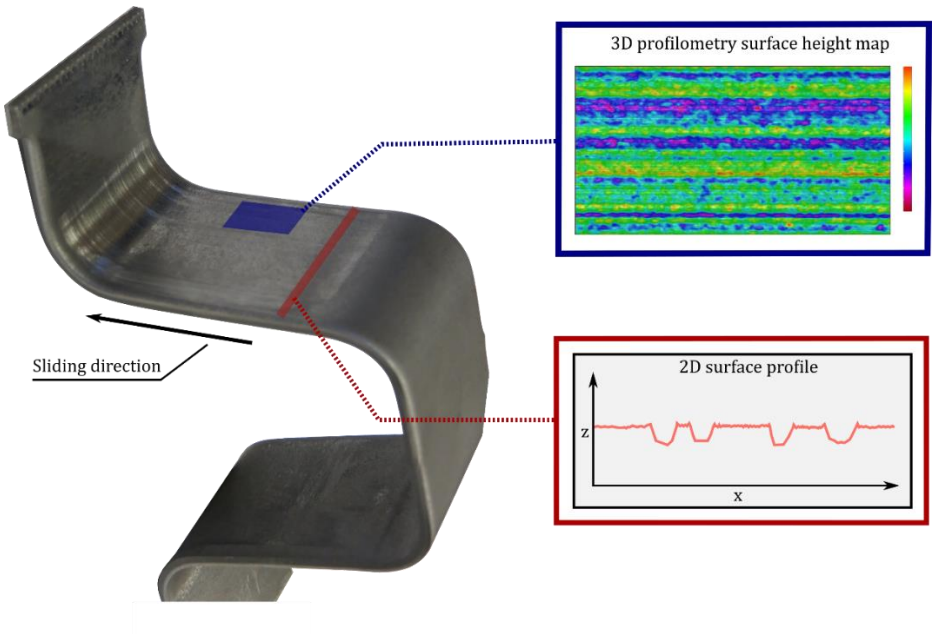

Figure 3.5: 2D and 3D profilometry collection schematic from channel part sidewall.

3.6 Signal analysis

3.6.1 Principal Component Analysis

As discussed in Section 2.2.3, Principal Component Analysis (PCA) is an image recognition technique that has been used for the analysis of punch force signatures for detection of part failure (Doolan et al., 2003) and process variation (Jin and Shi, 2000). The PCA method has been applied to isolate punch force signature variation that relates to tooling wear and related friction drivers in the stamping process. The PCA method isolates the Principal Components, major forms of shape variation, in a training set of punch force signatures. The process can then be used to reduce any punch force signature of the same length to a number of coefficients, b-values, that characterise the signature shape in terms of the Principal Components or form of shape variation. The PCA method is applied such that a punch force signature can be described by the following:

$$\hat{X}_i = \bar{X} + \boldsymbol{P}\boldsymbol{b}_i \quad (1)$$

Where $\bar{X}$ represents the mean vector of the punch force signature training set, and $\boldsymbol{P}$ is the matrix of significant eigenvectors determined for the covariance matrix of

the training set matrix. The vector $\boldsymbol{b_i}$ is the vector of weighted coefficients or b-values that describe the punch force signature $\hat{X}_i$ in terms of each Principal Component. Rearranging equation (1) $\boldsymbol{b_i}$ can then be determined using equation (2):

$$\boldsymbol{b_i} = \boldsymbol{P}^{+}\left(\hat{X}_i - \bar{X}\right) \tag{2}$$

Where $\mathbf{P}^{+}$ is the pseudo inverse of the **P**. By calculating b-values for each punch force signature, it is possible to track the changes in specific form signature shape change from part to part.

3.7 Summary

This Chapter has outlined in detail the common experimental methods and techniques that are utilised throughout this thesis. These include the semi-industrial and laboratory channel forming deep drawing processes, characterisation of worn part surfaces, and the signal analysis technique used on process signals captured during the semi-industrial trials.

The wear and process data has been collected from semi-industrial trials conducted on the channel forming deep drawing presses. The press geometry and process variables have been designed to replicate wear prone regions in automotive industrial deep drawing process. Data collected from these trials has be utilised throughout this thesis and ensures that results presented in subsequent Chapters have a direct link to industrial stamping and deep drawing.

Worn part surface characterisation and measurement are fundamental for the research objectives of this thesis, specifically the development of new galling wear targeted severity measures and galling wear process monitoring techniques. The methods for visual assessment, 2D profilometry, and 3D profilometry have been clearly established and will be utilised throughout this thesis.

PCA has been outlined as the main signal analysis technique that is applied to punch force signals captured during the semi-industrial trials. PCA provides a clear breakdown and representation of punch force signature variation, which will form the foundation for further understanding of the link between punch force, friction,

and galling wear. This understanding will in turn be crucial for developing process wear and friction monitoring techniques.

Subsequent Chapters refer to the generalised methods outlined in this Chapter and any deviation from the methods presented in this Chapter are detailed where appropriate.

CHAPTER FOUR

Punch force signature variation

4.1 Introduction

In Section 2.2.2, the close link between punch force signature variation and significant forms stamping process variation, including part failure, were discussed. In this Chapter, the link between punch force variation and the subtler process changes due to wear and other friction influencing factors such as blank holder force and lubrication will be investigated.

In order to establish if punch force signatures can be used to track and detect tooling wear onset and progression, a series of initial channel forming trials have been conducted. Firstly, a base case for channel forming punch force signatures was established and assessed, followed by a series of trials under different conditions for comparison. These trials have been conducted to determine if any forms of punch force signature shape variation, isolated through PCA, can be linked to specific friction influencing factors such as die wear. Punch force signatures have been collected under different lubrication conditions, different blank holder force (BHF), and distinct levels of die wear. PCA was then used to isolate the dominant forms of punch force shape variation associated with changes of the different friction influencing factors. These experiments show that punch force signatures vary in a detectable manner with changes in wear level, but the forms of variation are not unique to changes in wear. The main outcomes to be presented in this chapter were published in the proceedings of the International Deep Drawing Research Group conference 2014 (Voss et al., 2014).

4.2 Base case punch force signatures

In order to determine how punch force signatures are affected by wear on dies an understanding of unaffected punch force signatures must be established. Understanding the features and variation of punch force signatures under 'normal' conditions unaffected by wear provides a base case to which effected signatures can be compared. In this Chapter, the effects of a change in die wear have been assessed as well as changes of lubrication and BHF, that also affect friction.

Initial channel forming trials were conducted using the semi-industrial channel forming press (Section 3.3.1). To ensure that wear progression was removed as a factor in these initial channel forming trials two die sets have been used, one for the wear comparison and another for the other friction conditions. A set of polished hardened AISI D2 tool steel 7.5 mm radius die inserts (set labelled A09-A10) were used for the wear comparison, with sample punch force signatures taken at the beginning and the end of an extended wear trial. Wear progression was assumed to be negligible in these subsets of the trial. In the case of assessing other friction conditions wear was removed as a factor through the use of a set of hardened and coated inserts (referred to as PVD dies from this point forward). The PVD inserts consisted of hardened AISI D2 tool steel that were plasma-nitrided and PVD coated with TiCN.

The selected base case conditions for punch force signatures was signatures collected from parts formed using unworn die corner inserts and lubricated with anti-corrosive mill oil applied automatically with the semi-industrial presses lubrication roller. The data collected for both die sets is examined here so as to provide some insight into punch force signatures recorded under normal or base case conditions. The PVD inserts could not economically be allowed to develop severe galling wear and so, the A09-A10 die set wear trial was used to provided severe wear data. As a result, two specific base cases were required due to the difference in material and die radii of the PVD and A09-A10 set. These differences mean that the punch force signatures collected using each die set cannot be directly compared. The differences between these base case signatures are highlighted and discussed in this section. The details of the two base case trials are presented in Table 4.1.

Table 4.1: Base case trial press condition details.

Base case conditions						
Die set	**Lubricant**	**Average BHF**	**Wear level**	**Number of parts**	**Die corner radius**	**Blank material**
A09-A10	Mill oil	28 kN	No-wear	50	7.5 mm	HLSA400
PVD	Mill oil	28 kN	No-wear	50	5 mm	HLSA300

Punch force signatures for each part formed in the two base case trials were captured according to Section 3.3.2 and mean punch force signatures were calculated. Mean signatures were calculated by determining the mean punch force value at each sampled punch displacement for all signatures collected in the trial, and is equivalent to $\bar{X}$ (Section 3.6.1). Figure 4.1 shows the mean punch force signatures for the two base case trials with punch force against punch displacement.

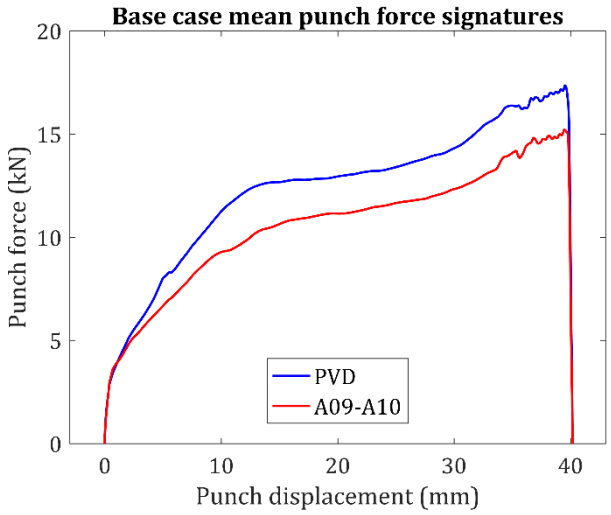

Figure 4.1: Base case trial mean punch force signatures.

These mean punch force signatures provide an indication of standard punch force signatures. There is a clear difference in magnitude, that is likely due to the tighter radii of the PVD inserts, which requires larger punch force to bend the blank around (Boljanovic, 2004). The mean signatures have similar general shape and progression of punch force over the course of the stroke, characterised by rapid increase in force in the first 13 mm of punch travel followed by a gradual increase cumulating in peak punch force at 39.5 mm of punch displacement and rapid drop to zero as the punch reaches maximum travel and retracts. Also notable is the

instability of the punch force progression in the last 5 mm of punch travel that is apparent in both average signatures.

4.3 Wear and other friction conditions

In this section the base case condition punch force signatures are compared to punch force signatures collected with worn die corner inserts and under various lubrication and blank holder force regimes. These condition comparisons were designed primarily to determine if punch force signature shapes varied significantly with wear of the tooling. Other friction conditions (lubrication and BHF) were also compared to the base case in order to establish if these friction influencing factors affect the punch force signature in ways that are distinct from wear.

4.3.1 Comparisons experimental setup

The initial experimental deep drawing trials were conducted using the semi-industrial channel forming process (Section 3.3.1). The punch force data collected for these trials highlighted punch force signature changes due to variation in lubrication regime, blank holder force variation, and distinct increases in galling wear severity on the tooling.

In order to collect data for the wear comparison, an extended series of 1850 channel parts were formed using the A09-A10 die set until severe galling wear was observed on both the formed channel parts and die corner radius inserts. Lubrication was kept constant according to the default application and type as described in Section 3.3.1, i.e. automated roller applied anti-corrosive mill oil. Two series of parts from the extended trial at distinct levels of galling wear were isolated. The first series consisting of 50 parts collected from the beginning of the trial, representing no-wear, and the second series consisting of parts from the end of the trial, representing severe die wear.

In order to compare the base case punch force signatures to other friction conditions a series of channel forming trials were conducted under different lubrication and BHF regimes. Five distinct lubrication trials and one altered BHF trial were

conducted, details of these trials can be seen in Table 4.2. The other friction condition trials were conducted utilising the PVD die corner radius inserts. The PVD dies prevented the onset of wear and removed wear as a variable for the other friction condition trials. The different lubrication conditions included mill oil, unlubricated, a high performance drawing lubricant, a base mineral oil, and an experimental ionic liquid lubricant (IL) consisting of 3% by weight ionic liquid additive compound in base mineral oil (Somers et al., 2013). BHF was maintained at an average of 28kN for the trials, where lubrication was altered. The final trial of the other friction conditions comparison reduced the BHF, with channel parts formed with an average blank holder force of 17.5kN. This trial was conducted using standard lubrication conditions outlined in Section 3.3.1.

Two types of blank materials have been used in the comparison trials. For the wear comparison using the A09-A10 die set a HSLA400 blank material has been used, trade name Xtraform 400. For the other friction conditions comparison using the PVD die set a HSLA300 blank material has been used, trade name Xtraform 300.

Table 4.2: Lubricant and wear comparison set experimental details.

Wear comparison						
Lubricant	**Average BHF**	**Wear level**	**Number of parts**	**Die insert material**	**Die corner radius**	**Blank material**
Mill oil	28 kN	No-wear	50	Polished D2 tool steel	7.5 mm	HLSA400
Mill oil	28 kN	Severe wear	50	Polished D2 tool steel	7.5 mm	HLSA400
Other friction conditions comparison						
Lubricant	**Average BHF**	**Wear level**	**Number of parts**	**Die insert material**	**Die corner radius**	**Blank material**
Mill oil	28 kN	No-wear	50	PVD	5 mm	HLSA300
Unlubricated	28 kN	No-wear	50	PVD	5 mm	HLSA300
Drawing lubricant	28 kN	No-wear	15	PVD	5 mm	HLSA300
Ionic liquid	28 kN	No-wear	15	PVD	5 mm	HLSA300
Mineral oil	28 kN	No-wear	15	PVD	5 mm	HLSA300
Mill oil	17.5 kN	No-wear	50	PVD	5 mm	HLSA300

Punch force signatures were recorded for each part formed in the trials outlined in Table 4.2 and the variation in punch force signatures shape within and between the comparisons were analysed. PCA has been used to analyse the punch force signatures of each comparison. This analysis provides a representation of the dominant signature variation types in the form of Principal Components (PCs). The PCs represent the dominate axis along which the signature shapes vary in the higher dimensional space. These axes are defined by the variables measured in each collected example of the data set, which in this case is the punch force level at each punch displacement step in the signature.

The form of punch force signature shape change that each PC represents can be visualised by plotting positive and negative example curves with the mean punch force signature of the data set, these example curves are determined using equations (3) and (4):

$$PC_i\ positive\ example\ curve = P^{(i)} b_{i,max} + \bar{X} \quad (3)$$

$$PC_i\ negative\ example\ curve = P^{(i)} b_{i,min} + \bar{X} \quad (4)$$

Where $P^{(i)}$ represents the PCA $\boldsymbol{P}$ matrix (discussed in Section 3.6.1) with all PC vectors except the one of interest are set to zero. $b_{i,max}$ and $b_{i,min}$ represent the maximum and minimum b-values for PC_i. By using both the maximum and minimum b-values it is possible to gain an understanding of the signature shape variation that the PC of interest describes, and the extent of that variation in the data set. Each signature has a series of b-values that correspond to each of the PCs isolated using PCA. Through assessment of b-values of parts formed under different conditions, it is possible to determine changes in punch force signatures that can be linked to that condition change. Enabling for the isolation of information in the punch force signature that allows for tracking changes in tooling wear and other influencing factors.

4.3.2 Wear comparison

The mean punch force signatures of the two conditions in the wear comparison are seen in Figure 4.2. A distinct difference in the magnitude of the mean signatures is

immediately apparent, with the severe wear mean signature larger in punch force magnitude. This initial result suggests that die wear can have a significant effect on punch force signatures.

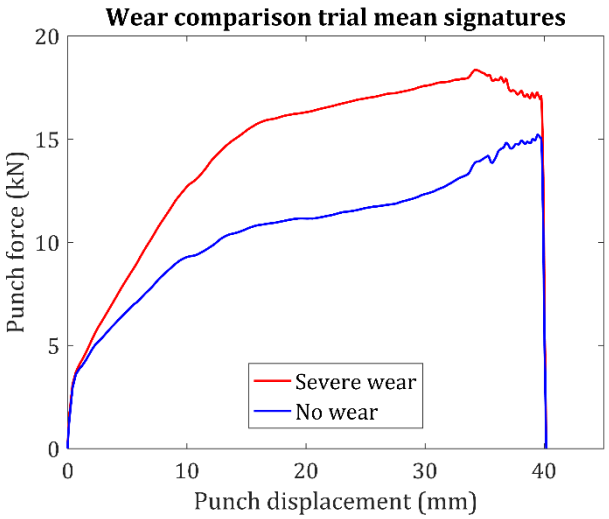

Figure 4.2: Wear comparison trial mean punch force signatures.

The wear comparison trials were assessed using PCA, where $\bar{X}$ was calculated using the A09-A10 base case signatures only. The first four dominant PCs are shown in Figure 4.3. The percentage of explained variation of each of the first four dominant PCs is listed in Table 4.3.

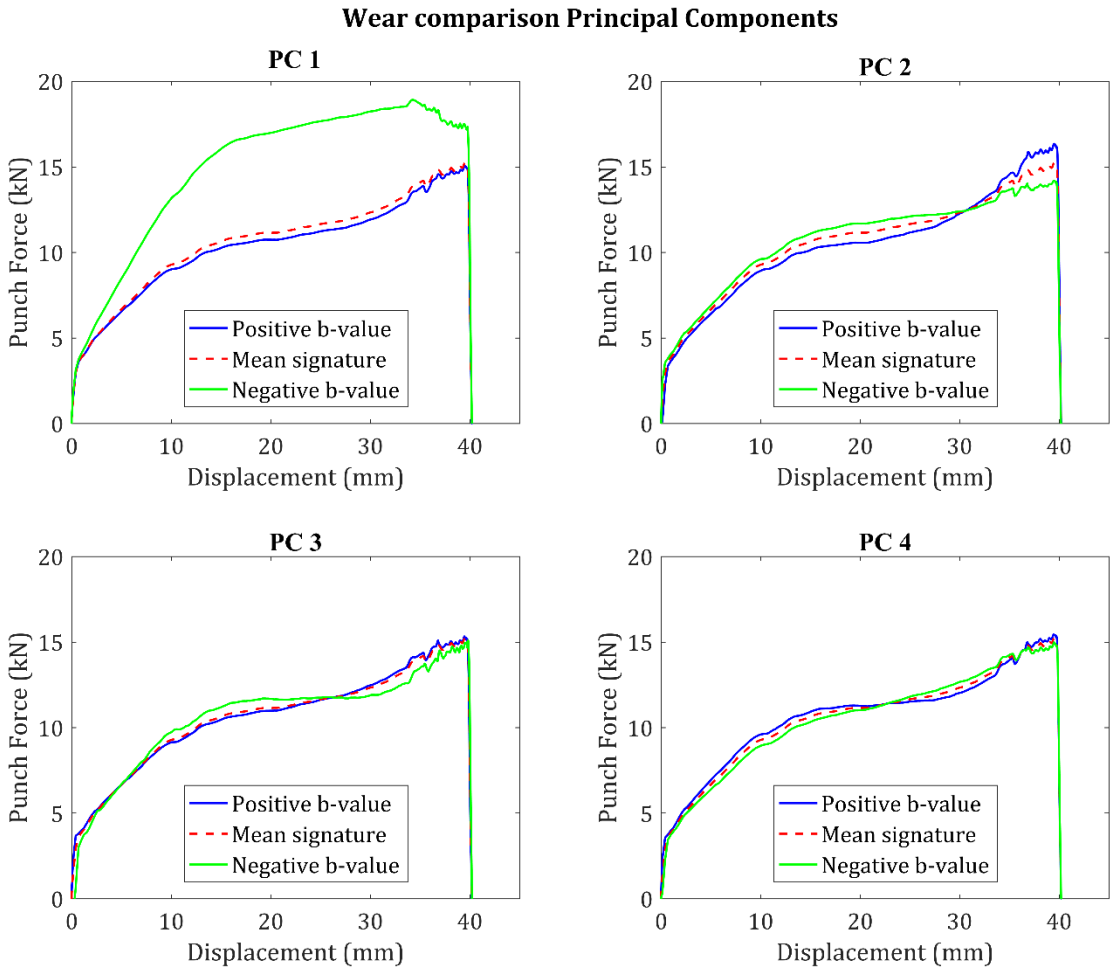

Figure 4.3: Wear comparison dominant Principal Component representations.

Table 4.3: Wear comparison set Principal Component percentage of explained variation.

Principal Component	Percentage of explained variation
1	97.84%
2	1.20%
3	0.52%
4	0.48%
Total	99.76%

PC1 appears to describe variation in the overall magnitude of the signature, and accounts for 97.84% of the explained variation in the data set. In addition to magnitude, this PC also captures variation in the slope of punch force progression for the last 5 mm of punch displacement. The features of this PC match the distinct difference in magnitude apparent between the mean signatures shown in Figure 4.2, which indicates that this PC will allow for distinction between the no wear and

severe wear signatures. PC2 appears to describe variation in the progression of punch force over the entire stroke, with positive and in particular late stroke progress between a displacement of 30-40 mm, PC2 accounts for 1.2% of the explained variation. PC3 appears to describe slight variation in progression of punch force, with positive and negative b-values representing steady progression or plateauing between displacement 15-30 mm respectively. PC4 appears to describe similar features as PC3, collectively PC3 and PC4 account for 1% of the explained variation in the data set. The b-values for the first four PCs were calculated, according to Equation (2), for each signature in of the wear comparison. The b-values that correspond to Principal Components 1-4 (Figure 4.3) are represented in Figure 4.4, in box plots. By comparing the mean and distribution of the b-values for each trial in each of the PCs it is possible to gain an understanding of how each PC relates to a change in conditions.

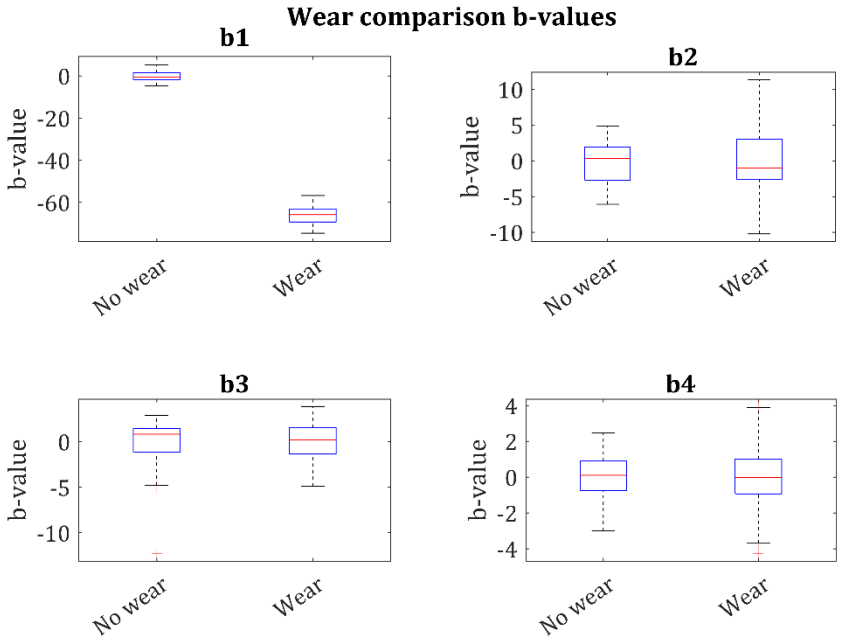

Figure 4.4: Wear comparison trial b-value box plots.

The b1 values show some strong grouping of the individual conditions, and demonstrate that PC1 allows for clear distinction between the no wear and severe conditions. The b2 values do not appear to show any obvious separation for the individual trials, however the spread of b-values in the severe wear trial is

noticeable more than it is for the no-wear trial. The b3 and b4 values do not appear to show any obvious separation or trends for the individual trials.

4.3.3 Other friction conditions comparison

The mean punch force signatures of the friction condition trials are seen in Figure 4.5. As it was seen with the wear comparison, each of the condition mean signatures are distinct. Initial examination of different lubricant mean punch force signatures showed similar generic signature shapes for all trials with varying overall signature magnitudes, with the exception of the unlubricated trial. The unlubricated mean signature reached a relatively stable signature plateau while the other trials displayed distinct increase in force at the end of the stroke. This late stroke increase was also observed in the wear comparison base case mean signature. The late stroke increase was not observed for the lower BHF trial.

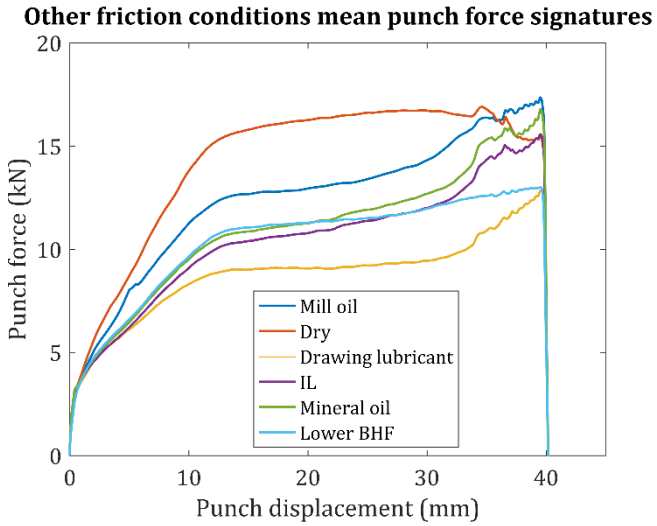

Figure 4.5: Other friction conditions comparison trials mean punch force signatures.

The other friction condition trials punch force signatures were compiled into a single data set and assessed using PCA, with $\bar{X}$ calculated using the PVD base case signatures only. The first four dominant PCs are shown in Figure 4.6. The percentage of explained variation of each of the first four dominant PCs are listed in Table 4.4. The first PC for the other friction conditions comparison accounts for 84.21% of the explained variation, with the second accounting for 14.00%, and together

accounting for 98.21% of the explained variation in the data set. PC1 appears to describe variation in the overall magnitude of the signature. With a positive b-value representing larger magnitude than the mean signature and a negative b-value representing lower than the mean signature. PC2 appears to describe the slope of the signature plateau, with a positive b-value representing an increasing trend in the signature over the stroke, and a negative b-value representing a decreasing trend. PC3 describes slight variation in the slope of punch force progression alternating at 'pivot' points found at 7 mm and 28 mm of punch displacement. PC4 also describes slight variation in the punch force progression alternating at pivot points found at 21 mm and 37 mm punch displacement. PCs 3 and 4 together account for 1.32% of explained variation in the data set.

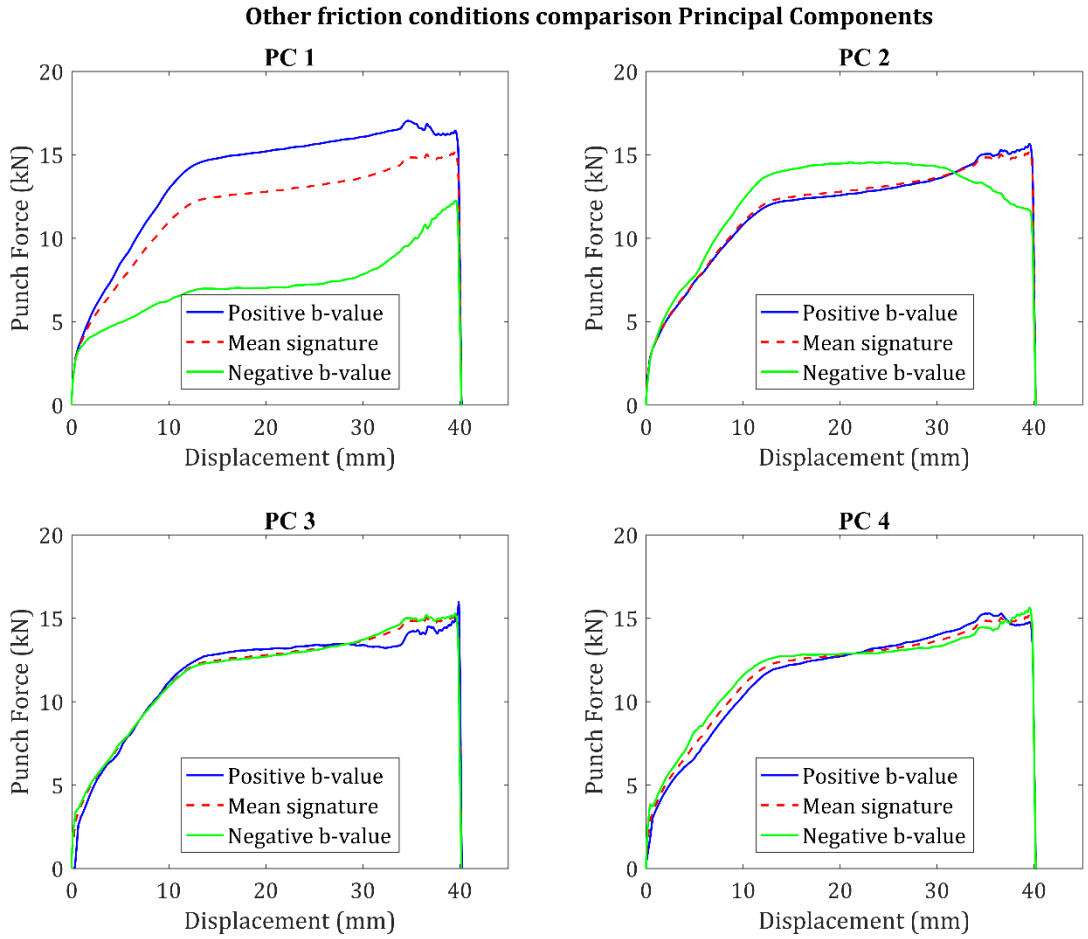

Figure 4.6: Other friction conditions comparison dominant Principal Component representations.

Table 4.4: Lubrication comparison set of Principal Component percentage of explained variation.

Principal Component	Percentage of explained variation
1	84.21%
2	14.00%
3	1.03%
4	0.29%
Total	99.54%

The b-values for the first four PCs were calculated, according to Equation (2), for each signature in the friction conditions comparison. The b-values that correspond to PCs 1-4 (Figure 4.6) are shown in Figure 4.7, as box plots.

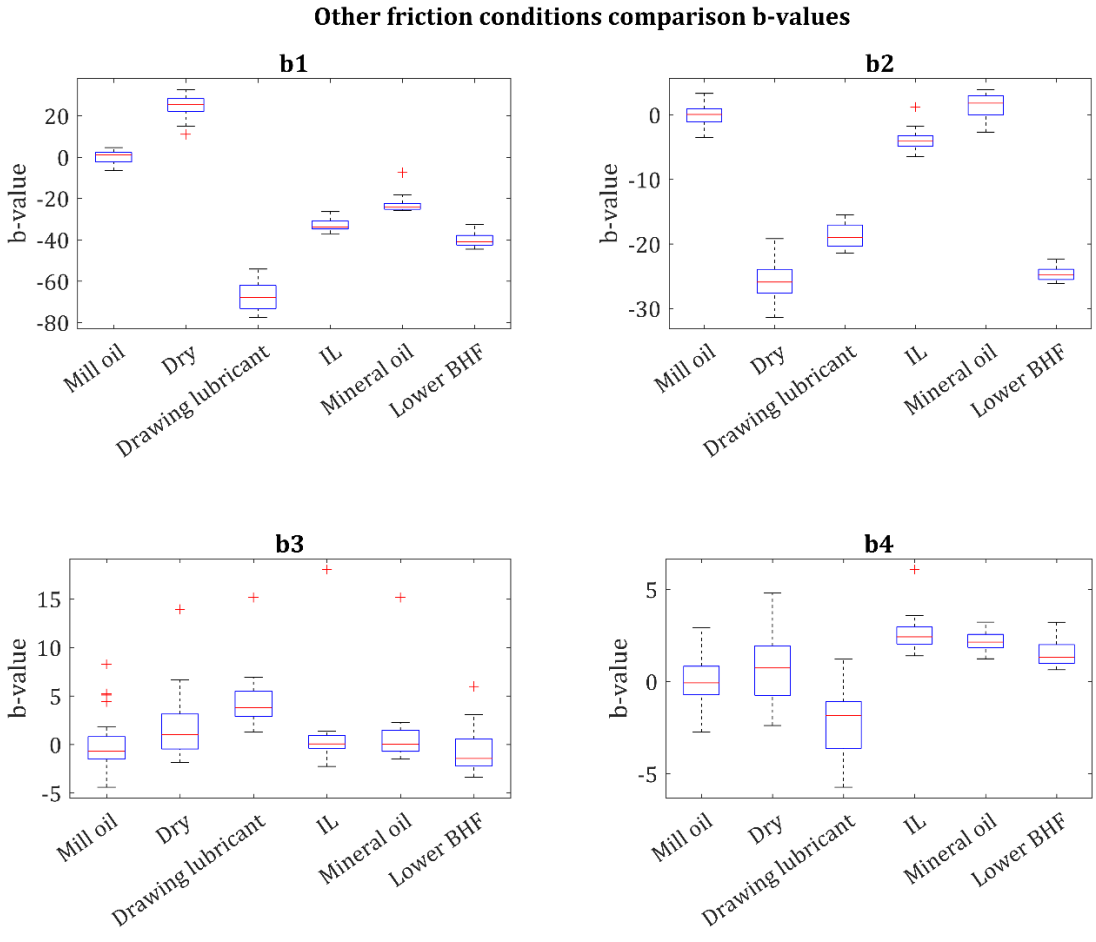

Figure 4.7: Other friction conditions comparison b-values.

The b1 and b2 values show some strong grouping and separation between individual trials within the data set. The b3 values do not appear to show any distinct differences in means or distribution between trials. There are positive outliers for each of the trials, these outliers correspond to the first signature of each trial, and the b-value can be explained by the slightly extended period of time over which the initial stroke is performed. This extension of loading increases the punch force at maximum punch travel. The increased force in the last period of punch travel is described by PC3 and the corresponding b-values. The b4 values show a noticeable difference in the mean values for the mineral oil, IL, and low BHF trials from unlubricated and the base case mill oil.

4.4 Wear and friction condition comparisons discussion

The distinct difference in median b1 values of the no wear and severe wear trials and increased range observed in the b2 values of the severe wear trial indicate that wear effects the punch force signature in a significant and measurable way. These results provide justification for further investigation of punch force based prediction of die wear progression. However, in order to accurately quantify galling wear severity for comparison to punch force signature features a targeted measure of galling wear severity is required, as was highlighted in the Section 2.4.

The PCA results of the other friction condition trials also prompt further investigation regarding the similarity of PC shapes from this comparison to those PC shapes isolated from the wear comparison. This similarity of general PC shapes prompts the question of whether changes in other friction influencing factors can be distinguished from wear development using punch force analysis.

Direct comparison of the b-values of PCs for the two comparison data sets cannot be made due to the difference between base case mean signatures. However, in general terms the PCs of the two data sets appear to capture similar variation in the shape of the punch force signature. The similarity of the dominant PCs for the two comparison sets indicate that there are no specific forms of punch force signature shape variation that are driven by any individual influencing factor that has been

assessed. However, the different response of b-value separation and distribution seen in the two comparison data sets could be used to characterise influencing factors.

PC1 for both comparisons allows for distinguishing between trials, and in both comparisons generally describes the magnitude of the signature. As discussed in Section 2.3, punch force is directly related to friction, and so variation in the magnitude of the signature captured by PC1 in the comparison could be considered as an indicator of overall friction for the individual stroke. Different lubrication regimes and BHFs will result in different coefficients of friction, and so should drive variation in the magnitude of the punch force. Similarly, an increase in wear on the press tooling will also increase friction, explaining the clear divisions between trials for this PC.

PC2 allows for distinguishing between other friction condition trials in the comparison based on mean b-values and shows a clear distinction between the lower BHF trial and the mineral oil and IL trials, that was not seen with PC1. This PC appears to describe the slope or change in the punch force progression over the stroke, which could be considered an indicator of dynamic friction changes over the course of the stroke. As press acceleration profile and other press variables are kept essentially constant from part to part, the dynamic friction changes are likely to be the result of changes in lubrication or wear conditions over the course of the stroke. The wear comparison b-values for PC2 are spread far more than the no-wear b-values, suggesting that the presence of die wear is driving some variation in dynamic friction. Also noteworthy in the comparison of other friction conditions PC2 b-values is the distinction between the unlubricated, drawing lubricant and lower BHF trial and the remaining trials. These three trials displayed negative median b-values as opposed to the other fluid lubricants, indicating that these regimes have distinct and characteristic dynamic friction conditions. With the negative b-values indicating the unlubricated, drawing lubricant, and lower BHF having more stable dynamic friction conditions than the mill oil, mineral oil, and IL trials.

The PC3s and PC4s in both the comparisons describe variation in the progression of the punch force progression and localised slopes of the signature plateau. Again, both of these PCs are similar between the two comparisons, with the crossing locations of positive and negative b-value signature examples crossing at the same

locations in both comparisons. However, PC3 and PC4 do not appear to describe variation that allows for discrimination between the no wear and severe wear trials. The range of b4 values for the IL, Mineral oil, and lower BHF trials all have positive median values that separate the trials from the mill oil, unlubricated and drawing lubricant trials. The negative b-values for PC4 generally indicate lower initial punch force in the signature followed by a higher than base case force in the latter half of the stroke. This could indicate initial low friction performance of the IL and mineral oil followed by a late stroke increase in friction due to breakdown of those lubricants.

Comparison of the mean signatures and b2 values of the base case and lower BHF indicate that the lower BHF produced much more consistent punch force over the course of the stroke. These signatures were lower in overall magnitude as well and demonstrated more consistent punch force progression towards the end of the stroke. When testing a series of lubricants under different blank holder force Kim, Altan & Yan (2009) found a slight increase in the maximum punch force measured under higher blank holder force, but also observed fractures with most tested lubricants at higher blank holder force. This suggests higher and unstable frictional conditions and supports the observations made here. Hedrick (2010) also discussed the unstable frictional effects of increasing BHF. This suggests that for these experimental conditions BHF of 17.5kN provided more stable friction conditions than the base case BHF of 28kN.

4.5 Summary

The initial trials conducted in this Chapter found that the punch force signature varies significantly with wear, and PCA effectively captures this variation. This result supports further investigation of the effects of wear progression on the punch force signature.

A series of common forms of punch force signature shape variation were isolated for different comparisons data sets, including variation of lubrication, BHF, and wear. The results of the PCA indicated that there is no individual form of punch force signature variation that is exclusively linked to wear, as opposed to the other friction

influencing factors tested. However, the severe wear trial b1 and b2 values behave distinctly from the no wear trial, and other friction conditions given the PCs of both comparisons describe the same general changes in signature shape. This indicates that tracking the progression of multiple PC b-values may be necessary in order to monitor for specific wear related events.

Two important forms of punch force signature variation captured in all the data sets accessed in this Chapter describe the overall signature magnitude and variation in the slope of the signature plateau respectively. Both of these appear to be linked to the state of friction. From the results of the two comparisons it is possible to state with reasonable certainty that the overall magnitude form of punch force shape variation is related to the overall level of friction in the stamping system. This appears to hold regardless if the friction coefficient is changed by variation in lubrication, BHF, or changes in the amount of wear on the dies. There is less certainty about the form of punch force signature shape variation that describes the slope of the signature plateau or the progression of force during the stroke. However, given the increase or decrease in force, the form of shape variation could be linked to dynamic friction changes over the course of the stroke. This form of signature shape variation enables the distinction between many of the lubricants trialled in the lubrication comparison, and the different BHF levels. It was also found that the spread of b-values for this form of shape variation was significantly more for the severe wear trial than the no-wear trial in section 4.3.2. The effect of this form of shape variation, and specifically the effects of dynamic friction changes on punch force signatures, and how these relate to wear progression will be investigated in Chapter 7.

CHAPTER FIVE

Galling wear severity quantification

5.1 Introduction

In Section 2.4 the need for a targeted accurate and repeatable measure of galling wear severity was identified. The measurement and characterisation of galling wear in real deep drawing situations is a crucial component in the development and implementation of accurate real time wear monitoring systems. Current and past techniques and parameters that have been used for quantifying and characterising galling wear (Section 2.4) are often not targeted at the localised features that contribute to and are caused by galling wear. The current standard for assessing galling wear severity, namely visual assessment, does not provide quantifiable and repeatable results. Furthermore, these techniques discussed in Section 2.4 are not well suited for implementation in large scale industrial style stamping wear trials that are necessary for developing wear monitoring systems.

In this Chapter a new technique for quantifying galling wear severity is introduced. The new technique uses 2D profilometry measurement of the surface and wavelet transformation to analyse the resulting surface information. Wavelet transformation allows for the isolation of a wavelength bandwidth that effectively characterises the localised galling wear features in 2D surface profiles.

The outcome of this chapter is to provide an accurate quantifiable measure of galling wear severity that can be used for verification of tool wear monitoring techniques. The new technique is performed via measurement of the workpiece (i.e. part) surfaces and not the tool surfaces, and is therefore appropriate for application in both laboratory-based experiments and industrial style wear trials. Industrial style wear trials will be utilised throughout this thesis and this new measure will play an

important role in developing an understanding of the relationship between punch force signatures and galling wear.

The major findings and methodology to be presented in this chapter have been published in the peer-reviewed journal, *Wear* (Voss et al., 2017).

5.2 Galling wear features

Sliding abrasive wear damage produces typical cross-sectional profiles as shown by Varjoranta et al. (1981) and Yost (1983). These typical cross-sections are characterised by shoulders of raised material pile-up on either side of the depression gouge which drops below the bulk material of the surface, seen in Figure 5.1. The surface features seen with galling damage exhibit similar cross-sectional features in an intensified state, larger material pile up and greater depth of gouges (Karlsson et al., 2012). The shallow depth of abrasive damage preceding galling damage in SMF can often be on the same scale as bulk material asperities, which can make characterisation using 2D profilometry difficult (Gåård et al., 2009). Calculating an aggregate profile by taking the mean of multiple adjacent 2D profiles can assist with minimising the asperity noise ratio when attempting to isolate these galling related features. It is evident that all of the galling features mentioned above share the characteristic of sudden changes in height above and below the level of the bulk material. This characteristic can be captured well by aggregate 2D surface profiles perpendicular to the sliding direction and may be utilised for possible galling wear identification and quantification.

Siefert and Babu (2014) numerically described galling damage and a number of other damage stages for ASTM G98 tests in terms of R_y values for profiles collected perpendicular to sliding direction. R_y value being the maximum peak to valley distance for the sampled region of the 2D surface roughness profile. The damage types characterised correspond well with the stages of damage observed for the galling wear mechanism in SMF. The damage types 'Wear', 'Incipient galling', 'Transition to galling' match the initial asperity deformation and degrees of abrasion observed in SMF prior to galling. The 'Wear' stage was visible but not quantifiable with laser microscopy on the test material, Everit 50 alloy. The 'Incipient galling'

damage stage, was described to be at the scale of existing surface asperities, with features being less than 1 μm in size for the test material. The 'Transition to galling' stage was classified as features exceeding ½ R_y, or $> 2\mu m$ and $\leq 5\mu m$ in size for the test material. Finally, galling damage was classified as features greatly exceeding ½ R_y by at least an order of magnitude, or $\geq 10\mu m$ in size for the test material. Cross-sections of the damage stages exhibit the 'U' shaped gouge with raised shoulders that has been previously described, with the significant difference between the stages being scaled. Seifert and Babu's (2014) observations provide a numerical description of the difference between galling and abrasion damage that is typically observed in SMF as a precursor to galling damage.

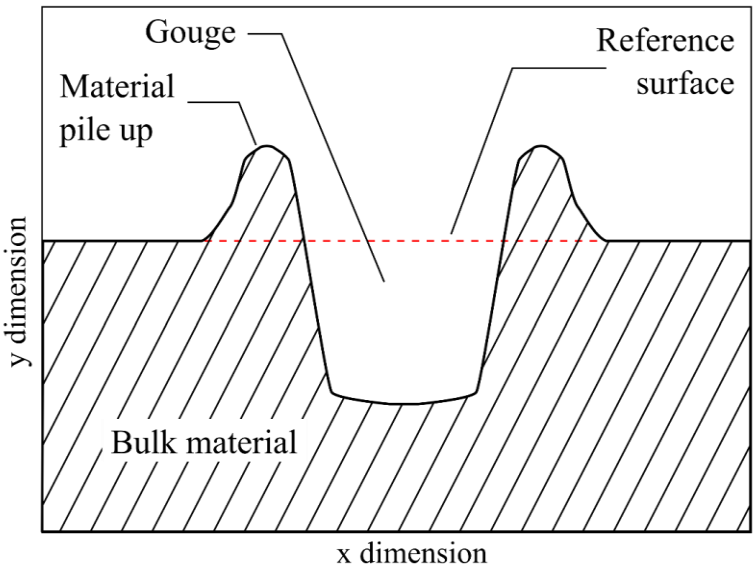

Figure 5.1: Typical simplified cross section of scratch gouge, characterised by the material pile-up either side of the gouge void in the surface.

5.3 Surface characterisation using frequency analysis

Engineering surfaces can be characterised by different spatial frequency or wavelength bandwidths. This form of surface characterisation is most evident with the common practice in surface metrology of using wavelength bandwidths to separate surface roughness, waviness, and form (Raja et al., 2002).

Characterising galling wear features in terms of spatial frequency allows for a targeted measure of galling wear severity. Wavelet Transform is a signal analysis technique that decomposes signals with localised wave-like functions, which represents signals in both the frequency domain and the spatial domain simultaneously and, as such, provides a good representation of localised signal features (Mallat, 2009). Wavelet Transform has been used extensively to analyse and process 2D roughness profiles, specifically for the detection of discontinuities in surfaces (Dutta et al., 2016; Fu et al., 2001; Josso et al., 2002; Lee et al., 1998; Lingadurai and Shunmugam, 2006; Papagiannakis et al., 2007; Rackov et al., 2000; Wei et al., 2005). However, Wavelet Transform has not yet been used for the characterisation and measurement of wear.

There are several wavelet functions or mother wavelets (denoted by $\psi(x)$) available for use in Wavelet Transform. A number of example wavelet functions can be seen in Figure 5.2. Numerous mother wavelet functions exist, and some are likely to be better suited for galling wear characterisation than others, this will be discussed further in Section 5.4.2.

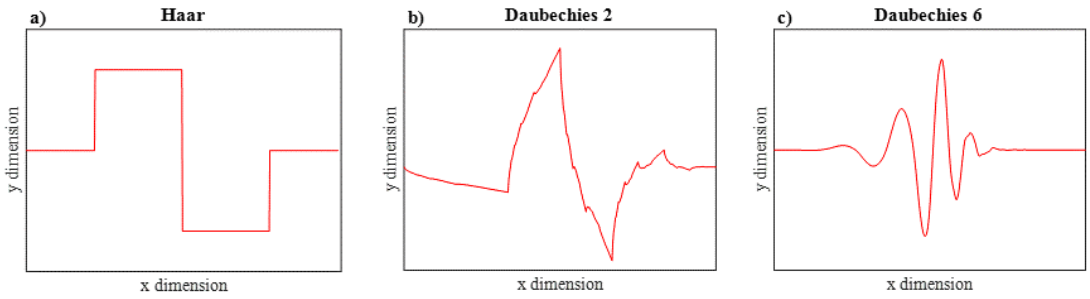

Figure 5.2: Example mother wavelet functions a) Haar wavelet, b) Daubechies 2, c) Daubechies 6.

The Discrete Wavelet Transform (DWT) is a common implementation of Wavelet Transform for practical applications using discrete data (Burrus et al., 1998). DWT decomposes a signal $f(x)$, where $-\infty \leq x \leq \infty$, by translating scaled copies of the mother wavelet, $\psi_{j,k}(x)$, across the signal and performing a convolution operation at each discrete translation step. Figure 5.3 shows the scaling and translation operations on the Daubechies 2 mother wavelet function. The wavelet base is defined as:

$$\psi_{j,k}(x) = 2^{j/2}\psi(2^j x - k) \tag{5}$$

Where j and k are integers, denoting the frequency or scale and space location or translation, respectively. The wavelet scaling function, $\phi_{j,k}(x)$, is defined as:

$$\phi_{j,k}(x) = 2^{j/2}\phi(2^j x - k) \tag{6}$$

In DWT the signal is broken-down into low pass approximation coefficients $c_j(k)$ and high pass detail coefficients $d_j(k)$, such that the wavelet expression of the signal is:

$$f(x) = \sum_k c_j(k) 2^{j/2}\, \phi(2^j x - k) + \sum_k d_j(k) 2^{j/2}\, \psi(2^j x - k) \tag{7}$$

Practically these coefficients can be determined using:

$$c_j(k) = \sum_k h(n)\, c_{j,k}(2k + n) \tag{8}$$

$$d_j(k) = \sum_k h_1(n)\, c_{j,k}\,(2k + n) \tag{9}$$

With $h(n)$ and $h_1(n)$ denoting quadrature mirror filters, a low and high-pass filter pair, where n is an integer in the sequence of discrete points of the input signal. The coefficients represent the level of correlation between the wavelet bases and the signal at each translation step. The approximation coefficients provide the low frequency component of the input signal and the detail coefficients capture the high frequency component.

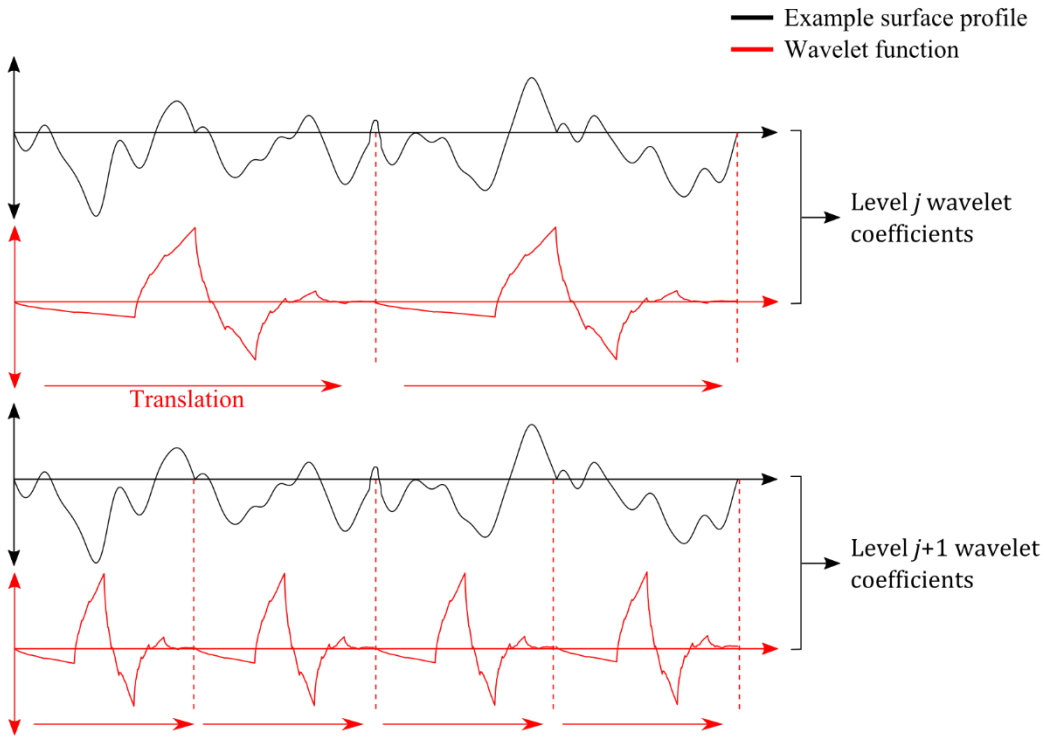

Figure 5.3: Schematic explanation of the Discrete Wavelet Transform operation, where the mother wavelet function is scaled and translated relative to the surface profile in order to calculate wavelet coefficients.

The multi-level decomposition DWT (Mallat, 1989) iteratively applies Equation (8) and Equation (9) on the current approximation coefficients (Figure 5.4). At each level the wavelet function is scaled to provide coefficients that represent different wavelet frequency bandwidths.

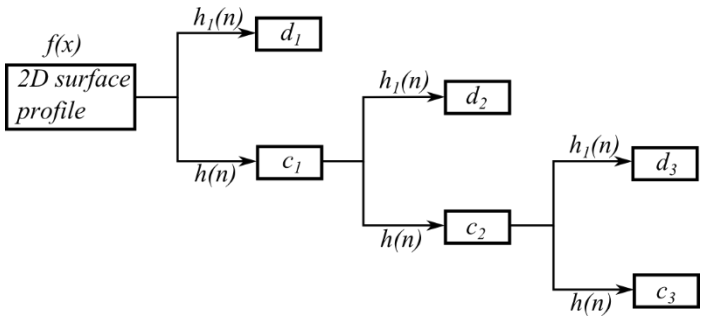

Figure 5.4: Multi-level DWT decomposition diagram, at each level detail and approximation coefficients are calculated and the decomposition is repeated on the approximation coefficients.

In sliding wear conditions it has been shown that the abrasive damage preceding galling can be of similar depth as the existing surface asperities or roughness (Gåård et al., 2009). From this it has been inferred that wear features will be active in the

same high frequency component of a surface profile as roughness. By assessing detail coefficients from different levels of the multi-level DWT, it will be possible to isolate specific bandwidths that best characterise galling wear features.

5.4 Discrete Wavelet Transform methodology

5.4.1 Surface profile collection

The new Discrete Wavelet Transform method requires the collection of 2D surface profiles perpendicular to the sliding direction, or the direction of galling wear features. These profiles must capture the cross-section of the galling wear gouge tracks (see Figure 5.5). Transfer of material that leaves debris adhered to the wear surface or adhesive tear-out scars are two other wear features that are observed on galled formed part surfaces (Gåård et al., 2008). These features are localised in both sliding and perpendicular to sliding directions and so are difficult to capture with individual 2D profiles. Therefore, they will not be targeted in the presented methodology.

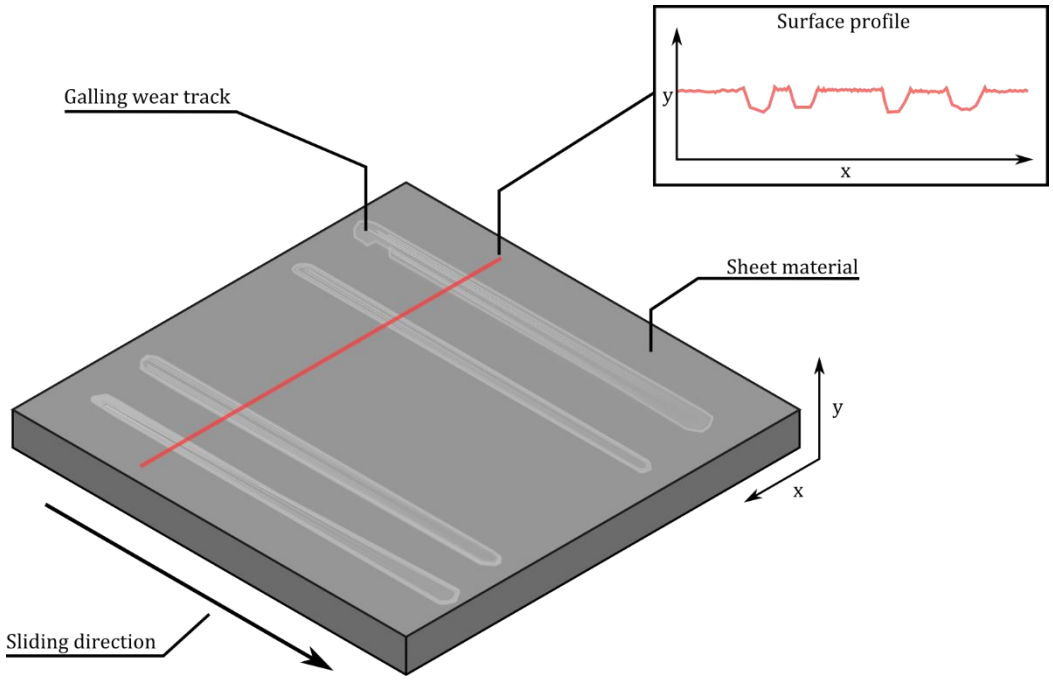

Figure 5.5: 2D surface profile collection schematic. The 2D profile is collected perpendicular to the sliding direction of the formed part in order to capture the cross section of any galling wear gouges.

5.4.2 Mother wavelet selection

There are numerous mother wavelet functions available with Discrete Wavelet Transform decomposition, and each of these will provide varying results. Selecting an appropriate mother wavelet that matches the signal or galling wear feature is crucial for effectively characterising galling wear. Qualitative comparison between the signal and mother wavelet is a common method for selection in other applications such as power quality assessment and medical Electromyograms (Ngui et al., 2013). In these cases, the shape of the mother wavelet is compared visually to the feature of interest in the respective signals. Example mother wavelet functions of the Daubechies wavelet family and the Haar wavelet can be seen in Figure 5.2. Visual comparison is simple in cases where the morphology of target features are known, as is the case here with the galling wear features highlighted in Figure 5.1.

For assessing galling, the shape of the selected wavelet function must resemble the increase and sudden drop in the 2D profile that occurs due to material pile-up on the edges of the gouge, as shown in Figure 5.6a. The Daubechies 2 mother wavelet represents a close approximation of these features. A large positive pulse immediately followed by a negative pulse corresponds well with the material build-up next to the wear gouge, as shown in Figure 5.6b. Because of these attributes the Daubechies 2 wavelet has been selected for the analysis of galling wear and preceding damage in this study. However, other galling wear features such as adhered material or adhesive pull-out scars may require selection of different mother wavelet functions for accurate measurement.

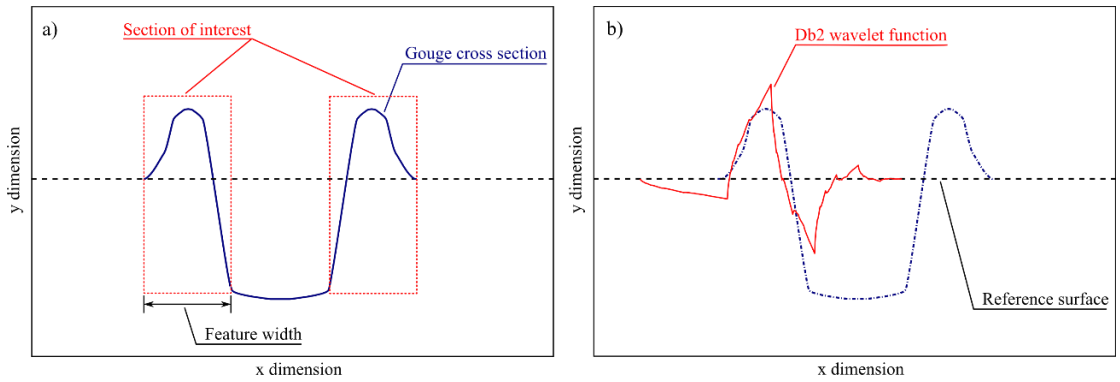

Figure 5.6: a) 2D profile galling wear cross section features. b) Selecting an appropriate mother wavelet function for galling wear feature of interest.

In cases where the feature morphology of the target wear damage is not well known, a quantitative technique for the selection of mother wavelet function may be required. For example, quantitative selection methods may be appropriate when attempting to quantify other forms of wear damage or wear in other applications. Minimum Description Length (MDL) criterion (Saito, 1994) is a quantitative technique that is commonly used in noise suppression and signal compression applications (Ngui et al., 2013), and will be highlighted as a quantitative alternative to visual comparison. The MDL criterion assumes that the 'best' wavelet function for describing a signal is given by the model that provides the most compact description of the data of interest. In situations where the morphology of the wear is not known, it is possible that application of MDL criterion with a range of mother wavelet function to a sample 2D profile of the wear feature of interest could assist with selection.

MDL criteria of a wavelet decomposition of the 2D surface profiles of galling wear regions has been calculated using equation (10) (Hamid and Kawasaki, 2002).

$$MDL(k,n) = min\left\{\frac{3}{2}\, k \log N + \frac{N}{2}\log\left\|\tilde{\alpha}_n - \alpha_{\boldsymbol{n}}^{(k)}\right\|^2\right\}, 0 \le k \le N \qquad (10)$$

Where N represents the number of wavelet coefficients or length of the decomposed signal, n is the wavelet filter, $\tilde{\alpha}_n$ represents the wavelet decomposition coefficients of the 2D surface profile determined using wavelet filter n, and $\alpha_{\boldsymbol{n}}^{(k)} = \Theta^{(k)}\tilde{\alpha}_n$ where $\Theta^{(k)}$ represents a hard-thresholding operation such that the k largest values of the vector $\tilde{\alpha}_n$ are maintained as absolute values and the remaining values are set to zero. The number of retained coefficients k where MDL reaches its minimum is deemed the optimal value. This process is repeated for different wavelet filters, n, utilising different mother wavelet functions in order to determine which mother wavelet provides the minimum MDL value for the tested 2D surface profile.

In order to compare the selection using MDL and visual comparison MDL values were determined for a series of test 2D surface profile of galling track regions. A series of wavelet functions available from the MATLAB wavelet toolbox were assessed with the series of test 2D surface profiles and the MDL criteria values were

determined, Table 5.1 shows the 5 'best' mother wavelets for each of the test profiles. These test profiles (label using the notation: die name – part number) exhibited a range of quantities and severities of galling wear damage on different materials in order to provide a representative sample for demonstrative purposes.

Table 5.1: Minimum Description Length values for test surface profiles of galling wear damage regions. See Appendix A for full wavelet names and functions.

Rank	Galling feature profile regions MDL results for various mother wavelets									
	#31 - 4200		#31 - 4600		#30 - 400		#30 – 1600		7 - 14	
1	***Haar***	489.98	***Haar***	374.59	***Haar***	573.95	***Haar***	418.22	***Haar***	517.54
2	***bior3.1***	551.23	***bior3.1***	426.83	***bior3.1***	584.63	***bior3.1***	436.22	***rbio3.1***	523.14
3	***db2***	587.19	***db2***	450.49	***db2***	631.12	***fk4***	495.83	***db2***	528.96
4	***fk4***	613.52	***fk4***	453.18	***fk4***	651.47	***db2***	496.85	***rbio2.2***	535.17
5	***rbio3.1***	618.14	***rbio3.1***	472.17	***bior2.2***	664.94	***rbio3.1***	524.40	***rbio1.3***	537.70

The Daubechies 2 wavelet, which was selected based on visual comparison, ranks highly based on the MDL criteria for all the test 2D surface profiles of galling wear regions. However, based on the criteria, the Haar and Biorthogonal 3.1 wavelets both rank higher for the majority of the test cases. As shown in figure 4.2a, the Haar wavelet is a square shaped wavelet, and the Biorthogonal 3.1 wavelet is a complex function with numerous pulses. MDL criterion is based on efficiency of encoding the data, so even if a model or wavelet may match the data more accurately, it may not be as efficient in encoding as other functions and so will be ranked lower by MDL criterion. The demonstrated application of MDL criterion shows that it is a viable alternative for mother wavelet function selection in cases where morphology of the targeted wear damage is unknown. However, given the knowledge of the targeted galling wear features in 2D surface profiles, visual assessment will be used for mother wavelet function selection in this work.

5.4.3 Selection of detail coefficient level

In order to quantify the severity of galling wear a detail level must be selected that has a wavelet frequency bandwidth that corresponds to the scale of the wear damage features. This can be achieved by examining example features from the

relevant data set and by noting the scale and width at which those features exist, as shown for the example gouge cross-section in Figure 5.6a.

Once the width of the wear features has been determined, the appropriate detail coefficient level must be selected. The detail coefficient level wavelength bandwidths can be determined as a function of the sampling frequency f_s of the acquired surface profiles. Table 5.2 shows wavelet wavelength bandwidths of detail coefficients for a 6-level decomposition as a function of sampling frequency, and bandwidths for a sampling frequency of 1766 samples/mm. This sampling frequency and the detail coefficient level selection for this case study will be described in Section 5.5.3.

Table 5.2: Discrete Wavelet Transform decomposition detail level wavelet frequency bandwidth ranges in terms of surface profile collection sampling frequency f_s.

Detail level	Wavelet wavelength bandwidth	Bandwidths for f_s
d_1	$2/f_s - 4/f_s$	1.13 – 2.27 µm
d_2	$4/f_s - 8/f_s$	2.27 – 4.53 µm
d_3	$8/f_s - 16/f_s$	4.53 – 9.06 µm
d_4	$16/f_s - 32/f_s$	9.06 – 18.12 µm
d_5	$32/f_s - 64/f_s$	18.12 – 36.24 µm
d_6	$64/f_s - 128/f_s$	36.24 – 72.48 µm

5.4.4 Detail coefficient calculation and wear severity quantification

Once the mother wavelet and the decomposition detail level are selected, the multi-level wavelet decomposition of the surface profile is completed and the specified detail coefficients determined according to Equation (8) and Equation (9). Large detail coefficient values indicate a high likelihood of a distinct wear feature of the corresponding scale. The detail coefficients also provide the relative location in the profile of the wear features.

In visual assessment the apparent severity of galling wear is in part related to the overall area of galling damage. As such, localised large coefficients do not necessarily indicate an immediate overall increase in severity of galling wear on the surface that

would be apparent using visual assessment. Rather, large coefficients indicate a high likelihood of distinct wear features, that may be important to note as transition points for galling progression.

5.4.5 DWT wear severity parameter

The raw detail coefficients provide information about the location and significance of galling wear features on the surface. However, it is difficult to gain an understanding of the relative overall severity of galling wear on the surface by assessing the raw detail coefficients. The detail coefficients can be processed to provide a single galling wear severity value by taking the mean of absolute values of the detail coefficients, Equation (11):

$$W_{DWT} = \frac{1}{N}\sqrt{\sum_{i=1}^{N} {d_j}^2} \tag{11}$$

Here N is the number of coefficients, and d_j are the detail coefficients of the selected level. The individual W_{DWT} values can be compared with values from the same mother wavelet function and wavelet frequency bandwidth, but cannot be directly compared to values determined under different DWT conditions.

This parameter results in the loss of spatial information, but provides a snapshot of the overall severity of galling wear damage through processing the detail coefficients. In order to minimise the dilution of large magnitude detail coefficients that will correspond to galling wear locations, the sum of the squares is performed. The parameter allows for easy comparison of relative galling wear severity between measured locations, and should be considered in conjunction with raw detail coefficients to provide a complete assessment of galling wear.

The closer a W_{DWT} value is to zero the less severe the measured galling wear damage, and larger values must be interpreted relative to other measurements in order to assess the severity of wear. Further work is required in order to develop typical values for different levels of galling severity on different materials. However,

when assessing detail coefficients collected at the same location on consecutively formed parts sudden increases in coefficient values at a location will indicate galling wear damage development.

5.5 Case study: Galling initiation

An important factor in measuring galling wear severity is registering initial phases of galling wear damage, as detecting these stages are crucial for preventing further galling progression. Registering these early stages of galling wear damage can be difficult because damage features can develop at the same scale as the base roughness of the surface, as was highlighted in section 5.2.

This case study has been conducted to demonstrate the DWT galling wear methodology application and accuracy in identifying galling initiation damage on channel parts. The results of the DWT galling wear methodology consists of two components, the detail coefficient values and the W_{DWT} parameter. This case study aimed to implement tests that assessed both of these components of the methodology. A series of channel parts were formed until galling wear was visually observed on the die corner inserts, and then the DWT methodology was applied to the parts. In order to assess the accuracy of the detail coefficients for characterising and locating galling wear damage, the coefficients were compared to images of the sidewall. The performance of the detail coefficients was assessed based on how well the detail coefficient activity aligned with visible features on the sidewall. The performance of the W_{DWT} parameter was assessed through comparison to visual assessment rankings and other surface roughness and texture parameters. These tests demonstrated that the DWT method provides a result that is less subjective and time consuming to collect than visual assessment, while maintaining the accuracy of visual assessment. The methodology also outperforms standard surface roughness and texture parameters based on comparison to visual assessment, while also providing additional insights in the form of localisation of galling wear initiation features through the assessment of detail coefficients.

5.5.1 Experimental method

A series of channel parts were formed using the laboratory stamping press (Section 3.3.3) until galling wear was visually observed on the dies and testing was ceased. This resulted in a total of 14 channel parts and the proposed DWT galling wear methodology was applied to 2D profile measurements of the part surfaces. Detail coefficients and the W_{DWT} parameter (see Equation (11)) for the parts were then compared to the sidewalls and visual assessment rankings respectively. Visual rankings are used as the reference measurement for the W_{DWT} parameter comparison because these are the current standard for evaluation and quantification of galling wear severity, as described in Section 2.4.1.

5.5.1.1 Surface characterisation

Three-dimensional surface scans were collected for each part sidewall using 3D focus-variation scanning microscopy (Alicona Infinite Focus), according to the process described in Section 3.5. The location of the 3D surface profilometry scans and the visual assessment region are shown in Figure 5.7. Aggregate 2D surface profiles perpendicular to the sliding direction of forming were then collected from the centre of these 3D surface scans, and calculated using the mean of 70 adjacent profiles spanning a region of width 50 μm (Figure 5.7). This ensured that sliding direction wear tracks were captured by the profiles and asperity noise was minimised. The sampling frequency or sample spacing of the 2D surface profiles was determined by the resolution of the 3D surface scans. For this study, the sampling frequency was 1766 samples/mm.

In order to assess and compare the W_{DWT} parameter to existing galling quantification options a number of roughness and surface texture parameters were determined for the collected 2D profiles and 3D surface scans – see Table 5.3. The Galling Severity Index (Vermeulen and Hobleke, 2003) is the only parameter directly targeted at galling quantification and requires the use of a reference unworn surface profile. The first part sidewall for each die were used as reference surfaces. A number of other 3D texture parameters and 2D surface profile parameters were also assessed, including: maximum valley depth (R_v), maximum peak height (R_p), root mean square of slope (R_{dq}), average height of area (S_a), and root mean square of

gradient (S_{dq}). R_{dq} has been linked to tool wear in machining (Petropoulos et al., 2010) and performed well in initial measurements, and so was included in this comparison.

Table 5.3: Alternate wear measures for the galling initiation case study.

Parameter	Description
R_a	Average roughness of profile
R_z	Mean peak to valley height of roughness profile
R_y	Maximum peak to valley height of roughness profile
R_p	Maximum peak height
R_v	Maximum valley depth
R_{dq}	Root mean square of slope
GSI	Galling Severity Index
S_{pk}	Mean peak height above core roughness
S_k	Height of core roughness
S_{vk}	Mean depth of valleys below core roughness
S_a	Average height of area
S_{dq}	Root mean square of gradient

5.5.2 Galling initiation case study visual assessment

Categorical visual rating scales of galling and wear damage have been used to provide subjective quantitative outputs of the visual assessment of galling wear damage on strip drawn samples (Andreasen et al., 1998), cylindrical cups (Olsson et al., 2010), and ASTM G 98 and G 196 test specimens (Budinski and Budinski, 2015). A tailored visual wear damage severity rating scale has been used to assess formed parts. The tailored visual wear damage severity scale has been developed to ease with assessment of the channel parts formed in this case study and is shown in Table 5.4.

Table 5.4: Visual assessment wear rankings for galling initiation case study.

Visual galling wear ranking	Definition
0	Smooth, no apparent wear
1	Very slight scratching
2	Mild scratching apparent
3	Obvious scratching in small proportion of side wall
4	Obvious scratching on significant proportion of sidewall half
5	Multiple scratching and/or galling site across entire sidewall half.

Images of the sidewalls were assessed by 9 assessors experienced with SMF, and a median rating for each part was determined. The channel forming operation was ceased when galling damage was observed on the die, with the counter surface on the formed parts exhibiting abrasive damage. The visual ranking score ranges from 0-5 in value; where a score of 0 is allocated if no wear is observed and 5 is allocated if severe damage is judged, as seen in Table 5.4. The issues with the application of numerical rankings to visual assessment of large worn surfaces have been discussed in Section 2.4.1. Considering these issues and to improve the accuracy of the rankings and the ease by which they can be applied, only the immediate wear region where sliding contact begins was assessed on each wear test sample, as seen in Figure 5.7. The assessment regions were considered to start 2 mm in from the edge of the parts to ignore edge effects and were divided into two equal regions perpendicular to the sliding direction such that each wear test sample was assigned 2 rankings. The width of the parts was 20 mm, which meant that wear development could occur at localised regions perpendicular to the sliding direction and therefore this division was conducted to improve ranking accuracy. A combined damage severity rating was then calculated for each wear test sample by summing the ratings assigned to the two regions to give a combined damage severity rating from 0 to 10. The resulting visual assessment rankings from the 9 assessors for the two dies are depicted with box plots in Figure 5.8, with the red line showing the median ranking for each part sidewall. Example median damage severity ratings are shown in the images of the corresponding part sidewalls in Figure 5.9.

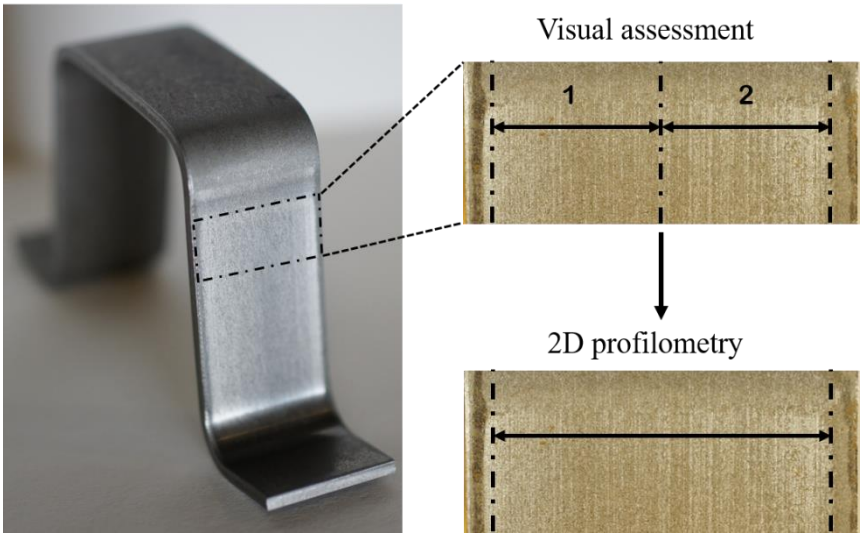

Figure 5.7: Part sidewall assessment division. Only the section at the initiation of steady state contact is considered and is subdivided into sections 1 and 2 for numerical ranking of galling wear severity. This same region is scanned using focus-variation scanning microscopy and a 2D aggregate profile is collected for the wear severity measurement.

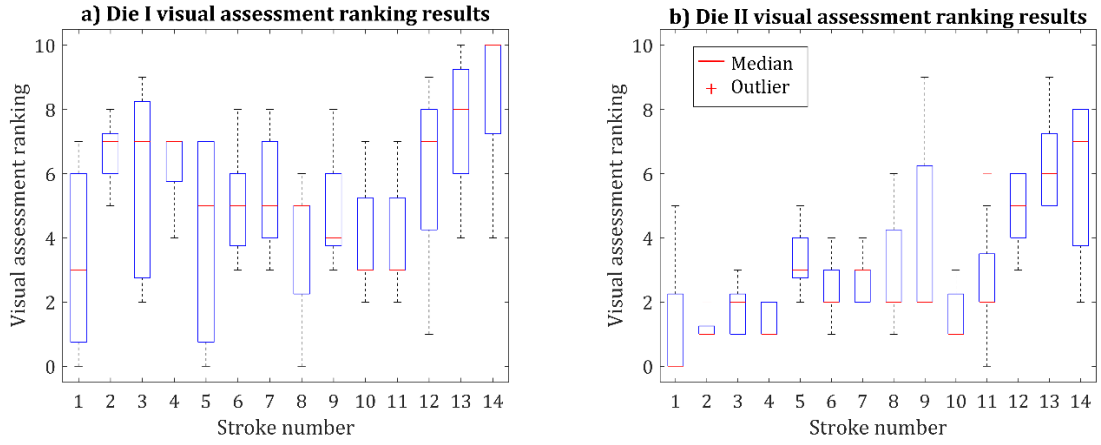

Figure 5.8: Box plots depicting part sidewall visual assessment rankings from 9 assessors who have ranked each of the 28 part sidewalls according to section 5.5.2. Red lines depict the median visual assessment ranking for each part sidewall, +symbols represent outlier ranking values for individual part sidewalls, whiskers represent the range of the ranking values and the blue boxes depict the range of quartiles 1 to 3.

Die	Part number	Median visual assessment ranking	Sidewall image
II	1	0	
I	12	7	
I	14	10	

Figure 5.9: Examples of the numerical wear severity rankings for three worn part sidewalls collected from the process described in Section 5.5.1.

5.5.3 Mother wavelet and detail coefficient level selection

Given the discussion of distinct wear features in sections 5.2 and 5.4.2, the Daubechies 2 mother wavelet was chosen for this application of the DWT galling wear methodology.

In order to select an appropriate decomposition detail level, a number of example galling wear gouges were isolated in the captured 2D surface profiles from Die I stroke numbers 4 and 14 and Die II stroke numbers 13 and 14. In these 2D surface profiles the edge transitions of the wear gouges, seen in Figure 5.6a, were measured and found to occur over a distance of 18μm. One example galling wear gouge and edge transition measurement can be seen in Figure 5.10.

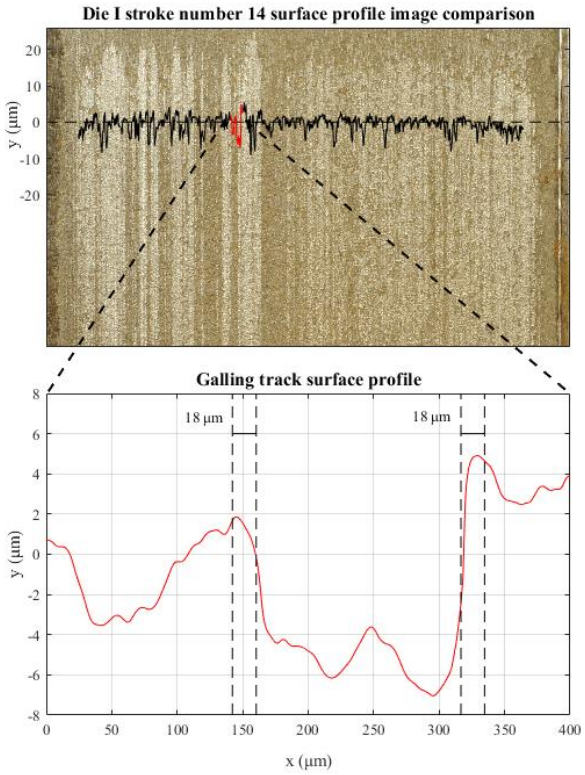

Figure 5.10: An example galling wear gouge track isolated from the 2D surface profile. Key gouge track edge transitions present at 150 µm and 325 µm are measured to determine the appropriate Discrete Wavelet Transform decomposition detail level.

The sampling rate at which the profiles were collected was 1766 samples per mm and so the detail levels correspond to the wavelength bandwidths seen in Table 5.2. Detail level 4 (d_4) approximately covers the 18 µm gouge edge transition and so has been selected as the output detail level.

5.5.4 Results and analysis

5.5.4.1 DWT detail coefficients

The detail coefficients provide an indication of the severity and location of galling wear damage on the surface. Overlaying the detail coefficients on images of the part sidewalls allow for assessing the accuracy of the detail coefficients for characterising and locating galling wear damage.

A DWT multi-level decomposition was performed on the collected roughness profiles using Mathworks MATLAB Wavelet Toolbox. The resultant Daubechies 2

level 4 detail coefficients (d_4) (Equation (9)) were overlaid on images of corresponding wear test samples to qualitatively check the correlation between the detail coefficients and the visual observation of scratches on the sidewalls of the parts (as shown in Figure 5.11 and Figure 5.12).

The channel part sidewalls exhibit areas of apparent wear damage running in the sliding directions, these areas are characterised in the images by their light colour. Based on the selection of mother wavelet and decomposition level it was expected that the wear damage on the sidewall would line up with large detail coefficients. Where large detail coefficient peaks notionally indicate a significant galling wear feature localised on the part surface. This component of the DWT methodology is designed to allow for the identification of galling wear damage locations in the surface profile data that would be difficult to achieve through assessment of raw profile data, particularly in situations such as this case study, where galling initiation is being assessed and features are expected to be on the same scale as base surface roughness. In order to demonstrate this, both raw surface profile and detail coefficients have been overlaid on to a part sidewall image (Figure 5.11). In this case of assessing galling wear initiation, the large detail coefficient values aligned with damaged areas provide a simple marker of the wear damage as opposed to features in the raw profile that are harder to discern amongst other features in the profile.

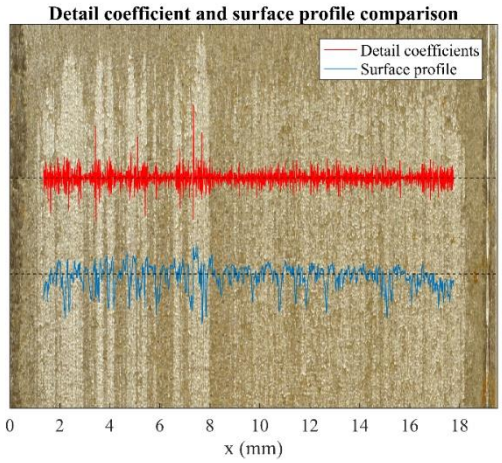

Figure 5.11: Example visual comparison of detail coefficients and surface profile on sidewall image (Die 1 - part 14).

Assessing the example detail coefficients overlaid on sidewall images in Figure 5.12 it is evident that there is generally a very good qualitative correlation (both in terms of the location and magnitude) between the detail coefficient parameter and the visual severity of the wear damage. In particular, this correlation can be observed with coefficients of value greater/less than ± 2 units on die I part 14 between 1-8 mm, die II part 13 between 16-18 mm, and die II part 14 between 5-7 mm and 15-18 mm. However, there is considerable noise in the detail coefficients and area of apparent wear that do not have corresponding large detail coefficients. For all sidewalls the coefficients exhibit a noisy response of ±1 unit regardless of the visible condition of the surface. This noise indicates a correlation between base surface roughness and the mother wavelet function, and highlights a need to focus on coefficients of greater magnitude when looking for galling initiation.

Also noteworthy is the lack of large magnitude coefficients for some visible surface damage regions, typified by the lack of significant detail coefficient for die I part 3, which has a number of visible marks on the sidewall. It is likely that the marks on die I part 3 are not the same scale as damage observed on later parts, which has resulted in them not being detected by the DWT methodology. Damage of the scale seen on die I part 3 was not observed on the preceding or following part sidewall, indicating that die damage was not significant galling.

Also noteworthy is the difference in magnitude of detail coefficients on die II parts 13 and 14 at 17-18 mm, having approximately ±7 and ±3 units respectively. The reduction of detail coefficient magnitude in this region could be explained by initial material adhesion and fracture causing significant damage followed by this material being further transferred or polished down during the stroke, leaving less material to gouge the opposing surface on subsequence strokes.

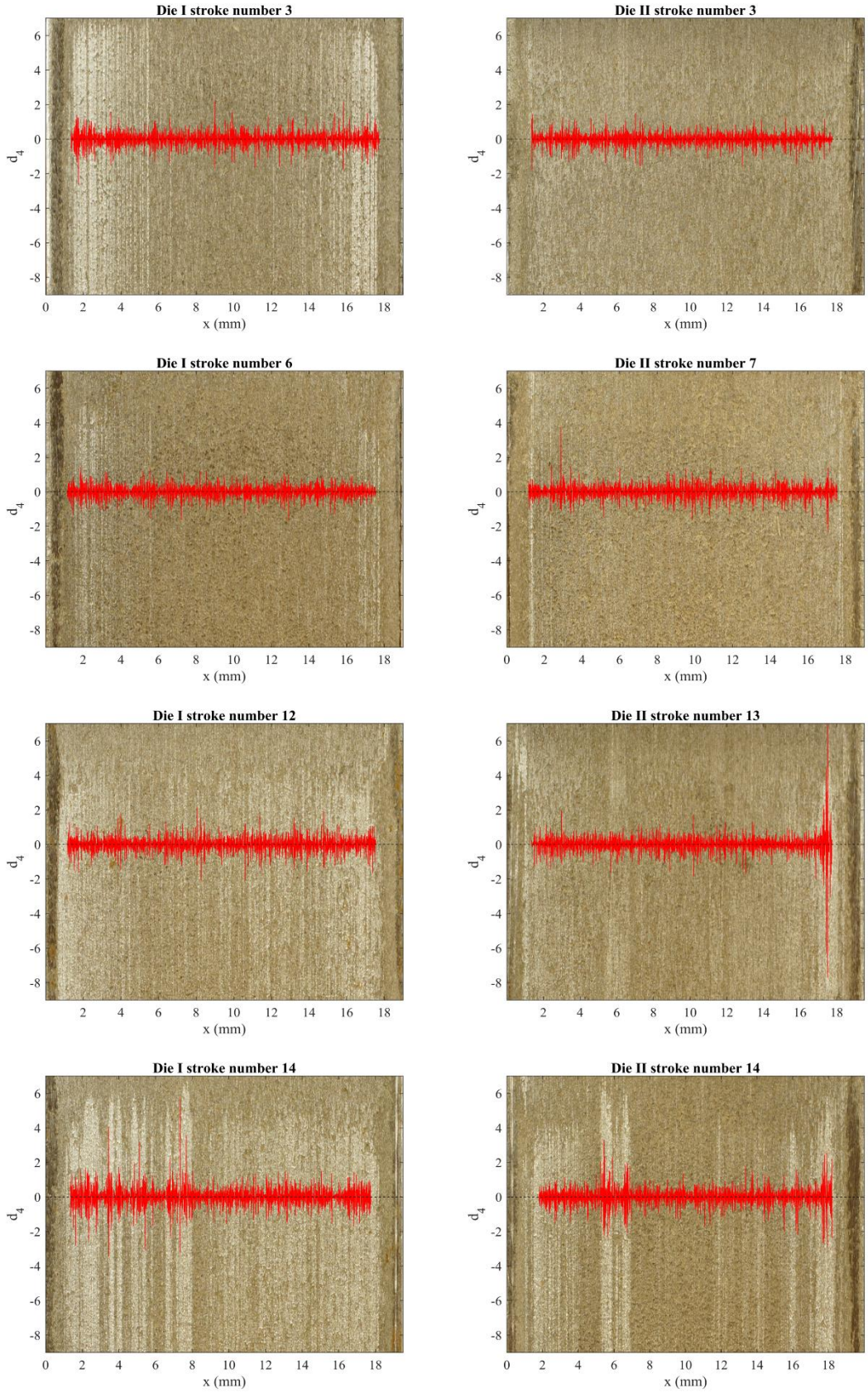

Figure 5.12: Detail coefficient (Daubechies 2 detail level 4) overlaid on worn sidewall images, demonstrating the detail coefficient response to galling wear features.

5.5.4.2 Wear parameters

The second result component of the DWT methodology is the galling wear severity parameter W_{DWT}. This parameter aims to capture the severity of the damage across the part surface in a single value by calculating the mean of the detail coefficient absolute values and should be used in conjunction with the raw coefficients to gain a comprehensive picture of the galling wear state. Measured W_{DWT} parameter values will be compared to visual assessment rankings as the new parameter and methodology aims to provide a faster and reliable measure of galling wear severity that is comparable in accuracy to visual assessment, which is time consuming to conduct and has issues with repeatability and subjectivity. A strong correlation with visual assessment rankings indicates that the W_{DWT} parameter provides a measure of galling severity that is comparable to the current standard as well as being less subjective and faster to obtain through the nature of being an automated calculation.

The progression of each galling wear measurement parameter or surface roughness parameter for both dies can be seen in Figure 5.13. As discussed, the visual assessment ranking (shown in Figure 5.13a) is the baseline measurement of galling wear for the parts. W_{DWT} values determined for a different wavelet function (Figure 5.13e) and different wavelet frequency bandwidth (Figure 5.13d) have been included as a comparison for a non-optimised DWT process. The values calculated with the Haar wavelet at detail level 4 (Figure 5.13e) and Daubechies 2 wavelet at detail level 6 (Figure 5.13d) represent values determined with sub-optimal wavelet function and wavelet frequency bandwidth respectively. Figure 5.13c also shows the calculated *GSI* parameter values, which is the only other galling wear targeted parameter. The best performing 'traditional' surface roughness-based parameter, R_{dq}, is shown in Figure 5.13f. Finally, R_a, S_{vk}, and S_{pk} have been included as representative examples of other traditional roughness and texture parameters.

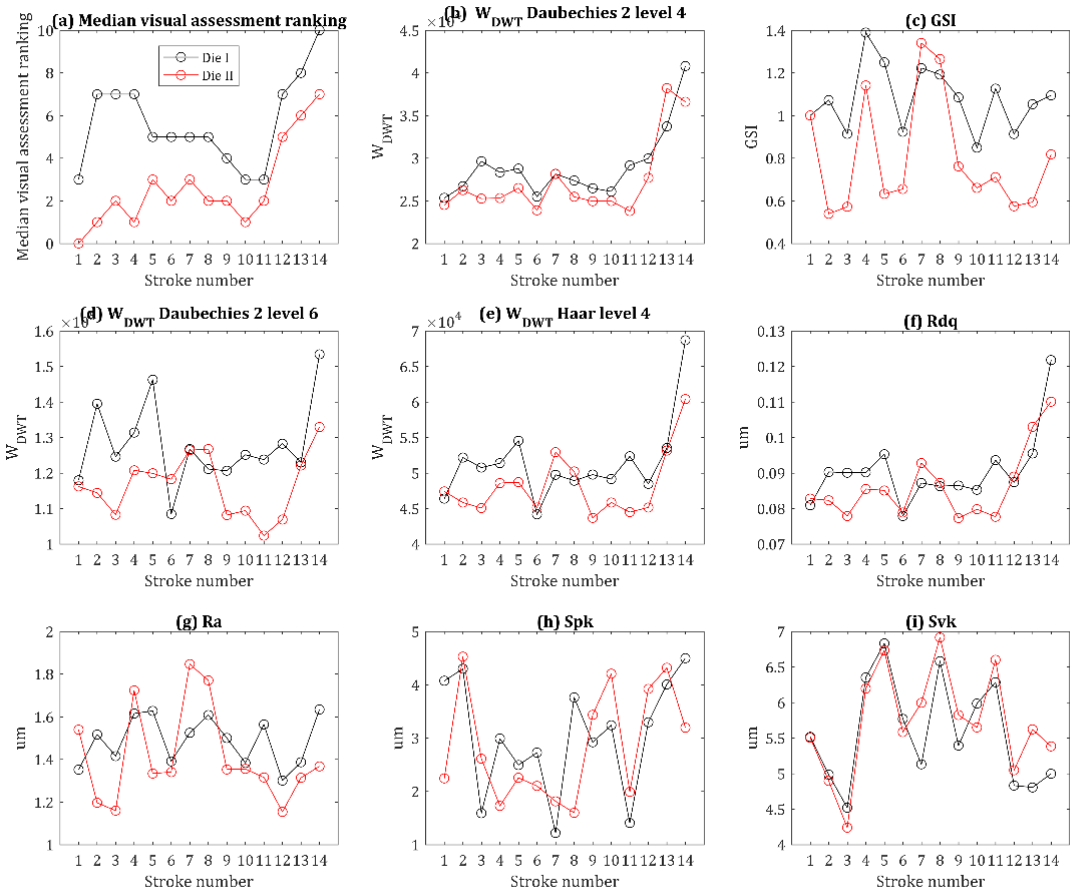

Figure 5.13: Assessed galling wear measurements for each die insert with stroke number, showing the progression of each parameter over the course of the wear trials for both dies.

The correlation between each of the wear measures and the visual assessment ranking was then measured using Spearman's rank Correlation Coefficients, r_s (Mendenhall and Sincich, 2016), using a total of 28 data points for each case. Spearman's rank correlation provides a measure of the rank correlation between two variables and is suitable for application to ordinal data, like the visual assessment rankings collected in this study. The performance of the parameters in Table 5.3 was measured against numerical rankings of galling wear severity based on visual assessment, which is the standard for the assessment of galling wear severity (ASTM Standard G196-08, 2016; ASTM Standard G98-02, 2009). Correlation coefficient and *p*-values for visual assessment ranking values with the parameters listed in Table 5.3 can be seen in Table 5.5. W_{DWT} was found to have a significant and highest correlation of r_s = 0.8411 with the visual assessment ranking.

Table 5.5: Spearman's rank correlation value for wear measures with median visual assessment ranking for galling initiation case study.

Median visual assessment ranking correlation results		
Parameter	**Correlation coefficient r_s**	***p*-value**
W_{DWT} Daubechies 2 level 4 (optimised)	0.8411	2.08E-08
W_{DWT} Haar level 4 (not optimised)	0.6241	3.87E-04
W_{DWT} Daubechies 2 level 6 (not optimised)	0.6246	3.81E-04
R_{dq}	0.7245	1.30E-05
GSI	0.2567	0.1873
R_a	0.1152	0.5595
R_z	0.0572	0.7731
R_y	0.0975	0.6277
R_p	0.2807	0.1479
R_v	-0.0498	0.8012
S_{pk}	0.2664	0.1707
S_k	0.0349	0.8601
S_{vk}	-0.3212	0.0956
S_a	-0.0642	0.7454
S_{dq}	-0.2315	0.2360

5.5.5 Galling initiation case study discussion

These results have demonstrated the two components of the DWT galling wear methodology, detail coefficients for assessing the location and relative severity of damage across the surface and W_{DWT} providing a total measure of severity of galling damage across the surface. For this case study, which focused on galling initiation, the DWT galling wear methodology has clear advantages over existing methods of quantifying and characterising galling wear severity in sheet metal forming. Generally, detail coefficients of significant magnitude (±2 units) show good alignment with galling wear features on the sidewall. The detail coefficients allow for the identification of galling location and respective severity of features that would otherwise be difficult to isolate in a raw surface profile. It should be noted that this threshold detail coefficient magnitude only holds for this mother wavelet and level of decomposition, and may also differ for other materials. There were some apparent damage features on part sidewalls that were not detected by the DWT methodology, and this was likely due to the scale of the damage. Failure to detect these features demonstrates a disadvantage of the methodology, and that the chosen

decomposition level may not capture all visible abnormalities on the surface. However, limiting the scale through decomposition level may help to classify different types of wear damage based on size.

The optimised W_{DWT} values have a strong correlation with visual assessment ranking and out performs other surface roughness and texture parameters based on the standard of visual assessment rankings. For galling initiation these results suggest the W_{DWT} parameter can provide a measure of galling wear severity that is comparable in accuracy to visual assessment and is faster to apply and less subjective in nature.

Visual assessment is a subjective process that is challenging to apply to large surface areas, and does not always lead to repeatable measurements of galling wear. The significant variability of visual assessment is demonstrated with the respondent assessment results shown in Figure 5.8. Numerical ranking provides a quantifiable output for visual assessment and median values address variability, however the subjective nature of the method and the difficulties with repeatability and application over large surface areas remain.

The DWT detail coefficients capture the important information about the wear features, and W_{DWT} converts the detail coefficient information into a form that is suitable for direct comparison to visual assessment rankings. However, condensing the wear information from the detail coefficients to the single W_{DWT} parameter results in the loss of spatial information. Therefore, the W_{DWT} values should be considered as one component in the presented methodology for measuring and characterising galling wear, rather than the definitive output.

There is a level of noise present in the detail coefficients that is due to low levels of wavelet correlation with other surface features. This is an issue that is exacerbated when using single 2D surface profiles as opposed to aggregated 2D surface profiles. While some noise still exists, it is apparent from the detail coefficient image overlay (Figure 5.12) that the wear features produce the dominant detail coefficient values. Utilising aggregate 2D surface profiles minimises this noise by reducing the prominence of non-wear related surface asperities and pitting. Figure 5.12 demonstrates that the galling wear features are well characterised by DWT detail coefficients for Daubechies 2 of wavelength 9.09-18.2μm, with the highest values of the detail coefficients at the galling wear features locations. The 9.09-18.2 μm

wavelength bandwidth that is associated with detail level 4 in this study is shown to cover the same spatial range as galling wear features in Figure 5.10.

The root mean square slope of the profile, R_{dq}, was found to have a significant correlation with visual assessment rankings; however, this correlation was not as strong as that found with W_{DWT}. R_{dq} gives a measure of variability of the surface and has been linked to wear in machining tools and has been used for assessing reflectivity and wettability of surfaces (Kuzinovski and Tomov, 2009; Petropoulos et al., 2010). It follows that this parameter will respond to the sudden drops below the bulk material level in the 2D profiles that are associated with galling related wear features (e.g. see Figure 5.1 and Figure 5.10). However, R_{dq} is likely to be more susceptible to the base surface roughness than the DWT methodology presented in this study. *GSI* is the only other parameter that is specifically targeted at galling wear measurement, and has been shown to be effective when measuring severely galled parts (Vermeiden and Hobleke, 2003). *GSI* performed poorly when compared to visual assessment ranking and W_{DWT} for the parts collected in the conducted case study. The collected parts exhibited primarily abrasive damage features that precede galling that are likely to be less prominent and less frequent in their occurrence than any features seen on parts exhibiting severe galling damage. By converting the profiles into the frequency domain without specifically targeting galling wear features, it is likely that if any frequencies potentially linked to those features are lost in the frequency response of the general surface roughness.

5.6 Case study: galling progression

Having demonstrated the DWT galling wear methodology on a galling initiation trial (section 5.5), a second case study has been conducted to test the methodology on an extended trial. Quantifying the progression of galling wear development over an extended period in sheet metal forming operations is an important component of further work linking process signals to galling wear and the development of galling wear monitoring systems. As with the galling initiation case study, both components of the DWT galling wear methodology will be demonstrated, detail coefficients and the W_{DWT} parameter. The performance of the detail coefficients was assessed based on how well the detail coefficient activity aligned with visible features on the

sidewall. The performance of the W_{DWT} parameter was assessed through comparison to visual assessment rankings and other surface roughness and texture parameters.

This will show that the DWT galling wear methodology can provide an accurate measure of galling wear severity past the point of initiation and into significant galling damage at multiple locations on the die. Galling wear progression provides an additional challenge to that seen with the galling initiation case study in that different scales of damage are expected for the different stages of galling severity, which may also be developing at different rates at different locations on the dies. An extended series of channel parts have been formed until significant galling wear damage was observed in multiple locations on both parts and die inserts. The proposed DWT galling wear severity parameter (W_{DWT}, see Equation (6)) was calculated from 2D profile measurements of part surfaces and was again compared to visual rankings. Visual rankings were used as the reference measurement for galling wear severity, however a new rating scale was developed for this case study. A different material was utilised for the extended wear trial that exhibited different characteristics of wear development, and so a new rating scale was required.

5.6.1 Experimental method

5.6.1.1 Channel forming operation

An extended channel forming wear trial was conducted using the semi-industrial stamping press (Section 3.3.1). A total of 4600 channel parts were formed in this extended trial, to replicate production lengths seen in industry. Significant galling wear was observed at multiple locations on both the die corner radius inserts at the conclusion of the trial. This die wear resulted in corresponding galling damage on the channel part sidewalls that have been measured for demonstration of the W_{DWT} parameter. Die corner radius inserts were hardened AISI D2 tool steel (60HRC) and precision ground, labelled inserts #30 and #31. Blank material was 1.8 mm thick HLSA300 (Section 3.3.1). A sample series of the formed channel parts were collected at regular intervals for further examination.

5.6.1.2 Surface characterisation

The series of 30 sampled channel parts were scanned on both sidewalls using focus variation microscopy see Section 3.5, and subsequent aggregate 2D surface profiles were collected according to the methodology outlined in Section 5.5.1.1. The sampling frequency for this case study was 1000 samples/mm.

For comparison, a number of roughness parameters were determined for the collected 2D profiles – see Table 5.6. 2D profiles from the sidewalls for part 1 of the trial were used as reference surfaces when calculating *GSI* for the parts of the trial.

Table 5.6: Alternate wear measures for galling progression case study.

Parameter	Description
R_a	Average roughness of profile
R_z	Mean peak to valley height of roughness profile
R_y	Maximum peak to valley height of roughness profile
R_p	Maximum peak height
R_v	Maximum valley depth
R_{dq}	Root mean square of slope
GSI	Galling Severity Index

5.6.1.3 Galling progression case study visual assessment

Visual assessment of the extended wear trial was conducted, and severity rankings were assigned for each part sidewall, according to an adjusted visual galling wear ranking scheme. As per the case study presented in section 5.5, part sidewalls were subdivided into two regions for assessment and a combined damage severity ranking was determined, see section 5.5. Due to the different material couple, the observed wear damage included galling damage on the part as opposed to the pure abrasive damage observed on parts in section 5.5 as a result of galling wear on the dies. The definitions of the 0-5 visual assessment wear severity rankings were adjusted to account for the presence of galling damage on the part sidewalls, see Table 5.7. Each assessment region was assigned a severity rating 0-5 and then a combined severity rating for the part was calculated by summing the two ratings to provide a combined damage severity rating from 0 to 10. The resulting visual

assessment rankings are depicted with stroke numbers in Figure 5.14. Example damage severity ratings are shown with the images of the corresponding part sidewalls in Figure 5.15.

Table 5.7: Visual assessment wear rankings for galling progression case study.

Wear ranking	Definition
0	Smooth, no apparent wear
1	Very slight wear damage
2	Mild scratching and/or galling apparent
3	Obvious scratching and/or galling in small proportion of side wall
4	Obvious scratching and/or galling on significant proportion of sidewall half
5	Obvious scratching and/or galling on entire sidewall half.

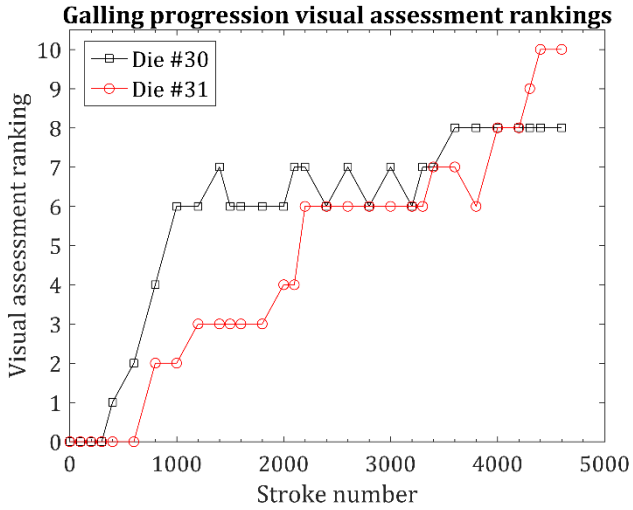

Figure 5.14: Visual assessment ranks for Dies #30 and #31 with stroke number.

Die	Part number	Median visual assessment ranking	Sidewall image
31	1200	3	
30	3200	6	
31	4600	10	

Figure 5.15: Examples of the numerical wear severity rankings for three part sidewalls formed in the trial outlined in section 5.6.1.1.

5.6.2 Mother wavelet and detail coefficient level selection

Given the discussion of distinct wear features in section 5.2 and the visual comparison conducted in section 5.4.2, the Daubechies 2 mother wavelet was selected for the DWT galling wear severity measurement methodology. For comparison the method was also applied using the Haar wavelet based on results of MDL criterion (Table 5.1) discussed in section 5.4.2.

Selection of detail coefficient decomposition level is complicated due to the extended nature of the trial, which leads to the possibility of different scales of galling wear damage over the course of the trial. In order to account for this added complexity a series of 2D surface profiles of wear damage regions at varying stages of development were isolated for assessment, see Figure 5.10. As outlined in section 5.4.3 the width characteristic edge feature of the galling wear damage tracks were measured and compared to wavelet wavelength bandwidths calculated based on the

sampling frequency of the surface profile. Detail coefficient decomposition level was then selected based on the measured features and the calculated bandwidths.

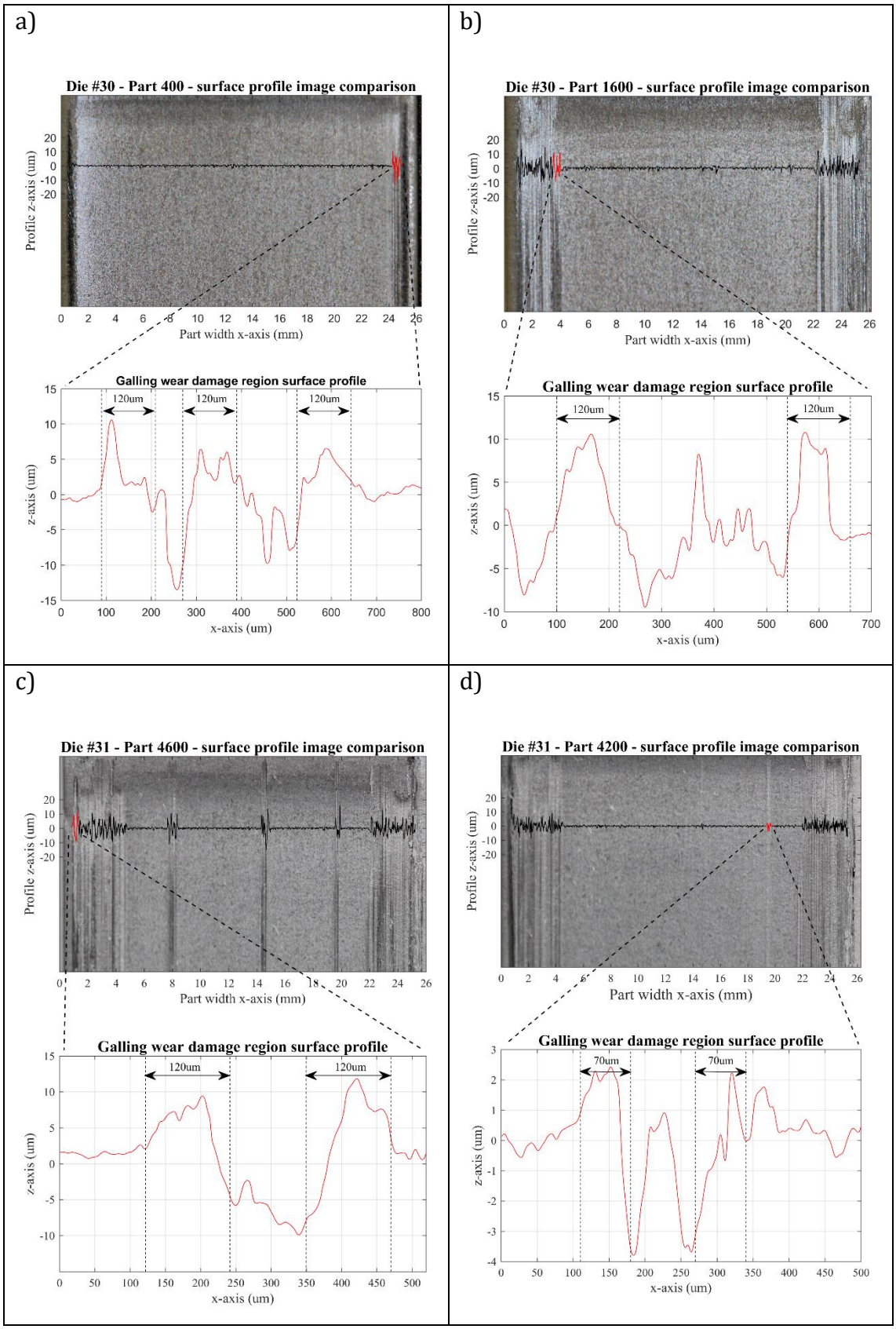

Figure 5.16: Galling progression case study galling wear damage region surface profile examples. a) Die #30 part 400 sidewall image and 2D profile section. b) Die #30 part 1600 sidewall image and 2D profile section. c) Die #31 part 4600 sidewall image and 2D profile section. d) Die #31 part 4200 sidewall image and 2D profile section.

Figure 5.16 shows the measured features sampled from various stages in the trials. The characteristic galling edge features in each of the example wear damage regions were found to range from 70-120μm. Table 5.8 shows the recalculated wavelength bandwidths for a 6-level decomposition given the sampling frequency used for this trial ($f_{s2} = 1000\ samples/mm$). As the characteristic galling edge features of the example wear regions were found to be 70-120 μm wide, detail level 6 was chosen for determining W_{DWT} values.

Table 5.8: Frequency bandwidth ranges for 6-level Discrete Wavelet Transform decomposition. Where $f_{s2} = 1000\ samples/mm$.

Detail level	**Wavelet wavelength bandwidth**	**Bandwidths for f_{s2}**
d_1	$2/f_s - 4/f_s$	2 – 4 μm
d_2	$4/f_s - 8/f_s$	4 – 8 μm
d_3	$8/f_s - 16/f_s$	8 – 16 μm
d_4	$16/f_s - 32/f_s$	16 – 32 μm
d_5	$32/f_s - 64/f_s$	32 – 64 μm
d_6	$64/f_s - 128/f_s$	64 – 128 μm

5.6.3 Results and analysis

5.6.3.1 DWT detail coefficients

Again, the detail coefficients provide an indication and the severity and location of galling wear damage on the surface. Overlaying the detail coefficients on images of the part sidewalls allow for assessing the accuracy of the detail coefficients for characterising and locating galling wear damage. Large magnitude detail coefficients should have good alignment with all visible regions of wear damage to demonstrate that the DWT methodology successfully identifies galling wear on the part surface.

As discussed in section 5.5.4.1, this component of the DWT methodology is designed to allow for the identification of galling wear damage locations in the surface profile data that would not be possible in the raw profile data. The strength of detail coefficient assessment for identifying galling wear damage was displayed in the galling initiation case study Section 5.5.

A DWT multi-level decomposition was performed on the collected aggregate roughness profiles using Mathworks MATLAB Wavelet Toolbox. The resultant Daubechies 2 and Haar level 6 detail coefficients (d_6), Equation (9), were overlaid on images of corresponding part sidewalls to qualitatively check the correlation between the detail coefficients and the visual observation of wear damage on the sidewalls of the parts (as shown in Figure 5.18). Both detail coefficients and raw surface profile have also been overlaid on a part sidewall image (Figure 5.17). Comparing both on the same sidewall image makes it possible to assess if detail coefficients reveal galling information that would otherwise be difficult to identify in raw surface profiles.

This case study focuses on galling wear progression and displays late stage wear damage at a larger scale than damage observed in the galling initiation case study (Section 5.5). Due to this difference in the scale and advanced stage of the galling it may be easier to distinguish galling wear damage features from unrelated roughness in the profile. This comparison aims to determine if detail coefficients continue to highlight galling information that would be difficult to assess in the raw profile.

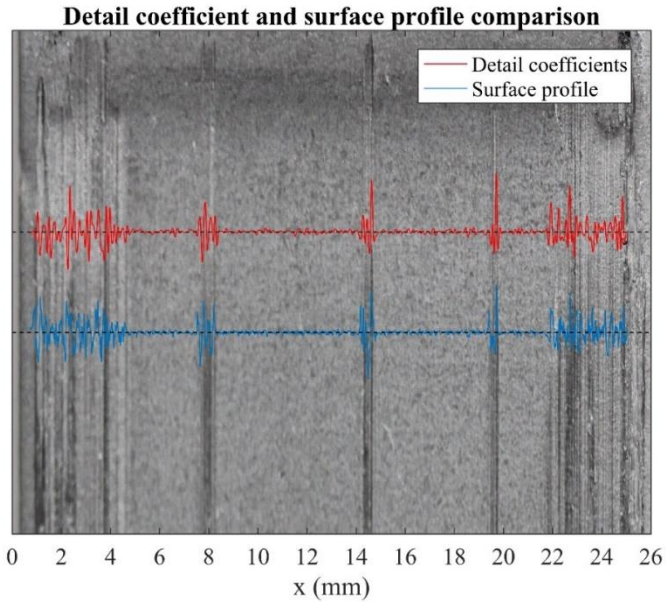

Figure 5.17:Example visual comparison of detail coefficients (db2 detail level 6) and surface profile on sidewall image (Die #31 - part 4600).

Dominant and clearly discernible features in the raw surface profile are well aligned with the visible galling damage on the part sidewall. This is also true for the detail

coefficients, but no obvious additional information is present in the coefficients that are not also present in the surface profile. These results indicate that assessment of detail coefficients for identifying galling wear features at advanced stages of wear is not as insightful as during the phase of galling initiation. This appears to be a result of the scale of the damage relative to the base surface roughness of the part.

Figure 5.18 displays part sidewall images overlaid with the chosen detail coefficient combinations, Daubechies 2 and Haar at d6. The chosen sidewalls demonstrate both advanced galling wear damage and recently initiated damage located at x = 4 mm on die #31 part 1200 (Figure 5.18a and b) and x = 14 mm and 19 mm on die #31 part 4200 (Figure 5.18c & d). These recently initiated vertical damage regions are characterised by their narrow width and lighter colour, as opposed to the wider and darker advanced damage regions on the edges of the two parts. Detecting both advanced and newly initiated galling damage on larger surfaces is an important performance criterion for the DWT methodology, as galling can initiate at multiple locations at different stages of continuous forming operations.

Again, as seen in section 5.5, it is evident that there is very good qualitative correlation, both in terms of the location and magnitude, between the detail coefficient parameter and the visual severity of the wear damage. The detail coefficients for both mother wavelets aligned with galling damage are distinct from the base level noise in the coefficients. The level of noise in the detail coefficients is not of the scale of the galling wear associated coefficients, this is different to what was observed in the galling initiation case study (Section 5.5), where wear associated coefficients were of the same scale of magnitude as the detail coefficient noise. This is likely due to the comparatively large scale of the advanced stage damage. Of the two mother wavelets tested, the Haar detail coefficients exhibits a larger response for the slight scratching or initiation sites that are separate from the established damage tracks, see at 14 mm in Figure 5.18*d* and at 4 mm in Figure 5.18*b*. This may be a result of the size of the galling feature and Haar wavelets being appropriate for edge detection, which could explain why it responds to smaller wear features. However, the db2 detail coefficients provide a larger response for the more obvious damage site at 19 mm on die #31 part 4200 (Figure 5.18c and d), indicating that db2 wavelet is more appropriate for the visible damage tracks. The feature at x = 19 mm is approximately 280 µm wide and 6 µm from peak material pile up to

gouge bottom, while the feature at x = 14 mm is approximately 190 µm wide and 4.5µm from peak material pile up to gouge bottom.

These results indicate that the detail coefficients determined using the DWT galling wear methodology detect visible galling wear damage in the surface profile of the part sidewall. In this case study of advanced galling wear progression the detail coefficients do not appear to provide any additional information about relative severity and location of the damage that is not already apparent from the surface profile. This appears to be a result of the significant scale of the damage features in the surface profile. It should be noted that the detail coefficients have been shown to track galling wear features (Section 5.5), and so if other unrelated features appear in the surface profile or a user is unsure if profile features correspond to wear, the detail coefficients can still assist with identification.

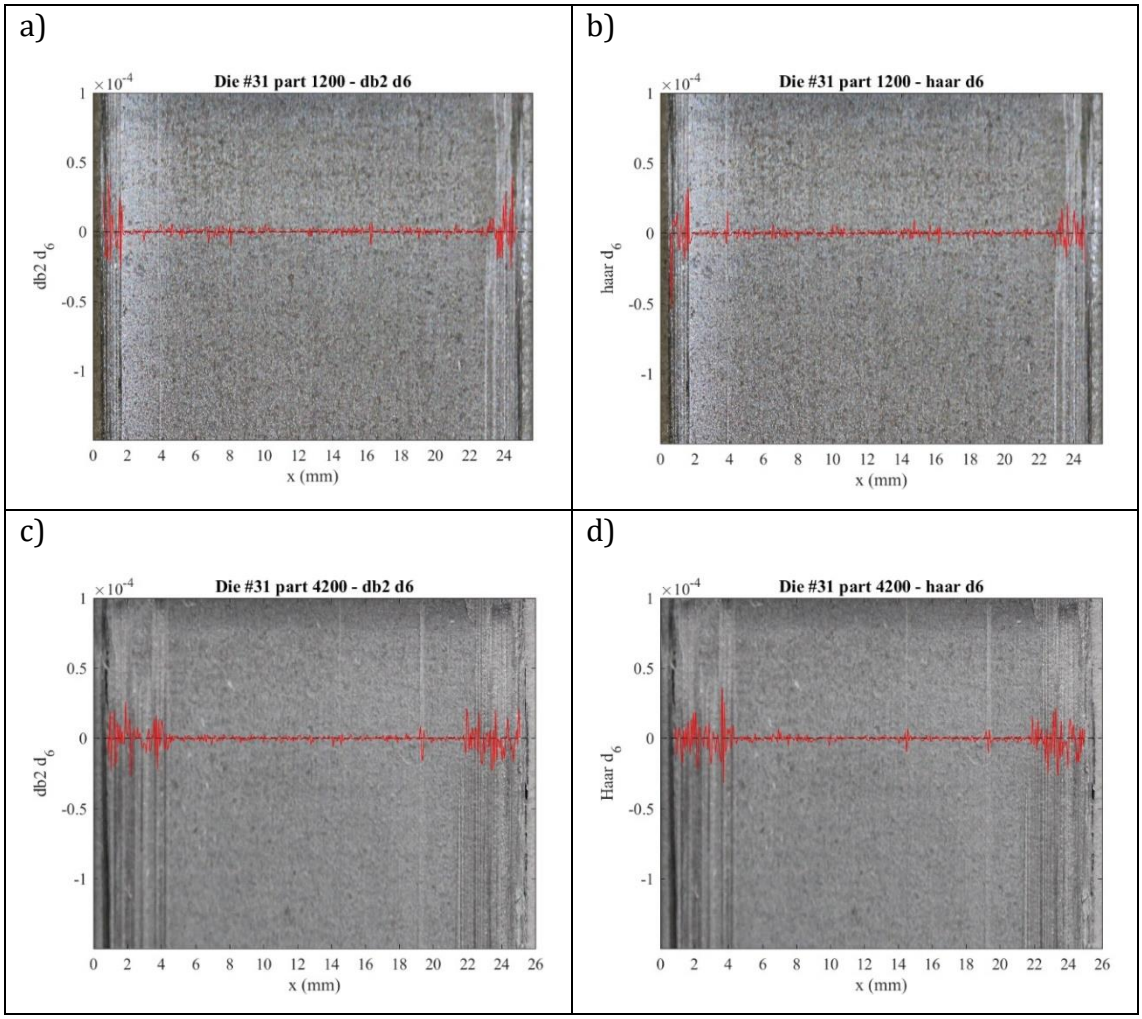

Figure 5.18: Detail coefficient overlaid on worn sidewall images demonstrating the detail coefficient response to galling wear features. a) Die #31-part 1200 sidewall with db2 detail level 6 coefficient overlay. b) Die #31-part 1200 sidewall with haar detail level 6 coefficient overlay. c) Die #31-part 4200 sidewall with db2 detail level 6 coefficient overlay. d) Die #31-part 4200 sidewall with haar detail level 6 coefficient overlay.

5.6.3.2 Wear parameters

The W_{DWT} parameter is the other component of the DWT methodology result that aims to capture the severity of the damage across the part surface in a single value. When assessed in conjunction with the raw detail coefficients the DWT methodology results aim to provide a comprehensive picture of the galling wear state, including relative magnitude and location of galling wear damage and the overall relative galling wear damage severity on the surface. In this section measured W_{DWT} parameter values are compared to visual assessment rankings. As was outlined in Section 5.5.4.2 the DWT methodology aims to provide a faster and reliable measure of galling wear severity that is comparable in accuracy to visual assessment. A strong correlation with visual assessment rankings indicates that the W_{DWT} parameter provides a measure of galling severity that is comparable to the current standard as well as being less subjective and faster to obtain through the nature of being an automated calculation.

The correlation between each of the wear measures and the visual assessment ranking was then measured using Spearman's rank Correlation Coefficients, r_s (Mendenhall and Sincich, 2016), using a total of 60 data points for each case. The performance of the W_{DWT} parameters and the parameters in Table 5.6 was measured against numerical rankings of galling wear severity based on visual assessment. Correlation coefficients and p-values for correlation with visual assessment ranking values for the parameters can be seen in Table 5.9. The Daubechies 2 d6 W_{DWT} parameter was found to have a very strong and the highest correlation with the visual assessment ranking over the Haar d6 W_{DWT} parameter, r_s = 0.8010 and 0.7684 respectively. Figure 5.19 shows visual assessment rankings and W_{DWT} (db2 d6) values with stroke for the extended wear progression forming trial. The visual ranking assessment and W_{DWT} show good agreement over the course of the trial, as the Spearman Rank Correlation Coefficient indicates. Discrepancies where W_{DWT} is much larger than visual rank (die #30 part 1400, die #31 parts 1000-2000) can all be explained by damage area remaining consistent while the localised severity and scale of damage on the parts has increased, and this means that visually the damage appears similar in severity as damage area contributes to the visual ranking however the W_{DWT} parameter quantifies this difference in severity. Similarly, discrepancies where visual assessment rank is

larger than W_{DWT} (#31 – 4200) can also be explained by the difference in scale and severity of galling damage in consistent areas part to part.

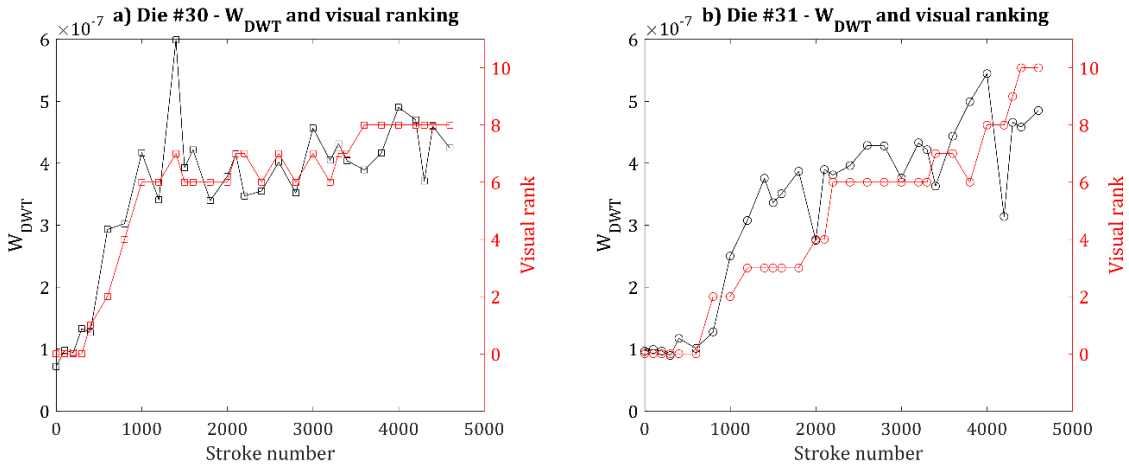

Figure 5.19: Die #30 (a) and #31 (b) W_{DWT} (db2 d6) values with visual assessment rankings with stroke number for the extended wear progression forming trial.

The roughness parameter R_a performed very well based on the correlation coefficients, r_s = 0.8253, the strongest correlation of the tested parameters. This result is likely due to the scale of the galling wear damage relative to base surface roughness on the part. The R_a parameter is the arithmetical mean height of the surface and so if damage features are large in scale, regardless of morphology, the parameter will provide an accurate indication of damage on the part surface. However, the Ra gave inaccurate results when wear features were on the scale of base surface roughness, Section 5.5.4.2. As shown in the previous case study in Table 5.5, the R_a parameter performed very poorly, with a correlation coefficient of just r_s = 0.1152 compared to r_s = 0.8411 for the W_{DWT} parameter. All standard roughness parameters had stronger correlation with visual assessment than was observed in the galling initiation case study, and this is likely due to the significant difference in scale between galling features and base surface roughness.

Table 5.9: Galling progression Spearman's rank correlation value for wear measures with median visual assessment ranking.

Visual assessment ranking correlation results – visual ranking finest detail 1unit		
Parameter	**Correlation coefficient r_s**	***p*-value**
W_{DWT} Daubechies 2 level 6	0.8010	1.54e-14
W_{DWT} Haar level 6	0.7684	7.71e-13
R_a	0.8253	5.08e-16
R_{dq}	0.7350	2.29e-11
GSI	0.5209	1.98e-05
R_z	0.7095	2.21e-10
R_y	0.6746	3.44e-09
R_p	0.6334	5.58e-08
R_v	0.5695	2.05e-06

The results of these comparisons indicate that for extended galling wear progression R_a and W_{DWT} provide the strongest correlation with visual assessment ranking. The DWT galling wear methodology still has the advantage of combining detail coefficients and W_{DWT} parameter to capture a more complete picture of the galling severity state. The results of the galling initiation case study also show that the standard surface roughness parameters do not accurately track the galling wear severity, giving the DWT methodology a distinct advantage given its accuracy in both case studies.

5.6.4 Galling progression case study discussion

Again, the presented DWT wear severity measurement methodology provides a measure of galling wear severity that maintains the accuracy of visual assessment, in this case study for extensive galling wear progression over thousands of parts.

Based on correlation with visual assessment rankings the R_a surface roughness parameter was found to give the most accurate measure of galling wear severity in this case study. As was discussed in Section 5.6.3.2, this result for the R_a parameter was due to the significant difference in scale between galling wear and the surrounding base surface roughness. Other standard surface roughness parameters were also found to be noticeably more accurate for the galling initiation case study (Section 5.5.4.2). In addition to the difference in scale of the galling wear features it

is also possible that the number of parts assessed could have influenced the observed improvement in accuracy in these surface roughness parameters. Approximately 1 in 150 parts were assessed due to the large number of parts formed in the trial, as opposed to every part in the small scale galling initiation case study (Section 5.5). As a result, in this case study the wear damage could progress significantly between sampled parts. Spearman's rank Correlation is used to assess the accuracy of the parameters, and distinct differences in the quantity and severity of wear damage between sampled parts could help to clarify the order of relative severity and hence give stronger correlation for all tested parameters. More frequent sampling of formed parts could possibly capture the progression of wear damage in finer detail, which would highlight the strengths of the DWT galling wear methodology over other standard surface roughness parameters, as demonstrated in section 5.5.

Both the Daubechies 2 wavelet and Haar wavelet derived W_{DWT} parameters have a very strong correlation with the visual assessment ranking. The MDL criterion suggested the Haar wavelet as the 'best' wavelet function for describing the isolated 2D profile wear sections (Section 5.4.2). There is a noticeable difference in strength of correlation between the visually selected db2 wavelet results and the MDL selected Haar wavelet. However, Figure 5.18 showed that the Haar wavelet detail coefficients had a more significant response for the smaller scale damage features than the db2 detail coefficients, for example at x = 4 mm (Figure 5.18b) and x = 14 mm (Figure 5.18d).

The square-wave shape of the Haar wavelet meant it was overlooked based on visual comparison to 2D profiles of galling wear features. However, its shape does make the Haar suitable for edge detection in other applications. Depending on the scale of the wear damage, Haar wavelets may approximate the distinct drop from the gouge shoulder to below the reference surface seen in the 2D cross-section of galling wear damage. This makes the Haar wavelet suitable for the detection of small scale wear damage features in the aggregate 2D surface profiles.

The 2D roughness parameter R_{dq} had a strong correlation with the visual assessment rankings. R_{dq} was the best performing standard 2D surface roughness parameter across both case studies (sections 5.5 and 5.6). R_{dq} gives a measure of the variability of the surface, as discussed in section 5.5.5, which makes it suitable for quantifying

the distinct features of galling wear damage on the part surfaces. *GSI* showed a moderate correlation with the visual assessment rankings, an improvement upon what was observed in section 5.5, but still not as effective as the W_{DWT} parameter or even some of the 2D roughness parameters.

As discussed in section 5.5.5, it should be noted that the DWT detail coefficients capture important information about the location and severity of the wear features on the part sidewalls, and the W_{DWT} parameter reduces this information into a form that is suitable for statistical analysis. However, by reducing the detail coefficients important information is lost, and so, for a comprehensive assessment of wear the W_{DWT} parameter should be considered in conjunction with the raw detail coefficients.

Galling wear progression can occur over the course of individual strokes, resulting in varying levels of galling wear severity on a single part. This was noticeable, in particular, for parts later in the forming trial, with more severe galling adhesive damage occurring late in the stroke, outside of the measurement and visual assessment region. The presented methodology is based on 2D profilometry, and so the resultant measure is dependent upon the surface profile location. Selecting a measurement location that corresponds to later in the stroke or taking multiple measurements will help to ensure an accurate measure of the wear severity is captured.

5.7 Summary

A new methodology and parameter for measuring the severity of galling wear has been presented that utilises DWT to target the distinct features of galling wear damage. The DWT methodology provides a targeted, repeatable and non-subjective measure of galling wear severity from the formed part that reflects visual assessment of part damage in SMF. This was developed to address the requirement for such a measure of galling severity in tracking galling wear development in sheet metal forming operations.

The DWT methodology has been applied in two case studies. In the first case study, the method was applied to a galling initiation trial (Section 5.5). In the second case

study, the method was applied to a long galling progression trial (Section 5.6). In each of these case studies the DWT methodology was compared to a number of other parameters that have been used to quantify wear. Of the parameters tested, the presented optimised W_{DWT} values in sections 5.5 and 5.6 were found to have a very strong correlation with visual assessment rankings, and the highest correlation of all the tested measures across both case studies, see Table 5.5 and Table 5.9.

In the section 5.6 where part sampling was infrequent, the standard roughness parameter R_a appeared to perform well for quantifying wear severity, having a very strong correlation with visual assessment rankings. However, this was not the case for section 5.5 where every part was collected and measured.

Of the existing wear measures assessed, R_{dq} was found to have a strong correlation with visual assessment rankings, and this performance was consistent for sections 5.5 and 5.6. R_{dq} was only outperformed by W_{DWT}, and that had a consistent very strong correlation for sections 5.5 and 5.6. *GSI*, the only other targeted galling wear measure, did not perform particularly well in either of the case study situations.

The DWT methodology was found to be appropriate for SMF tests that focused on galling wear in industrial style conditions. The method allows the quantification of multiple localised galling wear features over large surface areas, as opposed to fixed single tracks that are often studied in experimental wear trials. Therefore, this method will be ideal for quantification of galling wear severity in the industrial style channel forming trials, like the trial described in section 5.6, and will be used for testing galling detection and monitoring methodologies. Such a methodology will be presented in the subsequent chapters, and the DWT wear measurement methodology will be utilised to track the quantity and severity of galling wear throughout those trials.

CHAPTER SIX

Progression of galling wear

6.1 Introduction

In Chapter 4 a link between punch force signature and galling wear changes was established, and in Chapter 5 a new method for quantifying the severity of galling wear was presented. In this chapter the relationship between galling wear progression and punch force signature variation has been investigated.

Two extended deep drawing wear trials were conducted until significant galling wear damage was observed on the die inserts and part sidewalls to provide punch force and galling wear data for the investigation. The DWT galling wear methodology was applied to parts sampled from both extended trials and the W_{DWT} parameter and detail coefficients were assessed, providing another demonstration of the new methodology and a measure of galling wear severity for comparison to punch force variation. PCA was conducted on the punch force signatures of both extended trials and the dominant PC b-values for parts were then compared to W_{DWT} values using Pearson's correlation coefficients.

The relationship between peak force and W_{DWT} was also assessed to compare it to the forms of punch force signature shape variation isolated using PCA. Peak force is simpler to calculate and interpret than punch force signature shape variation, and so it was important to assess if the PCA of punch force signatures provide sufficient benefit over peak force to justify its use.

The results of these investigations showed that punch force signature magnitude, captured using PCA, has a strong linear relationship with galling wear severity, that is stronger than the relationship seen with peak force. This demonstrates the benefit of utilising PCA of punch force signatures over simple peak force values.

6.2 Wear progression experimental setup

Two extended wear trials of channel parts were conducted using the semi-industrial stamping press according to Section 3.3.1. Each trial utilised precision ground and hardened AISI D2 tool steel die corner radius inserts, and parts were formed until severe galling wear damage was observed on these inserts. Blank material for both trials were 1.8 mm thick HSLA300, and blanks were lubricated prior to forming according to Section 3.3.1. Extended trial 1 consisted of 1530 channel parts with die corner insert designations C01 and C02. Extended trial 2 consisted of 3310 channel parts with die insert designations #31 and #30. Die corner inserts #31 and #30 were also used in Section 5.6, and formed a total of 4500 channel parts as outlined in Section 5.6.1. However, a pause in the trial at stroke 3310 and subsequent movement and adjustment of punch force recording equipment led to significant noise being added to the punch force signals. This noise rendered punch force signatures after stroke 3310 unusable, and so for this analysis only strokes 1-3310 have been considered. As punch force was not required for the assessment of the W_{DWT} parameter, parts formed after stroke 3310 were included in the analysis conducted in Section 5.6.

A series of channel parts from both extended trials were measured on both sidewall and W_{DWT} values, and were determined using the same surface profile sampling frequency (1000 samples/mm), detail level (level 6) and wavelet type (db2), as outlined in Section 5.6. W_{DWT} values provide a wear value for individual sidewalls, however, a single wear measure was required per channel in order to compare to punch force. A W_{DWT} sum has been utilised in order to provide a single wear value for each part, this is simply the sum of the two W_{DWT} values calculated for each side of a part.

6.3 Wear progression results

W_{DWT} sum values were calculated for a selection of 39 and 36 channel parts from extended trial 1 and extended trial 2 respectively. These parts spanned the duration of the trials and provided a sampling of parts representing progressive levels of

galling severity. The development and progression of wear damage severity with stroke number are presented in Figure 6.1.

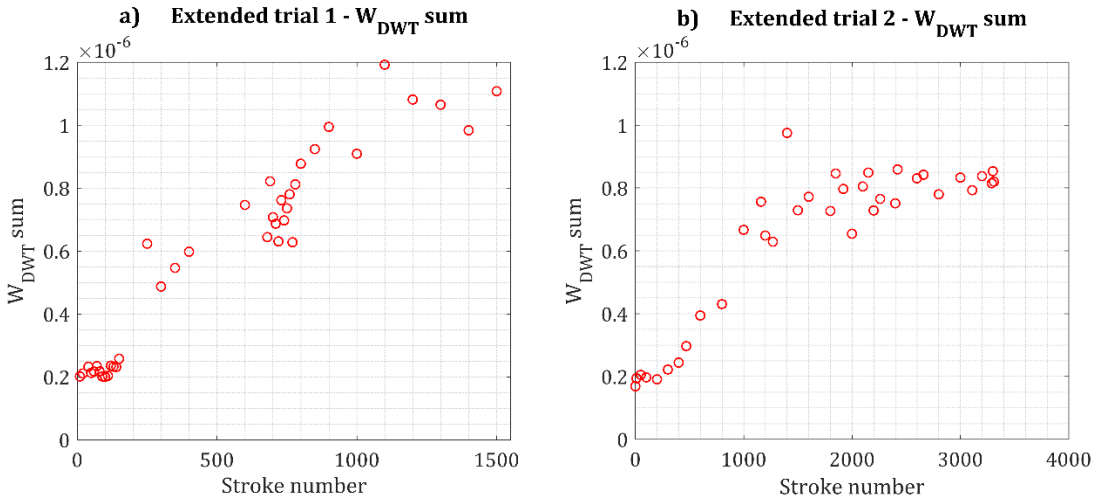

Figure 6.1: W_{DWT} sum progression for Extended trial 1 and 2. a) W_{DWT} values with stroke for extended trial 1. b) W_{DWT} values with stroke for extended trial 2.

Extended trial 1 (Figure 6.1a) shows an unworn period for strokes 1-150 followed by a sudden increase in galling wear severity at stroke 250, this is apparent from both detail coefficients and sidewall investigation. After stroke 250 there is continuous progression in galling wear damage severity for the remainder of the trial. Figure 6.2 shows the detail coefficient of both part sidewalls for parts at various strokes throughout the trial to demonstrate the sudden development of galling wear and its progression throughout extended trial 1. Figure 6.2 demonstrates the continuous progression of galling wear severity throughout the trial. With detail coefficients of the relatively unworn part 140, followed by part 250 that exhibits significant galling wear damage on the edges of the C01 sidewall. Damage then develops on the C02 sidewall, and damage sites grow resulting in galling wear damage sites across the C01 sidewall.

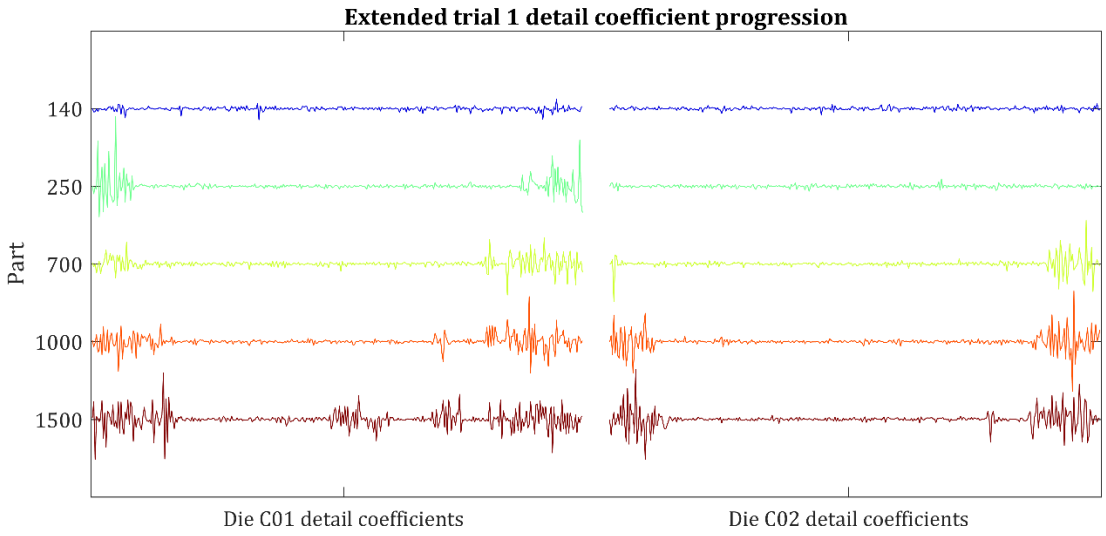

Figure 6.2: Extended trial 1 progression of detail coefficients for both die corner inserts, demonstrating galling wear development at locations on both dies for a series of parts from throughout the trial.

Extended trial 2 (Figure 6.1b) also showed an initial unworn period for strokes 1-300 followed by a gradual increase in galling wear damage severity up to stroke 1600. Stroke 1600 onwards sees a plateau in galling wear severity, this is also apparent from both detail coefficients and sidewall investigation. Figure 6.3 demonstrates this initial progression and plateau of galling wear severity. The detail coefficients of part 200 and part 800 show the relatively unworn surface and initial increase in galling wear severity respectively. The detail coefficients of parts 1600, 2800 and 3110 all exhibit the plateaued level of galling wear severity that begins after stroke 1600.

Figure 6.2 and Figure 6.3 also show the detail coefficients at the same scale without detail coefficient axis values, so as to demonstrate the relative severity and location. In both trials, galling wear damage develops first on the edges of the sidewalls and progresses towards the center over the course of the trials. This could be due to the anticlastic curvature of the blank and burring of its edges, which results in increased contact pressure at the edges where wear initiates.

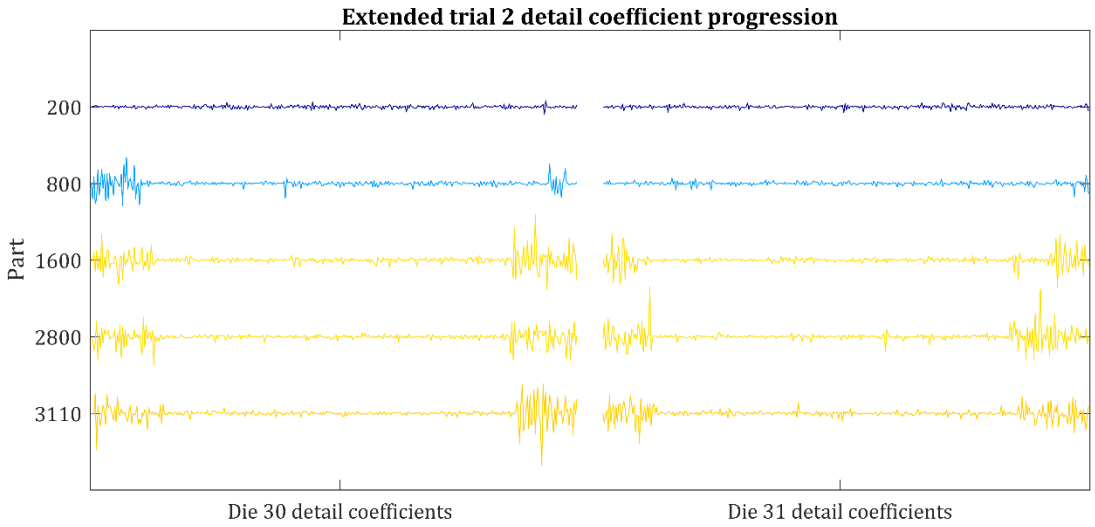

Figure 6.3: Extended trial 2 progression of detail coefficients for both die corner inserts, demonstrating galling wear development at locations on both dies for a series of parts from throughout the trial.

6.4 Principal Component Analysis

PCA was conducted on punch force signatures of the extended wear trials in order to determine the dominant forms of explained punch force variation in the extended wear trials. Determining these forms of variation and associated b-values for each punch force signature of the parts formed during the trial allows for two aspects of insight. The first provides an understanding of the response of punch force signature variation for wear progression, which can be compared to the variation isolated in Chapter 4 for the distinct differences in wear level. The second aspect of insight is determining the relationship, if any, between specific forms of punch force signature variation and wear progression which has been measured using the W_{DWT} sum (Section 6.2).

6.4.1 Extended trial 1

The first four PCs of the PCA of extended trial 1 (representations shown in Figure 6.4) accounted for 98.37% of the explained variation in the data set (Table 6.1). This justifies the assessment of only the first 4 PCs. Where PC1 appears to represent a change in the overall magnitude of the punch force curve. This general form of signature shape variation was observed in the wear and friction condition trials in

Section 4.3.2 and Section 4.3.3, and was theorised to be linked to and an indicator of overall friction for individual strokes.

PC2 appears to have a slight variation in the magnitude of the signature plateau but also a late stroke increase in punch force that is due to the slightly extended duration of the stroke holding or increasing punch force right up to maximum punch travel.

PC3 appears to describe variation in the slope of the signatures plateau, with positive and negative b-values representing varying degrees of slope in the progression of punch force with stroke. This general form of signature shape variation was observed and found to be significant in the friction condition trial in Section 4.3.3, and with it theorised to be linked to and an indicator of dynamic friction changes during the stroke.

PC4 appears to describe variation in the progression of the signature plateau with pivots between positive and negative examples at approximately 19 mm and 36 mm punch displacement. Again, this form of signature shape variation is likely due to dynamic friction changes during the stroke; however, this high frequency change in punch force trajectory suggests unstable friction conditions during the stroke. However, this PC only accounts for 0.62% of the explained variation.

Table 6.1: Extended trial 1 Principal Component percentage of explained variation for first 4 dominant Principal Components.

Combined data set PC	Percentage of explained variation
1	87.30%
2	8.37%
3	2.10%
4	0.62%
Total	98.37%

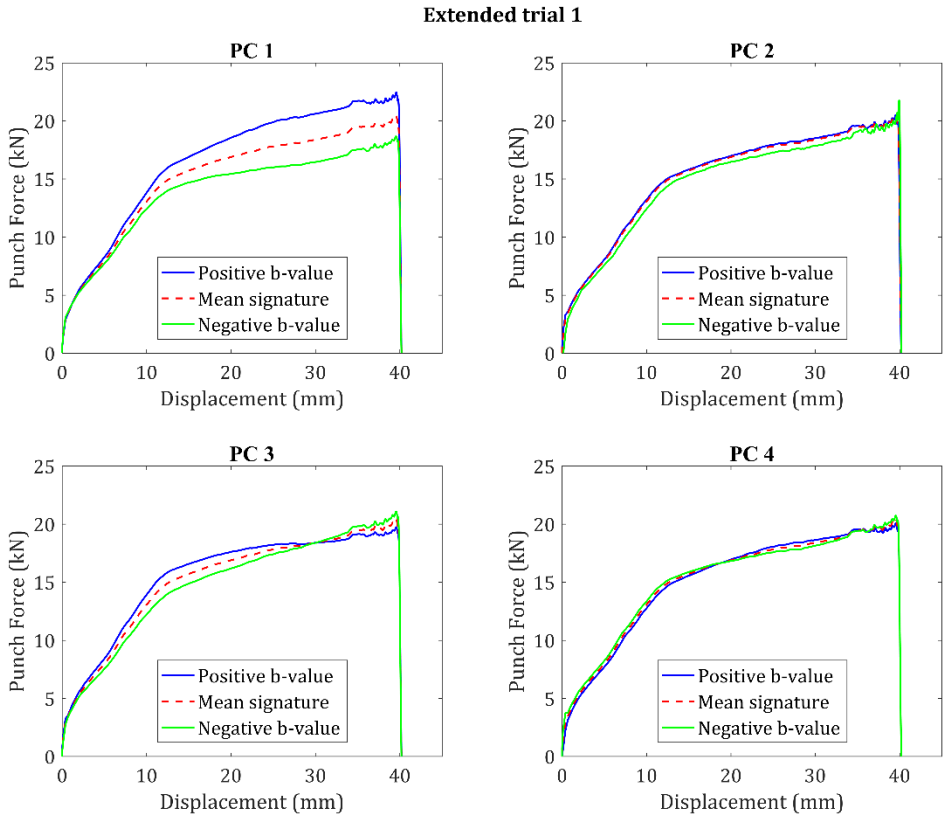

Figure 6.4: Extended trial 1 punch force signature PCA Principal Component 1-4 representations.

6.4.2 Extended trial 2

The first four PCs of the PCA of extended trial 2 (representations shown in Figure 6.5) accounted for 96.59% of the explained variation in the data set (Table 6.2). Again, justifying the assessment of only the first 4 PC.

The PCs calculated for punch force signatures of extended trial 2 appear to represent largely the same variation shapes in the same order of significance as those seen for extended trial 1. The main apparent discrepancy between results of extended trial 2 and extended trial 1 regards the sign of representative signature shapes being reversed. For example, PC1 in both analyses shows a signature of larger than average magnitude, however, the example is listed as a positive b-value for trial 1 and a negative b-value for trial 2, this is due to where the average sits. The sign/direction of these Principal Components are a result of the projection during the calculation and do not change the variation they describe, and so PC1 in both extend trials have been interpreted as describing the same general form of shape variation.

Table 6.2: Extended trial 2 Principal Component percentage of explained variation for first 4 dominant Principal Components.

Combined data set PC	Percentage of explained variation
1	65.62%
2	22.79%
3	7.04%
4	1.14%
Total	96.59%

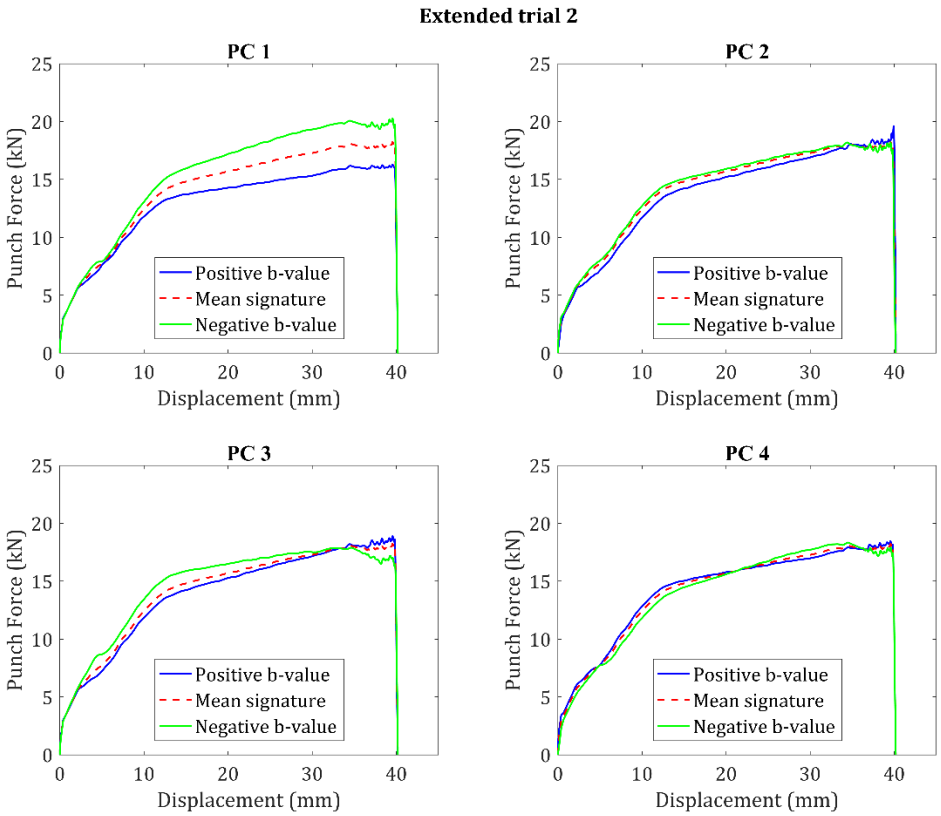

Figure 6.5: Extended trial 2 punch force signature PCA Principal Component 1-4 representations.

6.5 Principal Component and wear progression comparison

The b-values for PC 1-4 were calculated for each part in both extended trial punch force data sets and values for the parts with corresponding W_{DWT} measurements were isolated.

In order to determine if any of these individual PCs or forms of punch force signature shape variation are correlated with wear progression, an initial assessment of the

relationship between PC b-values and W_{DWT} sum was conducted through determining Pearson's correlation coefficients for extended trial 1 and extended trial 2. Pearson's correlation coefficient provides an indication of the strength of linear relationships between variables and an indication of the nature of that relationship, positive or negative, with values of -1 and 1 indicating perfect negative or positive linear correlation and a value of 0 indicating no linear relationship. The results of the Pearson's correlation calculations for extended trial 1 [n = 39] are reported in Table 6.3 and individual b-value with W_{DWT} sum scatter plots are shown in Figure 6.6.

Table 6.3: Pearson's correlation results for extended trial 1 PC b-values with W_{DWT} sum parameter.

Parameter	r	*p*-value
b1	0.9054	<0.001
b2	-0.0236	0.89
b3	0.0336	0.84
b4	-0.0068	0.97

The b1 values for extended trial 1 were found to have a positive correlation with W_{DWT} sum for the trial [r = 0.9054, p < 0.001], with increases in b1 corresponding to increases in W_{DWT} sum. The remaining b-values for PCs 2-4 were not found to have linear correlation with W_{DWT} sum in this trial based on Pearson's correlation coefficients. These results suggest a strong linear correlation between PC1 or overall punch force signature magnitude and W_{DWT} sum or galling wear severity progression. While the remaining dominant PCs, including PC3 that is theorised to be linked to dynamic friction changes, were not found to be correlated to galling wear severity progression.

Some clustering is apparent in the extended trial 1 b-value W_{DWT} sum scatter plots, where W_{DWT} sum equals approximately 0.2e-06, and this is a result of significant increase in galling wear damage severity between sampled parts, from essentially no wear to the development of a large galling wear damage track, as was highlighted in Section 6.3.

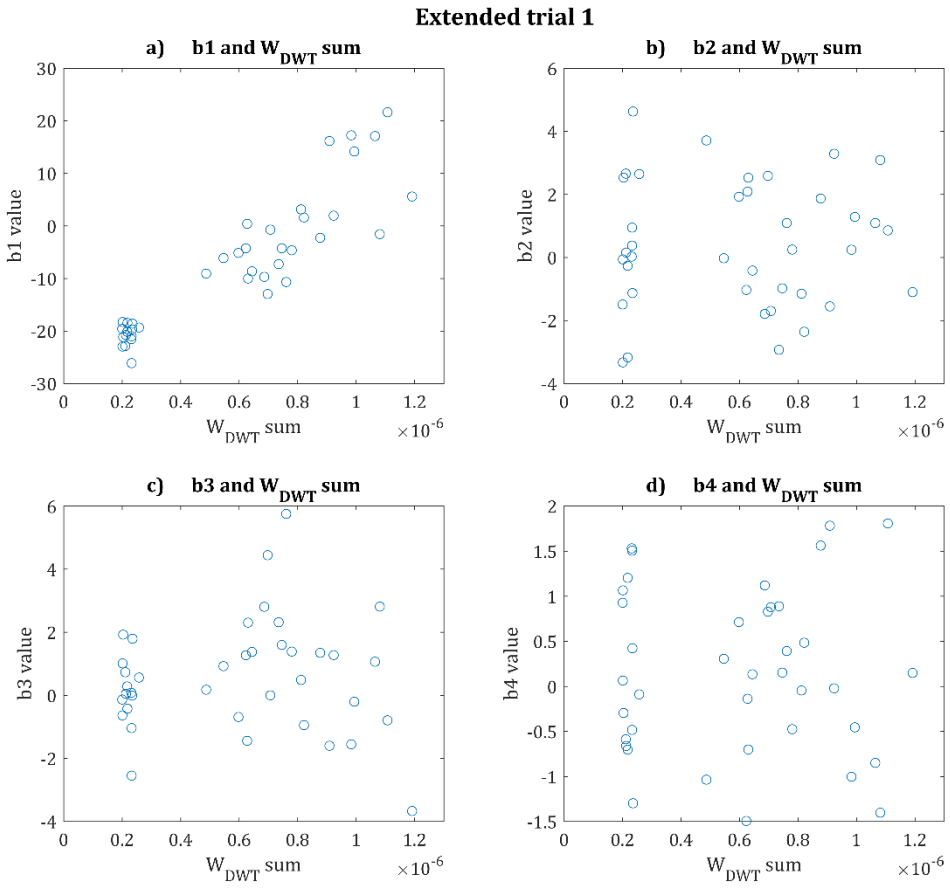

Figure 6.6: Extended trial 1 b-value with W_{DWT} sum parameter scatter plots. a) PC1 b-values (b1) with W_{DWT} sum. b) PC2 b-values (b2) with W_{DWT} sum. c) PC3 b-values (b3) with W_{DWT} sum. d) PC4 b-values (b4) with W_{DWT} sum.

The results of the Pearson's correlation calculations for extended trial 2 [n = 36] are reported in Table 6.4 and individual *b*-value with W_{DWT} sum scatter plots are shown in Figure 6.7.

Table 6.4: Pearson's correlation results for extended trial 2 PC b-values with W_{DWT} sum parameter.

Parameter	r	*p*-value
b1	-0.7024	<0.001
b2	-0.3018	0.074
b3	-0.5074	0.0016
b4	-0.1923	0.26

The b1 values for extended trial 2 were found to have a negative correlation with W_{DWT} sum for the trial [r = -0.7024, p < 0.001], with decreases in b1 corresponding to increases in W_{DWT} sum. This negative correlation is a result of the inverse direction of the PCs of extended trial 2 to what was seen in the PCs of extended trial 1. This PC represents the magnitude of the signature which is the same general form

of punch force signature variation isolated in PC1 of the extend trial 1 PCA. The b3 values were also found to have a moderate statistically significant negative correlation with W_{DWT} sum [r = -0.5074, p = 0.0016]. This PC represents the slope of punch force progression with negative b-values representing a decrease in force at the end of the stroke. This PC also represents a general form of signature shape variation that was also captured in the PCA of extended trial 1.

The analysis of punch force signatures from extended trial 2 also suggest a strong linear relationship between the magnitude of the punch force signature and galling wear progression. The results of the analysis also suggest a moderate linear correlation between galling wear severity and the slope of punch force progression during the stroke, however, this correlation was not observed in the analysis of extended trial 1. Some clustering of W_{DWT} sum values for extended trial 2, seen at approximately 0.2e-06 and 0.8e-06. These two values represent unworn surface and the steady state galling wear damage that was discussed in Section 6.3.

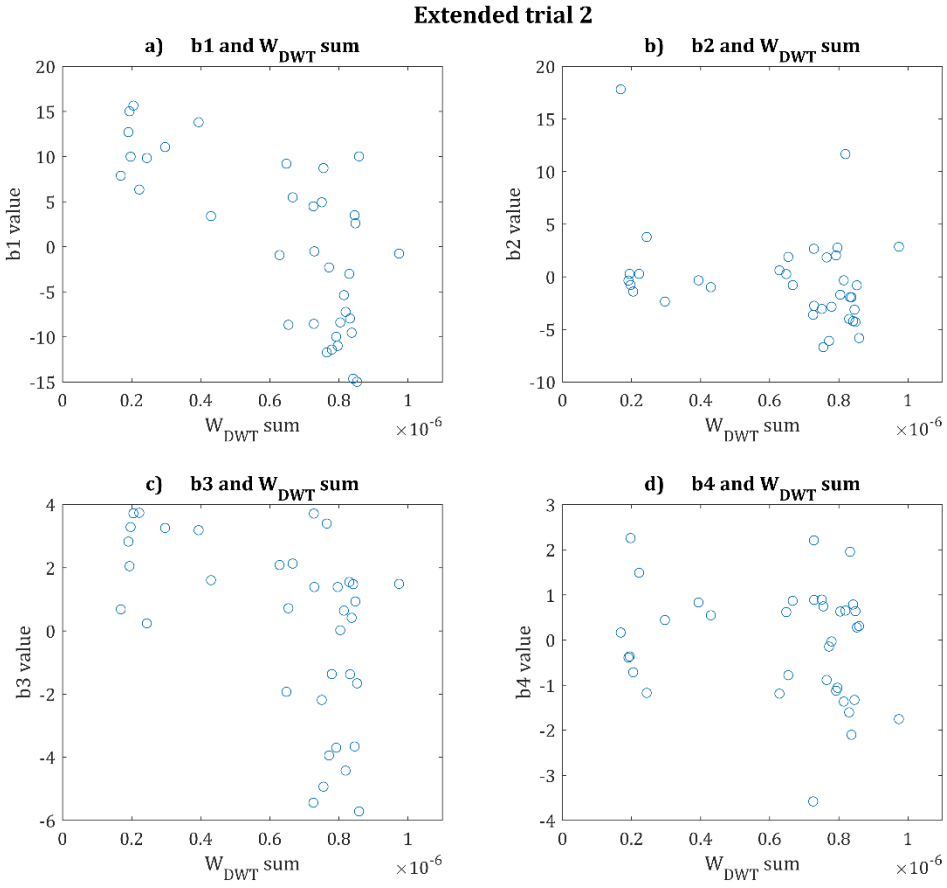

Figure 6.7: Extended trial 2 b-value with W_{DWT} sum parameter scatter plots. a) PC1 b-values (b1) with W_{DWT} sum. b) PC2 b-values (b2) with W_{DWT} sum. c) PC3 b-values (b3) with W_{DWT} sum. d) PC4 b-values (b4) with W_{DWT} sum.

These results indicate that the main form of signature shape variation found to be related to galling wear for this analysis was magnitude. Magnitude of the punch force signature is conceptually similar to peak force, which as a punch force signature feature is much simpler to collect than forms of signature variation. However, peak force reduces information from the entire stroke to a single data point and discards other potentially useful information. To compare peak force to the magnitude of the signature captured using PCA the relationship between peak force values and W_{DWT} sum value for the extended trials was assessed using Pearson's correlation coefficients, as shown in Table 6.5.

Table 6.5: Pearson's correlation results for peak force and W_{DWT} sum from extended wear trials.

Trial	r	*p*-value	*N*
Extended trial 1	0.8373	<0.001	39
Extended trial 2	0.5333	<0.001	36

Peak force for both extended trials was found to have statistically significant positive linear correlations. However, the linear relationship for peak force is weaker for both extended trials than punch force magnitude that was captured by PC1 in both trials. This indicates that punch force signature magnitude captured using PCA provides a more complete picture of the current state of galling wear severity.

6.6 Wear progression discussion

As part of this investigation into the link between galling wear progression and punch force signature variation, galling wear progression was measured in two extended wear trials. These measurements demonstrated the DWT galling wear methodology again for tracking localised wear development and spread. The results of these measurements showed two forms of progression: (i) continuous increasing progression for extended trial 1 and (ii) plateaued wear damage in extended trial 2. The wear severity progression in these two trials demonstrate one of the potential issues with quantifying galling wear in industrial forming situations, with very different types of severity progression under similar forming conditions. The

additional galling damage tracks in the center of the sidewall did not develop in extended trial 2, even after the formation of 3000 parts, as opposed to 1500 parts in extended trial 1. PC1 in both analyses generally described variation in the magnitude of the punch force, accounting for 87.3% and 65.62% of the explained variation in extended trial 1 and 2 respectively. PC2 in both trials captured the general form of shape change associated with slightly extended application of load at maximum displacement, that appears to be associated with the first stroke once the press is started. This form of punch force signature shape variation accounted for significantly more of the explained variation in extended trial 2 than in extended trial 1. Issues with emergency stop equipment on the press meant that extended trial 2 was stopped and restarted more frequently than extended trial 1, leading to an increased number of these over extended strokes, and hence the increased dominance of the associated PC.

Comparison of b-values to W_{DWT} sum values showed a relationship between punch force signature magnitude and galling wear severity progression. This linear relationship is intuitive, if magnitude of the punch force signature corresponds to an increase in the overall friction between blank and tooling. Given galling wear is the major changing factor in the trial, and increases in galling wear correspond to increase in friction, the punch force signature magnitude should increase accordingly. It should be noted that this linear relationship was weaker in extended trial 2, due to punch force magnitude (captured by PC1) increasing after the W_{DWT} sum values had plateaued. This indicates that some factor other than overall severity of galling wear damage is influencing an increase in friction and consequently punch force magnitude. A negative trend in b3 values is seen in extended trial 2 that is not observed in extended trial 1 (Figure 6.8d and b respectively). Figure 6.8 shows the progression of the relevant b-values (PC1 and PC3) with stroke for both extended trials, linear trend lines show the general direction of progression during the trials. The negative b3 values in extended trial 2 indicate higher early stroke punch force and a more consistent punch force over the course of the stroke. Given that other friction influencing factors were held constant for the extended trials, the higher than average early stroke punch force could be caused by a dominance of the adhesion mechanism in the galling that takes place. Adhesion results in higher friction than abrasion, the other mechanism observed with galling (Section 2.3.3). Therefore, if adhesion is the dominant mechanism early

in the stroke then that would explain the increase in punch force. A general increase in b-value scatter with stroke is also apparent in b-values for extended trial 1, indicating increased variability in both punch force magnitude and progression and unstable friction conditions. This could also be evidence of change in the dominant wear mechanism as the severity of galling wear damage increased.

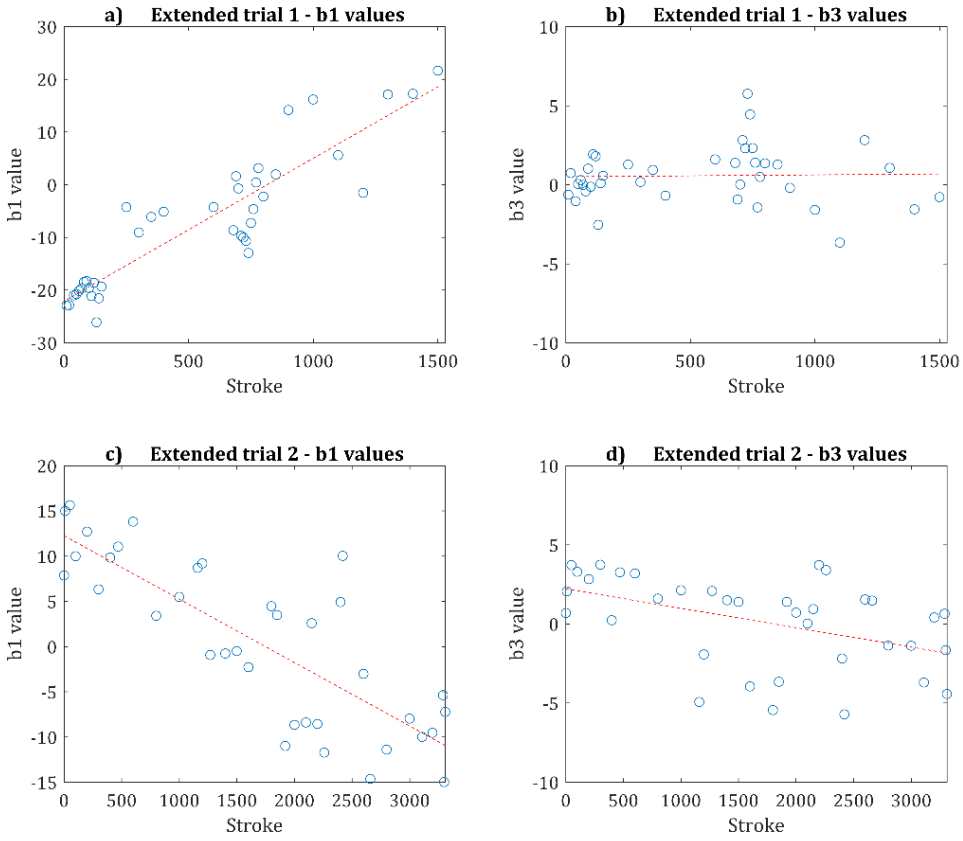

Figure 6.8: Progression of b1 and b3 values with stroke for extended trials 1 and 2. a) Extended trial 1 b1 values showing increasing trend that corresponds to increasing punch force signature magnitude. b) Extended trial 1 b3 values showing a neutral trend, indicating no linear bias in the variation of slope of punch force signature plateau for the trial. c) Extended trial 2 b1 values showing decreasing trend that corresponds to increasing punch force signature magnitude. d) Extended trial 2 b3 values showing a decreasing trend that corresponds to punch force signatures of the trial having higher force at the beginning of the stroke and a flatter signature plateau as the trial progressed.

Wear mechanism change during the stroke cannot be assessed using a single measurement on the part sidewall. It is also challenging to gain an understanding of how those changes effect friction and influence punch force signatures based on sparsely sampled parts, as growth of the damaged regions also changes friction conditions. Additional investigation is required to understand the effects of

dominant wear mechanism on punch force signatures, this is addressed in Chapter 7 by assessing consecutively formed parts so as to keep wear damage region size consistent and multiple galling wear measurements are taken down the sidewall of the parts.

One aspect of this thesis is to demonstrate that PCA is an appropriate tool for describing and tracking the relationship between punch force signatures and galling wear. PCA as applied in this thesis requires interpretation before it can be utilised for developing wear monitoring regimes, and so it is important that the method extracts additional useful information that simpler features such as peak force cannot provide. Only one form of signature shape variation captured using PCA was found to be strongly related to galling wear progression in this investigation, however, there is reason to believe that other forms of shape variation may contain information about wear state, such as PC3 from the analysis of the extended trials. These other forms of signature shape variation and their relationship to wear state will be investigated further in Chapter 7. This will strengthen the case for PCA of punch force signatures for use in wear monitoring regimes over simpler features of punch force signatures such as peak force.

6.7 Summary

In this chapter the relationship between galling wear progression in extended semi-industrial deep drawing trials and punch force signature variation was investigated. Two extended semi-industrial deep drawing wear trials were conducted, and galling wear severity measurements collected from throughout the trials were compared to PCA results of the corresponding punch force signatures.

The measurement of galling wear severity in the two extended trials again demonstrated the DWT galling wear methodology, showing growth of localised wear development. The results of these measurements showed two forms of progression, continuous increasing progression for extended trial 1 and plateaued wear damage in extended trial 2.

Pearson's correlation coefficients were used to determine if a linear relationship was present between individual forms of punch force signature shape variation and

W_{DWT} sum values for the parts. A strong linear relationship was found between the PCs that represent variation in the magnitude of the punch force signature and W_{DWT} sum for both extended trials. No linear relationships were found between other dominant PCs for extended trial 1 where wear progression was consistent for the trial.

A statistically significant but weak linear relationship between PC3 and W_{DWT} sum was found for extended trial 2, where PC3 represented dynamic changes in friction during the stroke, the same linear relationship was not seen in extended trial 1.

The relationship between peak force values and galling wear severity was also assessed for the extended trial. The peak force values were found to have a linear relationship with galling wear severity, but this relationship was weaker than that found with punch force signature magnitude captured using PCA.

These results have demonstrated a clear relationship between galling wear progression and punch force signature variation. Other observations, such as the trend in PC3 b-values of extended trial 2, indicate that additional information about wear state is also captured in the variation of the signature shape, however, further investigation is required in order to understand these relationships.

CHAPTER SEVEN

Wear and lubrication mechanism effects on punch force

7.1 Introduction

The results presented in Chapter 4 and Chapter 6 have demonstrated the link between punch force signature variation and wear and other friction influencing factors. The Principal Component Analysis (PCA) conducted on various punch force signature data sets found common general forms of shape variation in punch force signatures collected under progressive and distinct die wear levels, and various blank holder force (BHF) and lubrication regimes. Notable general forms of signature shape variation included one associated with the magnitude of the signature, and another associated with punch force progression or the slope of the signature plateau. In this Chapter these forms of punch force signature variation are investigated to confirm previous hypotheses of their cause.

Chapter 4 proposed that the form of signature shape variation linked to overall magnitude of the signature is associated with the friction between the blank and the tooling. This proposal was based on the observed difference in signature magnitude between the different tested forming parameters that are linked to friction: die wear level, BHF, and lubricant type. In Chapter 6 forms of punch force signature variation that describe the signature magnitude were found to have a strong linear relationship with galling wear severity. This again suggested that signature magnitude is driven by friction between the blank and the tooling, which increased with the development of galling on the die inserts.

To confirm that variation related to the magnitude of the signature is linked to the coefficient of friction, the b-values for the punch force signatures formed under different lubrication regimes have been compared to experimentally determined coefficient of friction results for the lubricants. The effects of BHF and wear on friction are also discussed.

The form of punch force signature shape variation associated with punch force progression or the slope of the signature plateau was hypothesised to be linked to mid-stroke changes in friction. This hypothesis was based on differences observed between unlubricated and lubricated punch force signatures (Section 4.3.3); and also, the increased magnitude and range of associated b-values when signatures were collected with die corner inserts effected by galling wear (Section 4.3.3 and Section 6.6).

To investigate these hypothesised links to lubricant and galling wear driven dynamic friction changes, two experiments were conducted. Firstly, the effect of lubrication was investigated by updating the friction condition punch force signature data set (Section 4.3.3) to include additional dry lubrication types. These new dry lubricants were assumed to maintain a consistent lubrication mechanism over the course of the stroke; allowing for comparison of consistent lubrication regimes to fluid lubrication.

Secondly, the influence of galling wear was investigated by assessing galling wear damage on consecutive formed parts and comparing this damage to b-values. It was assumed that friction changes during the stroke that influence punch force progression are due to mid-stroke wear developments. Galling wear is characterised by progression through multiple mechanisms, including abrasion and adhesion, that come with distinct levels of friction (Section 2.3.3). It was theorised that specific galling mechanism or localised severity of wear damage was driving the dynamic friction change. A change in the dominant mechanism, either adhesion or abrasion, over a series of consecutively formed parts could cause the variation in punch force signature progression or plateau slope that was isolated by PC2 in the wear comparison (Section 4.3.2). This was tested through assessment of galling damage at various locations on the part sidewalls and comparison to the associated b-values.

The main outcomes to be presented in this Chapter were published in the peer reviewed proceedings of the 36th International Deep Drawing Research Group conference 2017 (Voss et al., 2017).

7.2 Experimental design

A new set of lubrication trials were conducted to include dry film lubricant for investigation into dynamic friction during a stroke. Dry film lubrication regimes maintain boundary lubrication (Van Rensselar, 2017) and so two new dry lubricants have been added to the secondary lubrication comparison. The new lubricants were aerosol applied dry PTFE coating, and PTFE fiberglass sheeting. Both of the new dry film lubrication regimes were applied to the blank material prior to forming. To ensure that punch force signatures were consistent and comparable between lubrication trials, new iterations of lubrication trials were conducted for the regimes previously outlined in Section 4.3.3. These included: unlubricated, mill oil, drawing lubricant, mineral oil, and Ionic Liquid (IL). These trials were conducted using the semi-industrial stamping press channel forming process (Section 3.3.1) and full details of trial parameters are seen in Table 7.1.

Table 7.1: Secondary lubrication comparison data set details.

Secondary lubrication comparison set details						
Lubricant	**Average BHF**	**Wear level**	**Number of parts**	**Die insert material**	**Die corner radius**	**Blank material**
Mill oil	28 kN	No-wear	38	PVD	5 mm	HLSA300
Unlubricated	28 kN	No-wear	50	PVD	5 mm	HLSA300
Drawing lubricant	28 kN	No-wear	50	PVD	5 mm	HLSA300
Ionic liquid	28 kN	No-wear	50	PVD	5 mm	HLSA300
Mineral oil	28 kN	No-wear	50	PVD	5 mm	HLSA300
Dry PTFE coating	28 kN	No-wear	50	PVD	5 mm	HLSA300
PTFE sheet	28 kN	No-wear	50	PVD	5 mm	HLSA300

In addition to the investigation into the effect of lubrication, the effect of galling wear was also considered. This investigation required assessment of parts with different b-values for the Principal Component (PC) representing the progression of punch force, but with similar quantities of wear damage. As the severity and mechanism of the galling wear damage was the focus of this investigation, parts with the same level of galling wear severity in the same relative locations were required. In order to collect parts that met these conditions a series of 150 parts were formed with heavily worn die corner inserts, designation C01 and C02, and each of these formed parts were collected. These parts were considered to have largely consistent galling wear damage severity, however the trial was long enough to see some variation in b-values for the PC2, the form of shape variation of interest. The die corner inserts (C01 and C02) had previously formed 1530 channel parts for extended trial 1 detailed in Chapter 6.

7.3 Results

7.3.1 PCA results

Punch force signatures for the secondary lubrication trials were collated into a single data set and PCA was applied. The PC representations and b-value column scatter plot are shown in Figure 7.1 and Figure 7.2 respectively. For clarity the median b-values for each trial are shown in Table 7.2. The two most significant PCs represent the forms of shape variation associated with signature overall magnitude and progression of punch force over the stroke. These two forms of shape variation are the focus of investigation in this Chapter. This set of PCs and associated b-values are not directly comparable to those presented in Chapter 4 due to slight variation in press setup, lubricant batch variation, and die corner insert alignment. However, it is evident from the PC representations (Figure 7.1) that they describe the general forms of signature shape variation previously discussed in Chapter 4. As the two most dominant PCs represent the forms of punch force signature shape variation of interest (magnitude and progression slope), the P-matrix calculated using the secondary lubricant comparison data set will also be used to calculate b-values for the wear trial punch force signatures presented in Section7.3.4.

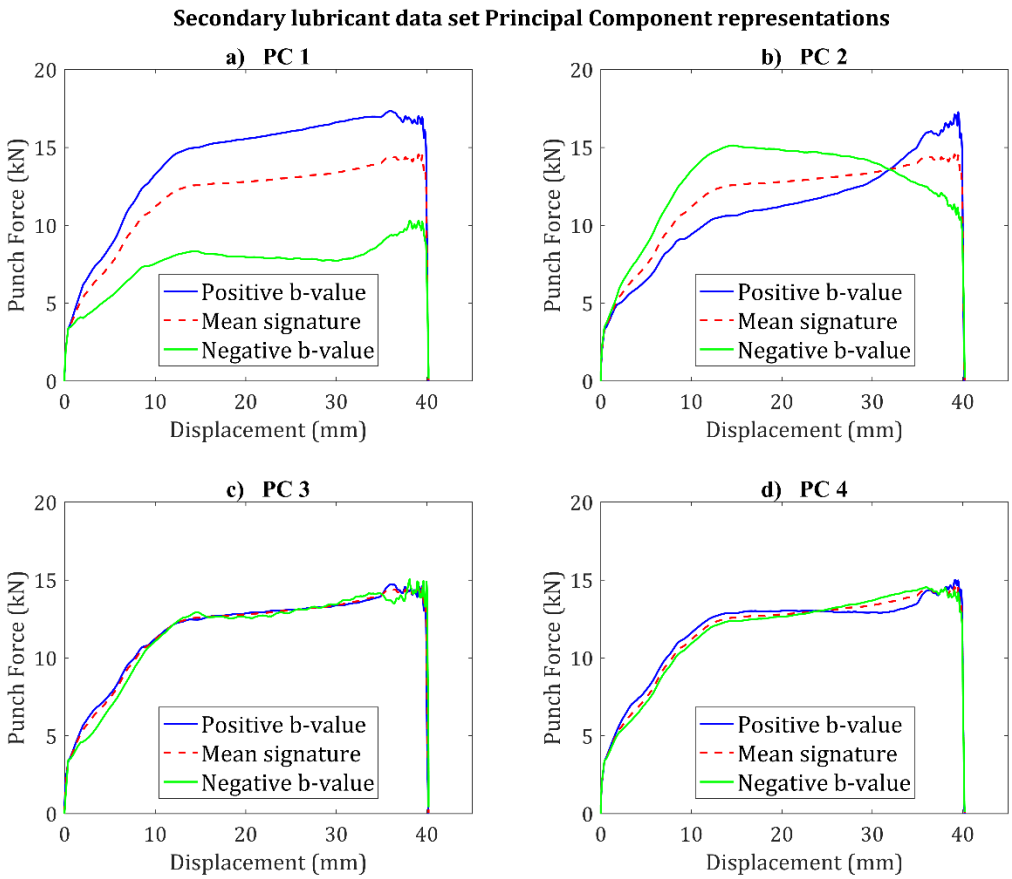

Figure 7.1: Secondary lubrication comparison data set dominant Principal Component representations. a) PC representation 1, b) PC representation 2, c) PC representation 3, d) PC representation 4.

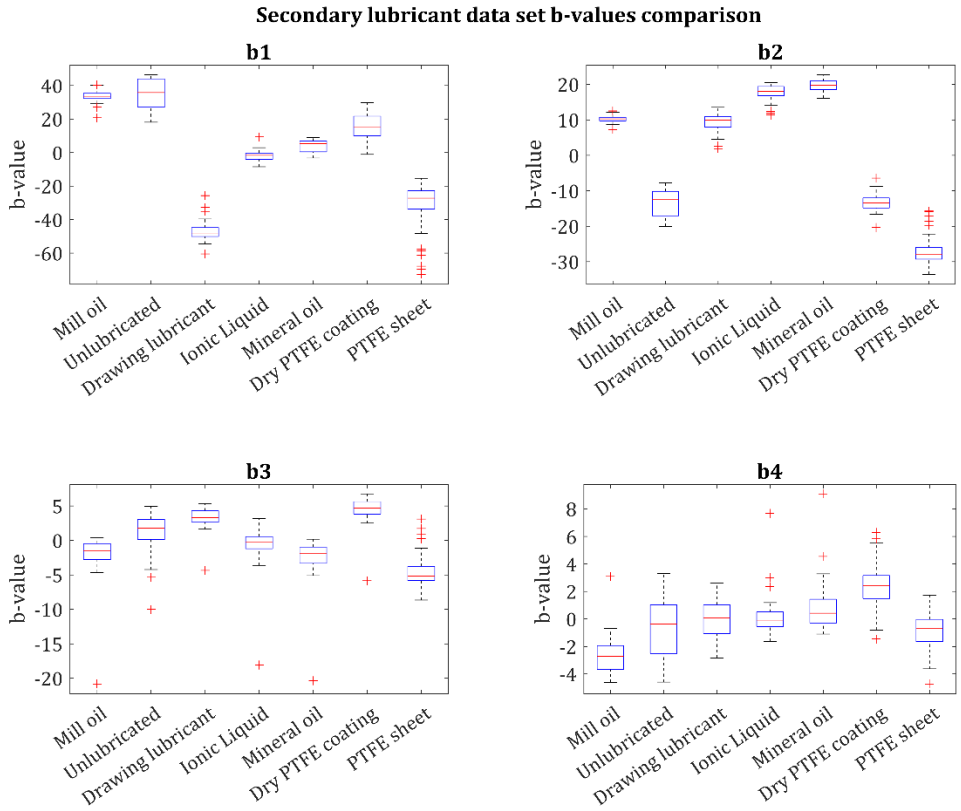

Figure 7.2: Secondary lubrication comparison data set b-value column scatter plots for 4 dominant PCs. a) b_1 values, b) b_2 values, c) b_3 values, d) b_4 values.

Table 7.2: Secondary lubrication comparison lubricant trial - mean b-values for 4 dominant PCs.

Lubrication	Median b1	Median b2	Median b3	Median b4
Mill oil	33.59	10.27	-1.48	-2.73
Unlubricated	35.75	-12.38	1.78	-0.37
Drawing lubricant	-48.04	9.94	3.27	-0.06
Ionic liquid	-1.71	17.98	-0.21	-0.09
Mineral oil	5.15	19.82	-1.94	0.42
Dry PTFE coating	15.38	-13.45	4.69	2.40
PTFE sheet	-27.25	-27.87	-5.18	-0.67

The b-value column scatter plots demonstrate the clear separation between lubricant trials in the two most significant PCs (Figure 7.2a-b). The only notable exceptions are the similarity of mean b1 values between mill oil and unlubricated and the similarity between mineral oil and the ionic liquid lubricant for both b1 and b2. The ionic liquid lubricant consisted of an ionic liquid additive in a mineral oil base, explaining the similarity between the ionic liquid lubricant and mineral oil despite marginally lower b1 and b2 values of the ionic liquid (IL) that indicate lower frictional performance. The separation between the unlubricated and mill oil trials was more distinct in the friction conditions comparison detailed in Figure 4.7. Separation of the median b2 values for these two conditions is still evident, however, b1 medians are very similar and the ranges have near complete overlap. To investigate this newly observed similarity the mean punch force signatures for the mill oil and unlubricated trials in both the original and secondary comparison data sets are shown in Figure 7.3.

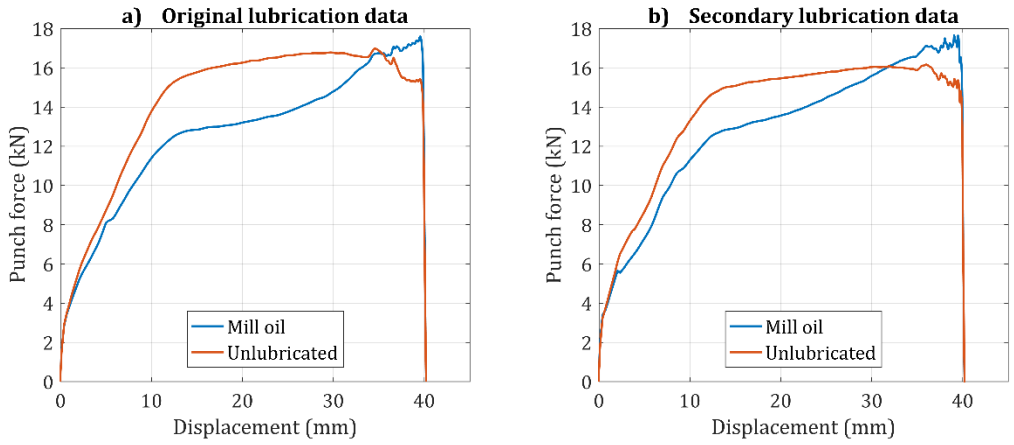

Figure 7.3: Mill oil and unlubricated trial mean signatures for original and secondary trials.

It is apparent from the mean punch force signatures in Figure 7.3 that the secondary unlubricated signatures are on average 1kN lower in magnitude than the original unlubricated signatures presented in Chapter 4. The two mill oil mean signatures appear similar in magnitude, however there is a slight difference in punch force progression. The original mean signature maintains a lower punch force level from 10 mm to 25 mm and then increases aggressively, and this would be unlikely to influence the magnitude form of signature shape variation. Blank material and tooling were cleaned with ethanol prior to forming in the unlubricated trials, and the consistent punch force level indicates that lubrication contamination is unlikely to have caused the disparity between unlubricated trials. Lin, Wang and Huang (Lin et al., 1992) noted increased drawing speed can reduce friction in low speed unlubricated deep drawing of aluminium, however, drawing speed was maintained constant for the trials. Slight variation in the average blank holder force between the original and secondary trials may explain the difference in magnitude and hence the lack of significant separation between secondary unlubricated and mill oil mean b-values.

7.3.2 Punch force signature magnitude

The most significant PC isolated in every comparison data set were associated with the overall magnitude form of punch force signature shape variation. The comparison data sets (Chapter 4) varied parameters that influence wear in sheet metal forming (lubrication, BHF, pre-existing wear). These parameters are also closely linked to friction between the blank and tooling (Kim and Kardes, 2012). Intuitively, if these parameters are varied the level of friction will also vary, and as punch force is strongly linked to frictional force restraining the blank, it is expected that the punch force signature will reflect this overall change in friction.

The effect of BHF on friction can be inferred from the mechanics of the deep drawing. Punch force acts in equilibrium with tension in the blank - a result of the restraining force applied and friction between the surfaces. An increase in this restraining force, or BHF, will necessarily increase the tension and drive an increase in punch force. Consequently, an increase in BHF should increase the magnitude of punch force signature, and this was observed in Section 4.3.3.

The quantitative effect on friction that a distinct increase in wear had on friction could not be measured in the semi-industrial channel forming trials. However, increased wear damage increases friction, and based on the same argument used for BHF, an increase in friction will increase tension in the blank and consequently increase punch force. This increase in punch force with wear was also observed in Section 4.3.3.

By assessing experimentally determined coefficients of friction for the lubricants listed in Table 4.2 and Table 7.1, it is possible to confirm the link between punch force magnitude and friction changes. It should be noted that friction varies over the course of the stroke, and this will be discussed in relation to the other dominant form of punch force signature shape variation in Section 7.3.3.

Pin-on-disc tests conducted by Raggatt (Raggatt, 2013) determined the frictional and wear characteristics of a number of the lubrication regimes examined in this thesis including unlubricated, mill oil, mineral oil, and IL. These coefficients of friction have been compared to average b-values for the trials of the secondary lubricant comparison. While the pin-on-disc experimental geometry differs significantly from the semi-industrial channel forming test, the difference between lubricant coefficients of friction determined in this manner still provide useful insight. The relative difference between lubricants can be reasonably compared b-values of the secondary lubrication data set. The median b-values for the PC1 (Figure 7.1a) are compared to the experimentally determined coefficients of friction in Table 7.3.

Table 7.3: Lubricant trial mean b1 value and experimentally determined coefficients of friction comparison.

Lubricant	**Median b1**	**Coefficient of friction**
Unlubricated	35.75	0.8
Mill oil	33.59	0.15
Mineral oil	5.15	0.1
Ionic liquid (IL)	-1.71	0.1

The order of coefficients of friction and mean b-values shown in Table 7.3 broadly correlate, implying the relationship between coefficient of friction and punch force magnitude. A clear disparity is the similarity of median b1 values for the

unlubricated and mill oil trials, that do not reflect the difference in coefficients of friction. This similarity in b-values was not observed in the comparison of friction conditions in Section 4.3.3, where mean b-values for these two trials showed a significant difference. As was previously discussed in Section 7.3.1, this is due to an increase in the mill oil signature magnitude.

7.3.3 Lubrication effect on punch force signature progression

Mean punch force signatures were calculated for each of the secondary lubrication trials to provide a representation of signature shape for each lubricant type. The mean signatures have been separated into groups of fluid lubricants (Figure 7.4a) and dry lubricants or unlubricated (Figure 7.4b). The mean fluid lubricant signatures demonstrate the late-stroke force increase that has been hypothesised to be associated with inconsistent lubrication regimes during the stroke. The dry PTFE coating and unlubricated signatures exhibit stable punch force over the course of the stroke. Finally, the PTFE sheet mean signatures shows decreasing punch force, suggesting a decrease in friction over the stroke.

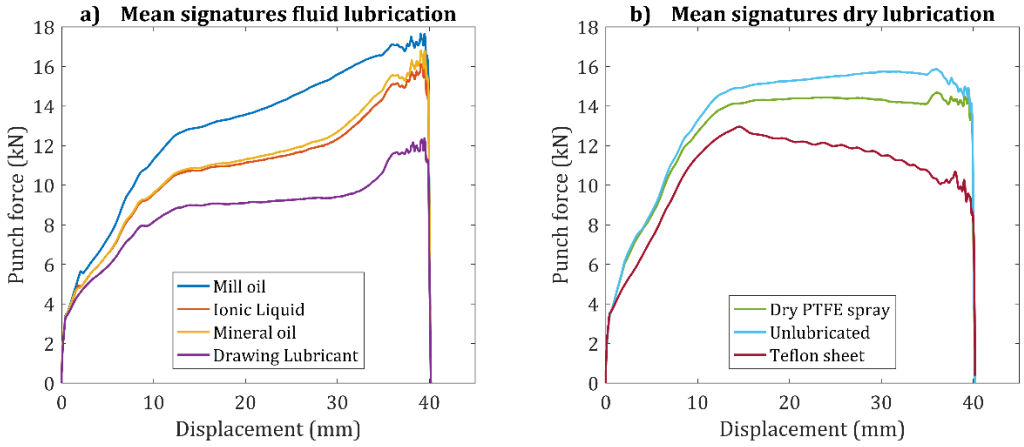

Figure 7.4: Secondary lubrication comparison trials mean punch force signatures.

PC2 and its associated b-values (Figure 7.1 and Figure 7.2b) show that dry PFTE coating and the unlubricated signatures are distinct from the fluid lubricants, with negative b-values that indicate more consistent punch force signatures or decreasing over the stroke. The mean signatures and b-values for these trials show

consistent punch force over the stroke and indicate stable friction conditions. These observations are consistent with dry lubricants maintaining boundary lubrication (Van Rensselar, 2017), and unlubricated maintaining consistent dry contact conditions. These observations also reinforce the theory that the late stroke increases in punch force seen with all of the fluid lubricant mean punch force signatures are the result of a transition from one lubrication mechanism to another mid-stroke; from mixed lubrication to boundary lubrication or even dry contact. It should be reiterated that the press ram speed changes from 300 mm/s to 0 mm/s during the stroke, as described in Section 3.3.1, however, this ram speed profile was consistent for all trials.

The PTFE sheet trial has a negative and the lowest median b2-value, indicating a downward trend in punch force over the stroke, as seen in Figure 7.1b. This suggests that friction is decreasing with stroke distance, which is contrary to the assumption that dry lubricants would maintain consistent friction levels over the stroke as a result of maintained single lubrication mechanism, boundary lubrication.

This initial high punch force and rapid decrease with stroke for Teflon/PTFE sheet lubrication has previously been observed in stamping (Bagheriasl et al., 2014) when assessing the effects of tool temperature. This punch force behaviour was not observed when a secondary fluid lubricant was tested in the study under the same conditions. The decrease in punch force with stroke could be a result of the low level of friction between blank and tooling when lubricated with the PTFE material. In this situation the punch force signature would steadily reduce with stroke as flange area decreases, matching the theoretical punch force – stroke curve described by Dieter (1961). Similar frictional behaviour was observed by Benati (2003) when assessing failure under different blank holder forces with Polyethylene sheeting, another low friction polymer sheet lubricant.

7.3.4 Wear effect on punch force signature progression

The PCs calculated for the secondary lubricant comparison punch force signatures have been used to determine b-values for the continuously sampled wear progression data. As outlined in Section 7.3.3, PC2 (Figure 7.1b) describes variation in the rate of increase or decrease in force over the course of the stroke. This form

of variation has been linked to mid-stroke friction changes due to lubrication mechanism in Section 7.3.3. The influence of the dominant sub wear mechanism within the broader galling wear on the form of punch force signature shape variation is assessed in this section. A positive b-value for PC2 indicates a distinct increase in punch force over the course of the stroke, and such a punch force signature shape suggests an increase in friction during the stroke. An increase in friction during the stroke in the wear trial may be a result of wear mechanism change to one associated with higher friction.

A selection of consecutively formed parts in the C01 and C02 extended wear trial were isolated for visual assessment, 2D profilometry, and b-value comparison, these selections formed 3 consecutive part sequences, see Table 7.4. These part sequences were selected due to significant changes in b_2 values.

Table 7.4: Extended wear trial consecutive part series'.

Consecutive part sequence	Included channel parts
1	1551, 1553, 1556
2	1559, 1560, 1562
3	1631, 1632, 1633, 1634

The focus of this initial visual assessment was adhesive wear damage late in the stroke, as the presence of the adhesive mechanism would drive an increase in friction over the abrasion mechanism. Comparing consecutively formed parts ensured that the area and number of galling wear sites remained relatively constant so that the galling wear mechanism was the only variable. This initial visual assessment and comparison of the parts in the consecutive sequences has shown that b_2 value increases correspond to an increase in adhesive wear damage on the late-stroke component of the galling tracks.

An example comparison of consecutively formed parts with a large range in b_2 values is seen in Figure 7.5. Each sidewall is subdivided into 8 sections labelled ***A*** through ***H*** to ease comparison of localised damage. An increase in adhesive wear damage can be observed on the late stroke regions of parts, from part 1632 to part 1634. When assessing part 1632 some adhesive damage including evidence of material pull out can be seen on sidewall C01 section E. On part 1633 the area of adhesive damage on

sidewall C01 section E has increased slightly, and additional adhesive damage is present in C01 section H and C02 section E. Finally, on part 1634 the area of adhesive damage in C01 section H and C02 section E has increased, while damage in C01 section E remains and new adhesive damage is present in C02 sections A and H. This progressive increase in adhesive wear damage, particularly on the late stroke regions of the sidewall, appears to correspond to an increase in b_2 value.

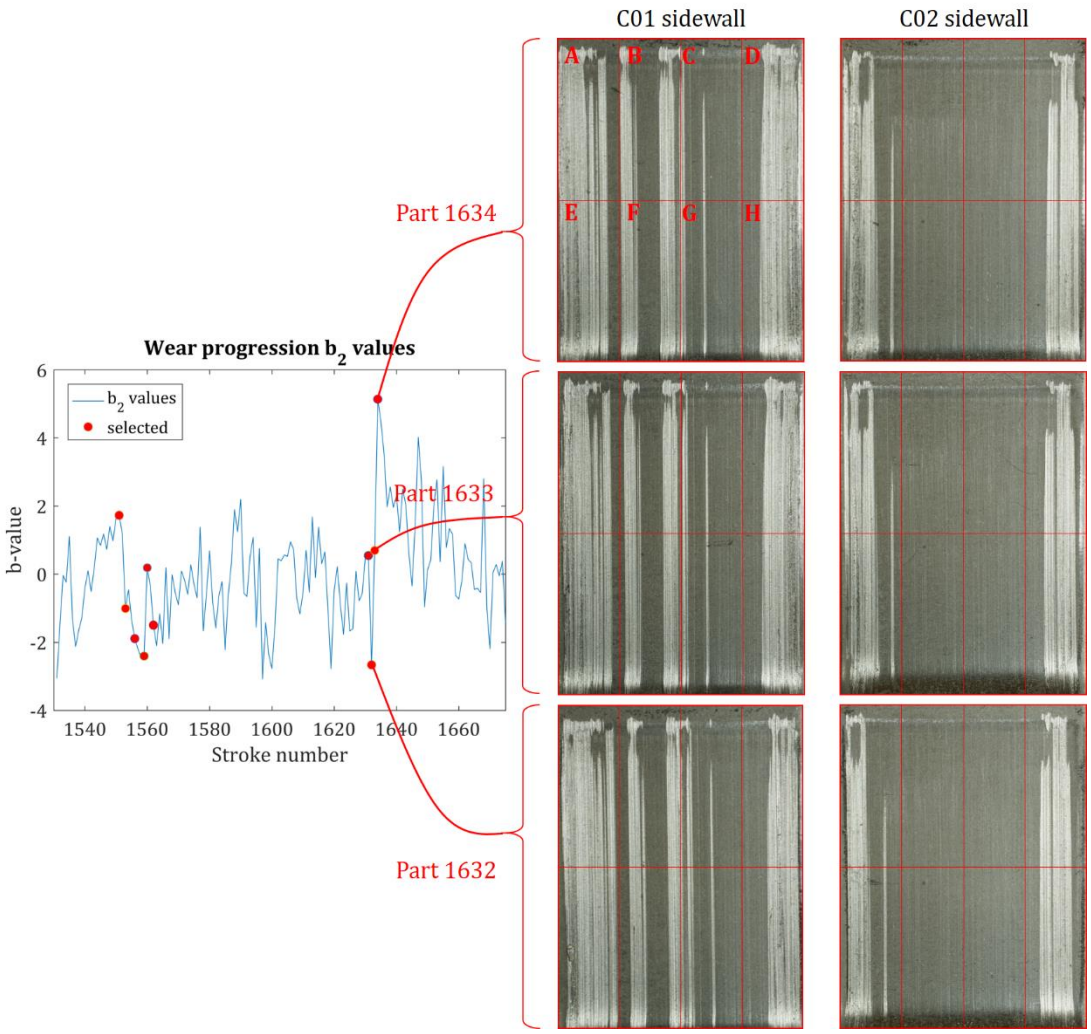

Figure 7.5: Depiction of b2 values for each part in the wear trial (left). Part sidewall photos of example parts are shown (right) that highlight the increased area of adhesive damage late in the stroke on parts 1632, 1633 and 1634.

This initial visual assessment revealed some qualitative agreement between an increase in late stroke adhesive damage severity and positive b2 values for the assessed consecutively formed parts, with more positive b2 values corresponding to a positive slope in punch force progression in an increase late stroke punch force.

In order to quantitatively test these observations a series of W_{DWT} wear measurements were collected for each of the parts in the consecutive sequences. The appearance of adhesive damage in galling wear tracks should increase unevenness of the existing damaged area, with deformed material and additional grooves. This will increase the quantity of abrupt changes in height in 2D surface profiles which in turn should translate into an increase in larger magnitude detail coefficient after DWT is applied. As a result, it was assumed that an increase in adhesive damage severity would correspond to an increase W_{DWT} value. Therefore, a part with a high positive b2 value would correspond to a part with higher W_{DWT}values late in the stroke, than a part with negative or near zero b2 value.

In order to capture the progression of wear over the course of the stroke, W_{DWT} measurements were taken on both part sidewalls at 3 locations, that corresponded to early, mid, and late in the stroke at approximately 15 mm, 25 mm, 35 mm punch displacement. W_{DWT} sum values were then calculated for the early, mid and late stroke locations on each part by adding the equivalent location W_{DWT}values from both sidewalls of the part. These localised W_{DWT}sum values provided three measures of wear severity over the course of the stroke for each of the assessed parts. These three values characterise the severity of galling wear at each stage of the stroke, however, a single value that describes the progression of galling wear severity over the stroke is required for comparison to the b-values for the part. In order to provide a single measure of the progression of wear severity over the course of the stroke for each part, a linear trend line was fitted to the three W_{DWT} sum values and the slope of this trend line was used to represent the progression. With a relatively positive value representing a general increase in the severity of galling wear and adhesive damage over the course of the stroke, while a value closer to zero or negative representing no increase in severity or adhesive damage. This process is illustrated in Figure 7.6. The slope of wear progression values were then compared to b_2 values for the parts. These comparisons for the three sequences of consecutive parts are shown in Table 7.5, Table 7.6, and Table 7.7.

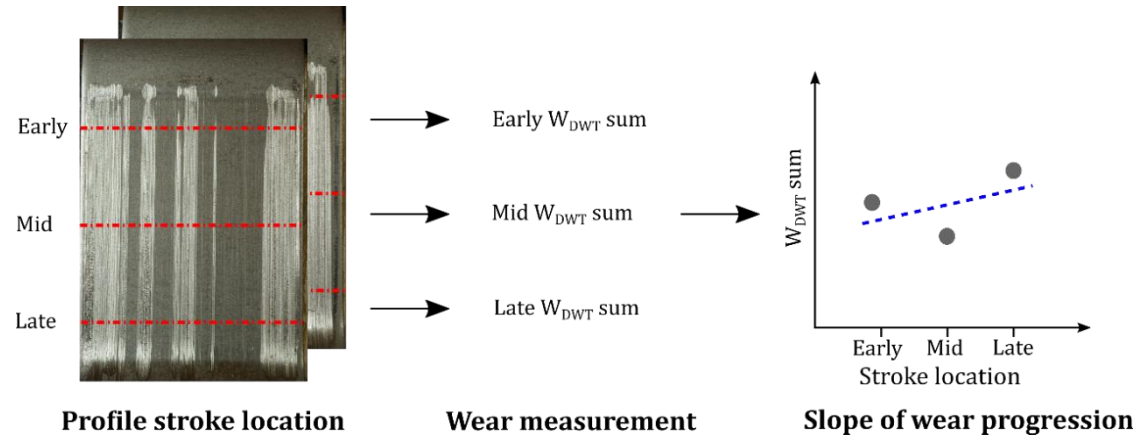

Figure 7.6: Slope of wear progression calculation processes diagram.

Table 7.5: Consecutive part sequence 1 b-value and slope of wear progression comparison.

Part	**PC2 b-value**	***W*$_{DWT}$ progression slope (x-10^{-7})**
1551	1.421	1.816
1553	-1.366	-2.000
1556	-2.798	-5.724

Table 7.6: Consecutive part sequence 2 b-value and slope of wear progression comparison.

Part	**PC2 b-value**	***W*$_{DWT}$ progression slope (x-10^{-7})**
1559	-2.887	1.482
1560	0.209	-1.709
1562	-0.879	0.536

Table 7.7: Consecutive part sequence 3 b-value and slope of wear progression comparison.

Part	**PC2 b-value**	***W*$_{DWT}$ progression slope (x-10^{-7})**
1631	1.554	2.932
1632	-3.361	3.080
1633	0.231	-2.077
1634	4.512	2.370

The results in Table 7.5 demonstrated the expected trend of positive wear progression slope value with positive b2 value. However, this trend was not observed in the results for the remaining consecutively formed channel parts

sequences (Table 7.6 and Table 7.7). Based on the collected W_{DWT} sum values and slope of wear progression results it is not possible to confirm a link between the form of punch force signature variation captured by PC2 and wear mechanism changes over the course of the stroke.

7.4 Discussion

In this Chapter two of the dominant PCs isolated in various wear and friction channel forming trials were assessed in order to develop an understanding of the relationship between punch force signature variation and press conditions. Additional lubrication and wear experiments were conducted to provide additional punch force signatures for evaluating the specific effects of friction changes on punch force signature shape variation.

The first dominant form of punch force signature shape variation investigated described the overall magnitude of the signature. In Section 4.4 the link between this form of signature shape variation and friction is proposed, and in Section 7.3.2 this link is investigated further. The b-values of the PC1 determined for a secondary lubrication comparison experiment were compared to experimentally determined coefficients of friction. A broad correlation between the order of mean b-values and the order of coefficients of friction was observed. These results, in conjunction with theoretical knowledge of the effects of BHF and wear on punch force, have reinforced the conclusion that the punch force signature magnitude form of shape variation is strongly linked to friction between the tooling and blank.

The second dominant form of punch force signature variation investigated described the progression of punch force or the slope of the signature plateau. In Section 4.4 and Section 6.6 this form of shape variation was discussed and the possible link to mid-stroke friction changes was proposed, in particular with regard to lubrication and wear. Assessing the mean signatures and b-values from the friction conditions comparison (Figure 4.5 and Figure 4.7) it was apparent that the unlubricated and drawing lubricant trials were distinct due to the consistent level of punch force in the signature plateau region. However, the drawing lubricant mean signature exhibited the same late stroke punch force increase that was present in

the mean signatures of the other lubricant trials (Figure 4.5). This feature was not observed in the unlubricated mean signature, leading to the hypothesis that fluid lubrication film thickness variation and lubrication mechanism change are driving the form of signature variation.

In Section 7.3.3 the effect of lubrication mechanism on progression form of punch force signature variation was investigated. There are a number of press variables that influence friction between the tooling and the blank. Lubricant viscosity, surface roughness, blank holder force and ram speed all play a role in this friction development (Kim and Kardes, 2012), however, these parameters were unchanged through-out the trials and so were assumed to have a minimal influence on the dominant forms of variation captured using PCA. This left only lubricant type as the major variable of the original and secondary lubrication comparison data sets.

The possibility of mid-stroke friction variation as a result of lubrication mechanism change was assessed by introducing additional dry lubricant trials to a secondary lubrication comparison data set. The mean signatures for the secondary lubrication trials (Figure 7.2b and Figure 7.4b) showed that punch force, and therefore friction increased during the stroke for fluid lubricants. This behaviour was not observed for unlubricated and dry-film lubricants. This observation suggested that a change in friction occurs when using fluid lubrication, and as dry/unlubricated regimes maintain a consistent lubrication mechanism, a change of lubrication mechanism explains the mid-stroke friction increase. The mean signature shapes (Figure 7.4) for different lubrication regimes demonstrate the distinction between fluid lubricated, dry-film lubricated, and unlubricated punch force signatures, and supports the hypothesis of fluid lubricant film reduction and mechanism change over the course of the stroke.

The deceleration of the press ram speed towards the end of the stroke also provides evidence to support the hypothesis that punch force signature variation is associated with a lubrication mechanism change. Andreasen et al. (2006) found that lower sliding speeds in Bending Under Tension tests led to significant increase in friction stresses and lubrication film breakdown, and so an increase in punch force should be expected as the ram speed decreases. Such an increase in the punch force signatures is only observed for the fluid lubrication trials, suggesting that lubrication film breakdown is occurring. The b-value column scatter plot of the

secondary lubrication comparison (Figure 7.2) therefore suggests that PCA of punch force signatures shape can be used to monitor lubrication mechanism changes over the course of the stroke for fluid lubrication.

A decrease in punch force over the course of the stroke was observed in the mean punch force signature of the PTFE sheet trial, Figure 7.4b. As the type of lubricant was the only press parameter varied in the lubrication trials, the decreasing force and friction seen with the PTFE sheet trial are assumed to be driven by the properties and behaviour of the PTFE sheet material. Some possible explanations for this behaviour were presented in Section 7.3.3. However, further investigation is needed to fully explain these observations.

The initial visual assessment results presented in Section 7.3.4 suggested that the plateau slope form of punch force signature variation can be used to detect changes in mechanism and amount of galling wear damage present on the formed sheet metal parts. Changes in b-values of the consecutive part sequences correlate with visual observations of increased quantities of galling wear adhesive damage localised at the end-of-stroke section of the part. The increased PC2 b-values assessed in the wear data correspond to a higher than average positive slope of the punch force plateau and an increase in area of adhesive wear damage in the galling track in the late-stroke region of the sidewalls. These observations indicate that localised increases in adhesive damage, a result of galling wear mechanism change, can be detected in punch force signature shape variation captured by using PCA and displayed by using b-values. However, these visual assessment results are qualitative in nature, and the 2D profilometry W_{DWT} results did not confirm the link between change in galling wear mechanism specific damage/severity and the form of punch force signature shape variation. One of the three consecutive part sequences demonstrated the expected trend of increasing W_{DWT} slope of progression with increasing b-value, however, this trend was not observed in the remaining consecutive part sequences. The 2D W_{DWT} parameter may not be capable of capturing the full extent of surface damage information needed to characterise the galling wear damage mechanism on part sidewalls with very similar quantities of overall damage. The parameter also includes a profile averaging step in order to minimise the detection of base surface roughness detection that comes with 2D profiles. However, this step will affect detection of important features within the

damage regions in the direction of sliding. This averaging step may be an influencing factor in the negative result, as the galling wear mechanism specific damage is also localised in the direction of the stroke.

As the results stand, it is not possible to confirm a link between galling wear mechanism and the form of punch force signature variation that describes punch force progression with stroke. Further investigation using 3D texture measurements could reveal additional information to support the hypothesis, however, the isolation of an appropriate measure would be required, in addition to characterisation of large areas of numerous part surfaces, which would be a very time-consuming process.

7.5 Summary

Two dominant forms of punch force signature variation, the first describing signature magnitude and the second describing punch force progression, have been investigated.

The first form of signature variation was linked to friction between the blank and press tooling. This was established through the comparison of b-values to experimentally determined coefficients of friction for lubricants used in the comparison data set.

The second form of signature variation that represents slope of the signature plateau or punch force progression with stroke, was linked to lubricant mechanism change. Dry lubricant regimes were found to maintain a consistent lubrication mechanism and punch force progression, which was not observed with fluid lubricant regimes. This result supported the hypothesis that this second form of variation captures late stroke lubrication mechanism change.

Finally, the link between the second dominant form of signature variation and galling wear mechanism change during the stroke was investigated. Although initial visual assessment supported the link, a quantitative analysis using the DWT methodology and W_{DWT} parameter was not conclusive.

These results provided further insight into the specific forms of punch force signature shape variation that were observed in all of the data sets collected in this thesis. This insight will prove useful for a future development of wear and lubrication monitoring systems based on punch force signatures.

CHAPTER EIGHT

Discussion

8.1 Introduction

The aim of the work undertaken in this thesis was to determine the relationship between punch force signatures and galling wear development and progression. The motivation of this work was to assist with addressing galling wear on sheet metal forming tools in the automotive industry. On-line wear monitoring systems will play an important role in solving the issue of galling wear on production dies, however, such systems cannot be effective without an in-depth knowledge of the relationship between galling wear and a range of process signals. Punch force is one of these process signals that is of particular importance due to its wide spread availability from industrial presses and its already confirmed relationship to various part quality and press condition issues. In this Chapter a summary of the work conducted in this thesis is provided, highlighting the initial aims of the work and logical progression of investigations. Then the relationship between punch force signature variation and galling wear is discussed. Specifically, the two key forms of punch force signature shape variation – the magnitude and the slope of progression. Finally, a summary of limitations of the work and key assumptions are discussed.

8.2 Summary of key findings

To investigate the relationship between punch force signatures and galling wear, the first component of this work aimed to determine if changes in galling wear and other friction influencing factors had a measurable effect on the punch force signature. PCA was applied to punch force signature data sets and signatures formed under the

different wear conditions and other friction conditions were found to have different b-values responses for 2 Principal Components. This result meant that changes in galling wear and other friction influencing factors had a clear influence on the punch force signature. Punch force signature shape variation captured using PCA and the b-values that describe each stroke in terms of these forms of variation allow for the distinction of signatures formed with and without galling wear on the tooling, and distinction between different lubricants and BHF levels.

These results provided justification for further investigation into the relationship between galling wear progression and punch force signature variation. This further investigation required a method to accurately quantify galling wear severity on the press tooling in industrial style forming situations. A review of the literature found a lack of accurate and targeted measures of galling wear that are suited to industrial situations. To meet this requirement a new galling wear severity quantification technique was developed. The new technique utilised discrete wavelet transformation of 2D surface profiles from the die counter surface and provided a means of targeted assessment of the relative severity of galling wear damage. This comes in the form of detail coefficients and a single relative severity measure for the 2D profile, the W_{DWT} parameter. This new methodology was demonstrated in case studies of galling initiation and galling progression and was shown to outperform alternative measures in the initiation case study and provided comparable accuracy to visual assessment. The methodology provided a means for quantifying the severity of galling wear on the channel parts formed in the semi-industrial trials utilised in this work and enabled further investigation into the relationship between galling wear progression and variation in punch force signatures. While further work is required to categorise what values to expect for certain materials, and threshold values for levels of wear, in its current state the method provides a useful targeted comparative measure.

The relationship between galling wear progression and punch force signature shape variation was then investigated using 2 extended galling wear trials. Galling wear severity measurements were found to have a strong linear relationship with b-values for the dominant punch force signature PC in both trials. These PCs both described variation in the magnitude of the punch force signature. No other strong linear relationship was found with other forms of punch force signature shape

variation despite the results of the initial investigation suggesting other forms of variation are sensitive to friction changes. The relationship between galling wear severity and the peak force feature of the punch force signature was also tested to determine its similarity to the magnitude form of shape variation. Peak force was found to have a weaker linear relationship with galling wear severity than signature magnitude, supporting the use of PCA for assessing the punch force signatures.

Finally, an investigation into the 2 general forms of punch force signature shape variation was conducted, these forms were those found to have a relationship with wear or have sensitivity to frictional changes. The investigation aimed to determine the frictional conditions they represent and how these conditions relate to galling wear development and lubrication. The magnitude of the punch force signature was linked to friction between the blank and the tooling based on assessment of experimentally determined coefficients of friction for a series of lubricants and the theoretical effects of wear and BHF on the friction level. The progression of punch force or slope of signature plateau was then linked to mid-stroke dynamic changes in friction. Assessment of this form of shape variation consisted of two aspects; one focusing on lubrication, and the other on galling wear. The lubrication assessment introduced new dry film lubricant regimes and proposed that differences in b-values observed for the relevant PC were the result of lubrication mechanism change during the stroke. This supported the hypothesis that signature variation related to punch force progress are driven by mid-stroke dynamic changes in friction.

The galling wear assessment proposed that mid-stroke change in dominant wear mechanism was responsible for this form of signature variation in the wear trials. Visual assessment and comparison supported the link, with increased amounts of adhesive damage on late stroke regions of part sidewalls corresponding to increases in late stroke punch force, captured in the PC. A quantitative study was conducted by collecting progressive W_{DWT} measurements with stroke, however, this study did not conclusively support the hypothesis. The results of the quantitative study found that only 1 of the 3 examined part series displayed the expected increase in galling severity during the stroke with a corresponding increase in late stroke punch force. Despite the inconclusive results of the quantitative wear study, the results of the lubrication assessment and visual wear inspection do suggest that the form of

signature variation that describes punch force progression is due to mid-stroke dynamic friction changes.

With regard to the motivation of the work, the results have shown that punch force can provide important galling wear information, specifically signature magnitude is strongly related to the progression of wear. Other forms of variation isolated from the data can also be linked to galling wear and friction changes due to lubrication and BHF. The work has also provided and demonstrated the appropriate tools for further investigation into the relationship between punch force signature and tool wear, specifically the use of PCA and the DWT galling wear severity quantification methodology.

8.3 Forms of punch force signature shape variation

The fundamental objective of this work was to determine the link or relationship between punch force signature variation and galling wear. During this work PCA was applied to punch force signature from a range of different semi-industrial channel forming trials, that included comparisons of distinct changes in wear, comparisons of changes in lubrication and BHF, and finally, extended wear progression. When applied to punch force signatures PCA isolates the dominant directions of variation in the punch force data points. This variation is interpreted as overall forms of signature shape change. As was summarised in Section 8.2, two distinct general forms of signature shape variation became focal points. The first generally describing the magnitude of the punch force signature and the second describing punch force progression or the slope of the signature plateau. In this Section these key forms of punch force signature variation and their relationships to friction conditions due to galling wear, lubrication, and BHF are discussed.

8.3.1 Punch force signature magnitude

The dominant form of signature shape variation in all the analyses in this work were found to be approximately represented as variation in the overall magnitude of the

punch force signature. Example PC representation that generally describe the magnitude form of punch force signature variation can be seen in Figure 8.1.

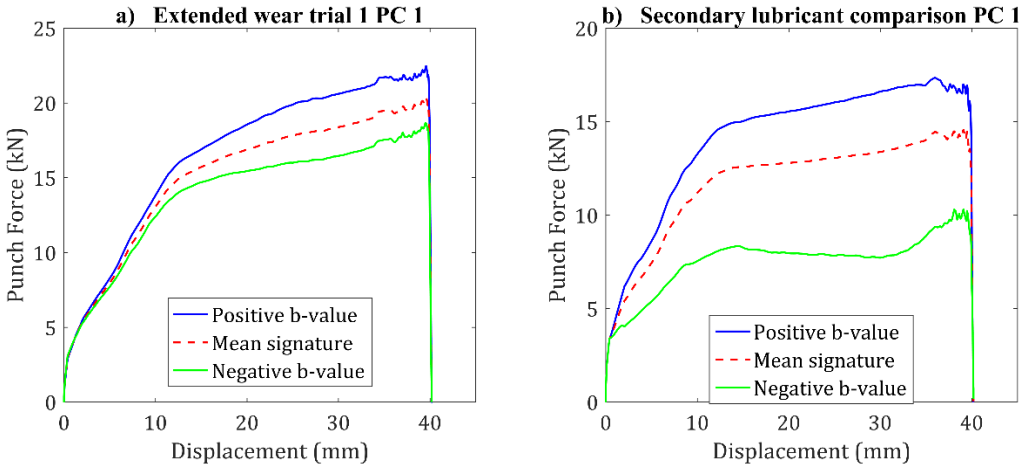

Figure 8.1: Principal Component representations for extended wear trial 1 Principal Component 1 (a) and the secondary lubricant comparison Principal Component 1 (b). These two Principal Components capture the magnitude general form of shape variation, despite differences in example b-value curves both PCs describe variation in the magnitude of the signature plateau.

Punch force signature magnitude captured using PCA and represented for each stroke by b-values has been clearly linked to friction between the blank and tooling. The results of Chapter 4 show that this form of shape variation can be used to distinguish between large increases in galling wear, the presence of which is known to increase friction (Akagak and Rigney, 1991). Variation of signature magnitude also allowed for the distinction between trials conducted with various lubricants and BHF levels. Again, these factors both strongly influence friction as discussed in Section 2.3.1.

In Chapter 6 punch force signature magnitude was also found to be strongly related to galling wear severity progression. This progression saw incremental increases in the severity of galling wear over 2 trials of 1500 and 3000 parts. The gradual increase in severity saw an increase in the effected area on the dies. This consequently increased friction between the sliding surfaces and drove the increase in punch force signature magnitude.

Importantly, it was the entire magnitude of the signature that was relevant for linking the signature to galling wear progression, as the results of the peak force comparison showed. Other forms of signature variation have shown that for the

semi-industrial trials used in this work, the early stroke punch force can be much lower than the late stroke punch force. In particular this is the case for fluid lubricants. As a result, peak force can easily give similar values for signature that have very different early stroke punch force magnitudes. The magnitude of signature as captured using PCA does not have this weakness.

Distinguishing between magnitude changes due to galling wear, as opposed to some other possible factor was not explored. However, this does not appear to be feasible, when based on this single form of shape variation. The magnitude of the signature is linked to the coefficient of friction between the blank and tooling, this is not the result of a single factor in the first instance and so separation based on magnitude alone is not feasible. However, it is possible that a distinct change in punch force magnitude could be a useful tool for identifying friction related issues that could then be diagnosed when based on other features of signature shape.

8.3.2 Punch force signature progression

A less dominant form of punch force signature shape variation was also observed in all the trials conducted. Generally, these PCs capture variation in the progression of punch force over the stroke, or the slope of the signature plateau, Figure 8.2. This as a consequence, will describe the initial level of punch force once the blank yields.

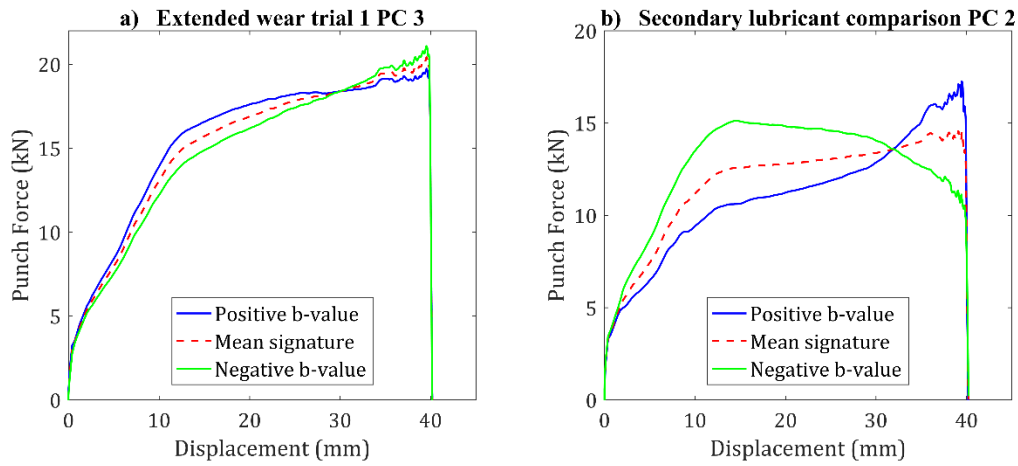

Figure 8.2: Principal Component representations for extended wear trial 1 Principal Component 3 (a) and the secondary lubricant comparison Principal Component 2 (b). These two Principal Components capture the progression of punch force over the stroke form of shape variation, despite differences in example b-value curves, both PCs describe variation in the punch force progression or slope of the signature plateau.

The slope of punch force progression was found to be related to dynamic changes in friction over the course of the stroke. This was supported by the differences in force progression observed between fluid lubricant punch force signatures and dry/unlubricated punch force signatures. The dry contact condition was found to have approximately consistent levels of punch force after the blank material yielded. Alternatively, all fluid lubricants were found to have increasing progression over the course of the stroke that was associated with friction increase that comes with lubrication regime change.

This form of signature shape variation allowed for clear distinction between various lubricant types and BHF levels (Section 4.3.3). The results Chapter 7 suggested that late stroke friction increase as a result of lubrication mechanism changes can be detected using this PC. The inclusion of dry film lubricants in addition to the unlubricated trials supported the hypothesis that the other fluid lubricant trials were experiencing late stroke lubrication mechanism change. The clear separation in b2 values for fluid lubricant trials and the dry conditions (Figure 7.2) demonstrates the detection of this late stroke mechanism change.

The relationship between the slope of punch force progression and galling wear was also assessed. The b-values associated with the slope of punch force progression form of shape variation were observed to have a significant increase in range for the high wear trial in Section 4.3.2.

A slight trend was also observed in this form of variation in extended wear trial 2 that continued after wear severity at the start of the stroke had plateaued. A similar trend was not observed in extended trial 1 indicating that the slope of punch force progression can be influenced by some inconsistent factor of galling wear.

Channel part sampling rate proved to be an issue for assessing the relationship between galling wear and punch force progression in the extended wear trials of Chapter 6. Large variations in b-values for the slope of progression PC occurred part to part for much of the extended trials. However, this variation could not be compared to the galling wear on the part as only every 10^{th} part was collected. To address this issue, extended trial 1 was continued in Chapter 7 and all parts were collected. Visual assessment of consecutively formed parts and comparison to changes in the associated b-value provided qualitative evidence that punch force progression form of signature shape variation is correlated to the presence of

adhesive wear damage late in the stroke. This correlation to late stroke adhesive damage was assessed quantitatively using W_{DWT} measurements to track galling severity over the course of a stroke, however, the results of this assessment were inconclusive. The W_{DWT} measurements did not demonstrate the expected relationship in 2 of the 3 test channel part series, with the remaining parts showing a clear increase in galling severity with stroke displacement for parts with signatures that had a higher than average positive slope for punch force progression.

In summary, there is qualitative evidence that the progression of punch force during the stroke is related to the dominant wear mechanism during the stroke. The different mechanisms that are observed in galling wear are associated with distinct levels of friction, and so it follows that a change will have an effect on the punch force progression. As galling wear develops, and more regions are damaged, multiple mechanisms can be present at the same time. Multiple damage complicates assessment and could have affected W_{DWT} measurements taken in the quantitative investigation (Section 7.3.4), where parts had at least 6 separate regions of damage across both sidewalls. Further work is required to clarify the quantitative link between punch force progression and galling wear, potentially by assessing parts with fewer damaged regions.

8.4 Limitations and assumptions

There are a number of limitations and assumptions in this work that must be considered with the results and conclusions. Firstly, this work has been conducted on relatively small channel parts, and so the proportion of wear damage area to total contact area is relatively large. In industry much larger parts are formed, which will make the ratio of wear to contact area much smaller. At this stage the sensitivity of the punch force signature is unknown, and very small changes in the amount of wear may not be detectable.

A significant assumption made throughout this work is that the PC determined for the analysis of different punch force signature data sets represent the same general forms of signature shape variation in the cases of magnitude and slope of progression. As the mean signature for each data set is not consistent, the PCs and

the corresponding b-values cannot be directly compared. However, in the analyses conducted the variation around the mean signatures for the dominant PCs appeared to represent the same general shapes. Hence the assumption that these different PCs represent the same general forms of signature shape variation and so are conceptually comparable.

Determining if a signature is affected by galling wear or other friction influencing factors is an aspect that has not been fully addressed, and so is a limitation of this work. Tests focusing on identifying if punch force magnitude variation is specifically due to lubrication changes or galling wear were not conducted. These factors were not assessed in the same trials in this work, with the trials focusing on varying either wear or other friction influencing factors, but not both simultaneously. It is feasible that either or both could occur in an industrial situation, requiring different remedial action, and as such, it would be beneficial to be able to distinguish between issues. With the data available it is not possible to make a direct comparison; however, a possible approach could involve combining b-values for both forms of variation in order to isolate specific issues. For example, the b2 values of the unlubricated conditions (Figure 7.2) were significantly different to the base case mill oil condition, and so in an instance where lubricant application failed it would be expected that b2 values would be very negative in addition to very positive b1 values. Based on observations from extended wear trial 1 (Figure 6.8b) the very negative b2 value would not be observed when wear is the issue, even though both situations would come with an increase in b1 values that correspond to increased signature magnitude. This, of course, has not been tested in the present work and requires further investigation to confirm. However, in an industrial situation, due to the cost of galling, any friction increases that will correspond to an increase in signature magnitude should merit inspecting the conditions of the press regardless of cause.

Another limitation relates to the DWT galling wear severity quantification methodology presented. The DWT methodology and W_{DWT} values are not currently linked to set severities of galling wear, making it difficult to infer the galling severity based off a W_{DWT} value. In this work the W_{DWT} have been treated as a relative measure with reference to values acquired for known unworn parts from the beginning of trials. If the technique is not applied similarly, as a relative measure, it

may be difficult to implement in industry or other trials immediately. Additional testing would be required to understand what values represent unacceptable levels of wear for different materials. The results of Chapter 7 also suggest that the W_{DWT} parameter does not conclusively show a distinguishable difference when measuring galling wear tracks of equal size but consisting of different wear mechanism specific damage. This may require further refinement of the W_{DWT} parameter to quantify these differences.

CHAPTER NINE

Conclusions and recommendations

9.1 Conclusion

This thesis has investigated the link between punch force signature variation and galling wear progression in deep drawing of sheet metal parts. This work has specifically addressed the problem statement (Section 1.2) and research objectives (Section 1.4). To conclude this thesis the significance and place of the work in the field will be discussed, the key contributions will be summarised, and avenues for further investigation will be recommended.

9.2 Summary of contributions

This work has made a number of contributions in the process of addressing the specific research objective outlined in Section 1.4. The contributions of this thesis build on and advance the fields of sheet metal stamping process signal analysis, process monitoring, and galling wear severity quantification. A new methodology for quantification of galling wear severity has been presented that illustrates a novel approach in targeting specific surface features. The new measure provides an accurate measure of galling wear severity for the use in developing wear monitoring systems as well as assessment of wear in industrial settings. The thesis also provides insight into the effects of galling wear and other friction conditions on the variation of punch force signatures. These insights provide a foundational understanding that can assist with the development of wear monitoring systems in sheet metal forming, a tool that will address the significant issue of tool wear in sheet metal forming

industries. The details of each of these contributions are summarised with respect to the research objectives of the thesis.

Objective: Determine if variation in wear and other friction influencing factors have a demonstrable effect on punch force signatures (Chapter 4).

- Punch force signatures from channel forming trials were found to be clearly affected by changes in galling wear severity on tooling, changes in lubricant type, and changes in BHF level.

- PCA of punch force signature data sets were shown to be an effective tool for isolating the effects of changes in wear and other friction conditions.

- A number of common general forms of signature shape variation were observed in the analysis of 2 punch force signature data sets focusing on variation of wear severity, and variation of other friction influencing factors. Two specific forms of signature shape variation allowed for distinction between signatures collected under different wear severities, lubricants, and BHF levels.

Objective: Develop an accurate method for quantifying galling wear severity that can be applied to channel forming experiments conducted in this work (Chapter 5).

- A new methodology for quantifying galling wear severity was presented in the form of the DWT methodology.

- The DWT methodology has a number of features that make it suitable for use in the channel forming experiments and also make it more accurate than alternative measures.

- The methodology uses Discrete Wavelet Transformation to target galling wear features in 2D surface profiles of the die counter surface, and no other galling wear measure aims to target galling specific features.

- The methodology provides an indication of the location and relative severity of localised galling wear damage in the form of detail coefficients, and a parameter that quantifies the overall severity of galling wear severity on the surface in W_{DWT}.

- The methodology was shown to provide an accurate quantifiable measure of galling wear severity in galling initiation and galling progression cases.

Objective: Examine if the onset and progression of galling wear has a quantifiable relationship with punch force signature shape variation (Chapter 6).

- The PCA of punch force signatures for extended channel forming trials in which galling wear progressed in severity has been presented. These wear trials demonstrated a progression of galling wear severity in two forms, continued increasing severity and plateaued severity.

- In the extended channel forming trials conducted, galling wear severity progression was found to have a strong linear relationship with punch force signature magnitude.

- In the same trials, peak punch force was also found to have a relationship with galling wear severity progression, however, not as strong as the relationship seen with punch force signature magnitude.

- The slope of the punch force signature plateau was not found to have a conclusive linear relationship with galling wear progression in both test trials.

Objective: Investigate how specific wear events and changes in friction influencing factors affect the punch force signature (Chapter 7).

- Using experimentally determined coefficients of friction for lubricant types the magnitude PC is linked to the coefficient of friction between the tooling and blank.

- This correlates well with theory relating to the effects of wear and blank holder force on friction, as well as observations from the trials conducted.

- The slope of the punch force signature plateau or the progression of the punch force was linked to the lubrication mechanism change experienced near the end of the stroke. Such a mechanism change is characterised by the lubricant film thinning, changing from a mixed lubrication regime to boundary lubrication or even dry contact as film thickness reduced.

- The slope of the punch force signature plateau or the progression of the punch force was qualitatively linked to changes in the dominant type of wear damage in galling wear tracks, either adhesive or abrasive wear damage.

9.3 Significance and place in the field

Previous work looking into the link between stamping and deep drawing process signal and tool wear has been limited. The relationship between punch force and wear was previously only discussed incidentally but not investigated. This work has demonstrated that punch force signatures have a close relationship to galling wear, and contains useful features and indicators that provide information about the current state of galling wear severity. Experimentally determined typical punch force signature responses to galling wear and friction changes have been highlighted and discussed. These results provide experimentally derived foundational knowledge for punch force-based process monitoring of deep drawing processes and sheet metal stamping more broadly.

PCA has been shown to be an effective tool for extracting wear and friction relevant information out of the punch force signature. Previously this technique had been applied to punch force or forming force signals to isolate larger distinct issues such as part failure. PCA enabled tracking of the gradual variation in the punch force signatures in a manner that could be linked back to the wear in the system. This application to process signatures for monitoring gradual state changes in the form of wear is a significant insight that opens up opportunities for implementation in

other manufacturing processes, including but not limited to other sheet metal stamping stages.

The DWT galling wear severity quantification methodology is a significant contribution to the field in two regards; firstly, it provides a new methodology for assessing and quantifying the severity of galling wear on galled surfaces. Secondly it presents a new way of thinking about galling wear measurement with 2D profiles by focusing on relevant features and using wavelet transformation to achieve this focus. Prior to this work, there were no standardised quantifiable techniques for measuring galling wear, and no prevalent method for measuring wear on sheet metal forming dies and parts. No work had compared results to visual assessment, which is used as a standard for assessing galling wear, and no utilised parameter targeted the features of galling wear damage on the surface.

9.4 Recommendations for future work

The results of this thesis have revealed a number of areas for further investigation and future work. These include continuations of topics addressed in this thesis, and further development of techniques outlined.

A limitation of the work conducted was the lack of investigation into distinguishing between the cause of punch force signature variation, whether that be galling wear or other factors, such as lubrication issues. This limitation presents an avenue for potential future work. It was proposed that distinguishing between friction influencing factors would be possible through the use of multiple PCs. Monitoring the behaviour and differences observed in punch force signatures collected from the various combined lubrication and wear progression trials could reveal distinct shifts in multiple PC b-values for the different conditions. A clear area for further work would involve experimentally confirming this theory.

Another area of potential future work involves the further development of the DWT galling wear quantification methodology. The DWT methodology meets the requirements of this thesis by providing accurate relative measures of galling wear severity, however, further broader application and adoption of the method requires refinement and standardisation. This would involve determining and defining

representative W_{DWT} values for different severities of wear on a number of materials. Followed by defining standard values or thresholds, so as to remove the current reliance on relative measurements to understand the severity of the damage on the surface.

Finally, future work that progresses the overall aim and motivation behind this thesis is recommended. The motivation of this work was to provide foundational knowledge for implementation of a sheet metal stamping tool wear monitoring system. The development of an experimental tool wear monitoring system based on punch force signature PCs highlighted in this thesis is an obvious recommendation for further work. Such a system could also potentially include other process signals, such as audio and acoustic emissions, to aid with the detection of wear onset and progression.

References

Akagak, T., Rigney, D.A., 1991. Sliding friction and wear of metals in vacuum. Wear 149, 353–374.

Andreasen, J.L., Bay, N., De Chiffre, L., 1998. Quantification of galling in sheet metal forming by surface topography characterisation. Int. J. Mach. Tools Manuf., International Conference on Metrology and Properties of Engineering Surfaces 38, 503–510.

Andreasen, J.L., Olsson, D.D., Chodnikiewicz, K., Bay, N., 2006. Bending under tension test with direct friction measurement. Proc. Inst. Mech. Eng. Part B J. Eng. Manuf. 220, 73–80.

Archard, J.F., 1953. Contact and rubbing of flat surfaces. J. Appl. Phys. 24, 981–988.

ASTM Standard G196-08, 2016. Standard test method for galling resistance of material couples, ASTM International. West Conshohocken, PA.

ASTM Standard G40-15, 2015. Standard terminology relating to wear and erosion, ASTM International. West Conshohocken, PA.

ASTM Standard G98-02, 2009. Standard test method for galling resistance of materials, ASTM International. West Conshohocken, PA.

Bagheriasl, R., Tari, D.G., Kurukuri, S., Worswick, M.J., 2014. Material properties for numerical calculations, in: Comprehensive Materials Processing. Elsevier, pp. 227–246.

Bassiuny, A.M., Li, X., Du, R., 2007. Fault diagnosis of stamping process based on empirical mode decomposition and learning vector quantization. Int. J. Mach. Tools Manuf. 47, 2298–2306.

Benati, F., 2003. Effect of surface topography upon the quality of autobody panels. Brunel University.

Bhushan, B., 2013. Introduction to tribology. John Wiley & Sons, New York.

Billur, E., 2012. Principles of sheet forming presses, in: Altan, T., Tekkaya, A.E. (Eds.), Sheet Metal Forming-Fundamentals. ASM International, Materials Park, Ohio, pp. 129–144.

Boljanovic, V., 2004. Sheet metal forming processes and die design. Industrial Press, New York.

Breitling, J., Pfeiffer, B., Altan, T., Siegert, K., 1997. Process control in blanking. J. Mater. Process. Technol. 71, 187–192.

Bubna, P., Humbert, M.P., 2016. 3D Metal printing of automotive stamping dies. Met. Mag. 34,36-39.

Budinski, K.G., Budinski, S.T., 2015. Interpretation of galling tests. Wear 332, 1185–1192.

Burrus, C.S., Gopinath, R.A., Guo, H., 1998. Introduction to wavelets and wavelet transforms : a primer. Prentice Hall, Upper Saddle River, NJ.

Christiansen, S., De Chiffre, L., 1997. Topographic characterization of progressive wear on deep drawing dies. Tribol. Trans. 40, 346.

Dieter, G., 1961. Mechanical metallurgy. McGraw-Hill Book Company, New York.

Ding, Y., Elsayed, E.A., Kumara, S., Lu, J.-C., Niu, F., Shi, J., 2006. Distributed sensing for quality and productivity improvements. IEEE Trans. Autom. Sci. Eng. 3, 344–359.

Doege, E., Meiners, F., Mende, T., Strache, W., Yun, J.W., 2008. Sensors for process monitoring: metal forming, in: Hesse, J., Gardner, J.W., Göpel, W. (Eds.), Sensors Applications. Wiley-VCH Verlag GmbH & Co. KGaA, pp. 172–202.

Doege, E., Schmidt-Jürgensen, R., Huinink, S., Yun, J.-W., 2003. Development of an optical sensor for the measurement of the material flow in deep drawing processes. CIRP Ann. 52, 225–228.

Doege, E., Seidel, H.-J., Griesbach, B., Yun, J.-W., 2002. Contactless on-line measurement of material flow for closed loop control of deep drawing. J. Mater. Process. Technol. 130–131, 95–99.

Doolan, M., Hodgson, P., Kalyanasundaram, S., Cardew-Hall, M., 2003. Use of image recognition techniques in the analysis of sheet metal forming force signature curves. J. Manuf. Sci. Eng. 125, 363–368.

Doolan, M.C., Kalyanasundaram, S., Hodgson, P., Cardew-Hall, M., 2001. Identifying variation in sheet metal stamping. J. Mater. Process. Technol. 115, 142–146.

Du, R., 2006. Monitoring and diagnosis of sheet metal stamping processes, in: P.Eng, L.W., Gao, R.X. (Eds.), Condition Monitoring and Control for Intelligent Manufacturing, Springer Series in Advanced Manufacturing. Springer London, pp. 193–218.

Dutta, S., Pal, S.K., Sen, R., 2016. Progressive tool flank wear monitoring by applying discrete wavelet transform on turned surface images. Measurement 77, 388–401.

Emmens, W.C., 1997. Tribology of flat contacts and its application in deep drawing. University of Twente.

Eppinger, S., Huber, C., Pham, V., 1995. A methodology for manufacturing process signature analysis. J. Manuf. Syst. 14, 20–34.

Fildes, J.M., Meyers, S.J., Mulligan, C.P., Kilaparti, R., 2013. Evaluation of the wear and abrasion resistance of hard coatings by ball-on-three-disk test methods—A case study. Wear 302, 1040–1049.

Fu, S., Liu, X., Muralikrishnan, B., Raja, J., 2001. Wavelet analysis with different wavelet bases for engineering surfaces. Proc. 16th Annu. Meet. Amer. Soc. Precis. Eng. 125, 249–252.

Gåård, A., Krakhmalev, P., Bergström, J., 2009. Influence of tool steel microstructure on origin of galling initiation and wear mechanisms under dry sliding against a carbon steel sheet. Wear 267, 387–393.

Gåård, A., Krakhmalev, P., Bergström, J., 2008. Wear mechanisms in deep drawing of carbon steel – correlation to laboratory testing. Tribotest 14, 1–9.

Galakhar, A.S., Gates, J.D., Daniel, W.J.T., Meehan, P.A., 2011. Adhesive tool wear in the cold roll forming process. Wear 271, 2728–2745.

Ge, M., Du, R., Xu, Y., 2004. Hidden Markov Model based fault diagnosis for stamping processes. Mech. Syst. Signal Process. 18, 391–408.

Ge, M., Du, R., Zhang, G., Xu, Y., 2004. Fault diagnosis using support vector machine with an application in sheet metal stamping operations. Mech. Syst. Signal Process. 18, 143–159.

Ge, M., Zhang, G.C., Du, R., Xu, Y., 2002. Feature extraction from energy distribution of stamping processes using wavelet transform. J. Vib. Control 8, 1023–1032.

Grand View Research, 2017. Metal stamping market analysis by process (blanking, embossing, bending, coining, flanging), by application (automotive, industrial machinery, consumer electronics), and segment forecasts, 2014 - 2025. Grand View Research Inc., San Francisco.

Groche, P., Moeller, N., Hoffmann, H., Suh, J., 2011. Influence of gliding speed and contact pressure on the wear of forming tools. Wear 271, 2570–2578.

Hamid, E.Y., Kawasaki, Z.-I., 2002. Wavelet-based data compression of power system disturbances using the minimum description length criterion. IEEE Trans. Power Deliv. 17, 460–466.

Hao, S., Ramalingam, S., Klamecki, B.E., 2000. Acoustic emission monitoring of sheet metal forming: characterization of the transducer, the work material and the process. J. Mater. Process. Technol. 101, 124–136.

Hedrick, A., 2010. Die Science: Drawing under pressure. Stamp. J. January/February.

Hou, Y., Zhang, W., Yu, Z., Li, S., 2009. Selection of tool materials and surface treatments for improved galling performance in sheet metal forming. Int. J. Adv. Manuf. Technol. 43, 1010–1017.

Hummel, S.R., 2011. Elements to improve galling resistance test results using the ASTM G98 method. J. Test. Eval. 39, 103214.

Inasaki, I., Tönshoff, H.K., 2008. Fundamentals: roles of sensors in manufacturing and application ranges, in: Hesse, J., Gardner, J.W., Göpel, W. (Eds.), Sensors Applications. Wiley-VCH Verlag GmbH & Co. KGaA, pp. 1–6.

Jin, J., Ding, Y., 2004. Online automatic process control using observable noise factors for discrete-part manufacturing. IIE Trans. 36, 899–911.

Jin, J., Shi, J., 2001. Automatic feature extraction of waveform signals for in-process diagnostic performance improvement. J. Intell. Manuf. 12, 257–268.

Jin, J., Shi, J., 2000. Diagnostic feature extraction from stamping tonnage signals based on design of experiments. J. Manuf. Sci. Eng. Trans. ASME 122, 360–369.

Jin, J., Shi, J., 1999. Feature-preserving data compression of stamping tonnage information using wavelets. Technometrics 41, 327.

Josso, B., Burton, D.R., Lalor, M.J., 2002. Frequency normalised wavelet transform for surface roughness analysis and characterisation. Wear 252, 491–500.

Karlsson, P., Gåård, A., Krakhmalev, P., Bergström, J., 2012. Galling resistance and wear mechanisms for cold-work tool steels in lubricated sliding against high strength stainless steel sheets. Wear, Tribology in Manufacturing Processes 286–287, 92–97.

Kennedy, D.., Hashmi, M.S.., 1998. Methods of wear testing for advanced surface coatings and bulk materials. J. Mater. Process. Technol. 77, 246–253.

Kim, H., Altan, T., Yan, Q., 2009. Evaluation of stamping lubricants in forming advanced high strength steels (AHSS) using deep drawing and ironing tests. J. Mater. Process. Technol. 209, 4122–4133.

Kim, H., Kardes, N., 2012. Friction and lubrication, in: Altan, T., Tekkaya, A.E. (Eds.), Sheet Metal Forming-Fundamentals. ASM International, Materials Park, Ohio, pp. 89–103.

Kirkhorn, L., Bushlya, V., Andersson, M., Ståhl, J.-E., 2013. The influence of tool steel microstructure on friction in sheet metal forming. Wear 302, 1268–1278.

Koh, C., Shi, J., Williams, W., 1995. Tonnage signature analysis using the orthogonal (Haar) transforms. NAMRI/SME Trans. 23, 229–234.

Koh, C.K.H., Shi, J., Black, J., Ni, J., 1996. Tonnage signature attribute analysis for stamping process. NAMRI/SME Trans. 24, 193–198.

Kotsiantis, S.B., Zaharakis, I.D., Pintelas, P.E., 2006. Machine learning: a review of classification and combining techniques. Artif. Intell. Rev. 26, 159–190.

Kuzinovski, M., Tomov, M., 2009. Effect of sampling spacing upon change of hybrid parameters values of the roughness profile. J. Prod. Eng. 12, 23–28.

Lee, J., 1995. Machine performance monitoring and proactive maintenance in computer-integrated manufacturing: review and perspective. Int. J. Comput. Integr. Manuf. 8, 370–380.

Lee, S.-H., Zahouani, H., Caterini, R., Mathia, T.G., 1998. Morphological characterisation of engineered surfaces by wavelet transform. Int. J. Mach. Tools Manuf. 38, 581–589.

Li, X., Bassiuny, A.M., 2008. Transient dynamical analysis of strain signals in sheet metal stamping processes. Int. J. Mach. Tools Manuf., Advances in Sheet Metal Forming Applications 48, 576–588.

Lim, Y., Venugopal, R., Galip Ulsoy, A., 2012. Auto-tuning and adaptive control of sheet metal forming. Control Eng. Pract. 20, 156–164.

Lim, Y., Venugopal, R., Ulsoy, A.G., 2008. Advances in the control of sheet metal forming. IFAC Proc. Vol. 41, 1875–1883.

Lin, J.F., Wang, L.Y., Huang, T.-K., 1992. Friction in deep drawing of aluminium sheet. Wear 156, 189–199.

Lingadurai, K., Shunmugam, M.S., 2006. Metrological characteristics of wavelet filter used for engineering surfaces. Measurement 39, 575–584.

Mallat, S.G., 2009. A wavelet tour of signal processing : the Sparse way, Third. ed. Elsevier /Academic Press.

Mallat, S.G., 1989. A theory for multiresolution signal decomposition: the wavelet representation. IEEE Trans. Pattern Anal. Mach. Intell. 11, 674–693.

Mendenhall, W., Sincich, T., 2016. Statistics for engineering and the sciences, Sixth. ed. CRC Press, Boca Raton, FL.

Ming, G., Xu, Y., Du, R., 2008. An intelligent online monitoring and diagnostic system for manufacturing automation. IEEE Trans. Autom. Sci. Eng. 5, 127–139.

Moore, D.F., 1975. Principles and applications of tribology. Pergamon, Oxford.

National Research Council, 1991. The competitive edge: research priorities for U.S. manufacturing. The National Academies Press, Washington, DC.

Ngui, W.K., Leong, M.S., Hee, L.M., Abdelrhman, A.M., 2013. Wavelet analysis: mother wavelet selection methods. Appl. Mech. Mater. 393, 953–958.

Nine, H.D., 1978. Drawbead forces in sheet metal forming, in: Koistinen, D.P., Wang, N.-M. (Eds.), Mechanics of Sheet Metal Forming: Material Behavior and Deformation Analysis. Springer US, Boston, MA, pp. 179–211.

Olsson, D.D., Bay, N., Andreasen, J.L., 2010. A quantitative lubricant test for deep drawing. Int. J. Surf. Sci. Eng. 4, 2–12.

Overly, S., 2001. Recovering from press overload: Protection systems help to sense overload and minimize machine, tool damage. Fabr. May.

Papagiannakis, A.T., Zelelew, H.M., Muhunthan, B., 2007. A wavelet interpretation of vehicle-pavement interaction. Int. J. Pavement Eng. 8, 245–252.

Pereira, M.P., Duncan, J.L., Yan, W., Rolfe, B.F., 2009. Contact pressure evolution at the die radius in sheet metal stamping. J. Mater. Process. Technol. 209, 3532–3541.

Pereira, M.P., Yan, W., Rolfe, B.F., 2010. Sliding distance, contact pressure and wear in sheet metal stamping. Wear 268, 1275–1284.

Pereira, M.P., Yan, W., Rolfe, B.F., 2008. Contact pressure evolution and its relation to wear in sheet metal forming. Wear 265, 1687–1699.

Petropoulos, G.P., Pandazaras, C.N., Davim, J.P., 2010. Surface texture characterization and evaluation related to machining, in: Surface Integrity in Machining. Springer London, London, pp. 37–66.

Podgornik, B., Hogmark, S., Pezdirnik, J., 2004. Comparison between different test methods for evaluation of galling properties of surface engineered tool surfaces. Wear 257, 843–851.

Pujante, J., Pelcastre, L., Vilaseca, M., Casellas, D., Prakash, B., 2013. Investigations into wear and galling mechanism of aluminium alloy-tool steel tribopair at different temperatures. Wear 308, 193–198.

Rackov, D.M., Popovic, M.V., Mojsilovic, A., 2000. On the selection of an optimal wavelet basis for texture characterization. IEEE Trans. Image Process. 9, 2043–2050.

Raggatt, J., 2013. Tribology in Sheet Metal Stamping - The effect of surface roughness and ionic liquid additive lubricants. Deakin University.

Raja, J., Muralikrishnan, B., Fu, S., 2002. Recent advances in separation of roughness, waviness and form. Precis. Eng. 26, 222–235.

Ravindran, D., Su, Y.-C., 2012. Sensors for sheet metal forming, in: Altan, T., Tekkaya, A.E. (Eds.), Sheet Metal Forming - Processes and Application. ASM International, Materials Park, Ohio, pp. 301–314.

Rolfe, B.F., Frayman, Y., Webb, G., Hodgson, P., 2003. Analysis of stamping production data with view towards quality management, in: Proceedings of the Ninth Internation Conference on Manufacturing Excellence (ICME 03). pp. 1–15.

Saito, N., 1994. Simultaneous noise suppression and signal compression using a library of orthonormal bases and the minimum description length criterion. Wavelets Geophys. 299–324.

Schedin, E., 1994. Galling mechanisms in sheet forming operations. Wear 179, 123–128.

Schedin, E., Lehtinen, B., 1993. Galling mechanisms in lubricated systems: A study of sheet metal forming. Wear 170, 119–130.

Schey, J.A., 1983. Tribology in metalworking : friction, lubrication, and wear. American Society for Metals, Metals Park, Ohio, USA.

Shaffer, S.J., Rogers, M.J., 2007. Tribological performance of various coatings in unlubricated sliding for use in small arms action components—A case study. Wear 263, 1281–1290.

Shui, H., Jin, X., Ni, J., 2015. An anomaly detection and diagnosis method based on real-time health monitoring for progressive stamping processes, in: Proceedings of The ASME International Manufacturing Science and Engineering Conference. Charlotte, North Carolina, USA.

Siefert, J.A., Babu, S.S., 2014. Experimental observations of wear in specimens tested to ASTM G98. Wear 320, 111–119.

Skåre, T., Krantz, F., 2003. Wear and frictional behaviour of high strength steel in stamping monitored by acoustic emission technique. Wear 255, 1471–1479.

Skåre, T., Thilderkvist, P., Ståhl, J.-E., 1998. Monitoring of friction processes by the means of acoustic emission measurements—deep drawing of sheet metal. J. Mater. Process. Technol. 80–81, 263–272.

Smith, D.A., 2001. Die maintenance handbook. Society of Manufacturing Engineers, Dearborn, MI.

Smith, R., Hawkins, B., 2004. Lean maintenance : [reduce costs, improve quality, and increase market share]. Elsevier Butterworth Heinemann.

Somers, A.E., Khemchandani, B., Howlett, P.C., Sun, J., Macfarlane, D.R., Forsyth, M., 2013. Ionic liquids as antiwear additives in base oils: Influence of structure on miscibility and antiwear performance for steel on aluminum. ACS Appl. Mater. Interfaces 5, 11544–11553.

Stavropoulos, P., Chantzis, D., Doukas, C., Papacharalampopoulos, A., Chryssolouris, G., 2013. Monitoring and control of manufacturing processes: a review. Procedia CIRP, 14th CIRP Conference on Modeling of Machining Operations (CIRP CMMO) 8, 421–425.

Swanson, P.A., Ives, L.K., Whitenton, E.P., Peterson, M.B., 1988. A study of the galling of two steels using two test methods. Wear 122, 207–223.

Taşan, Y.C., de Rooij, M.B., Schipper, D.J., 2005. Measurement of wear on asperity level using image-processing techniques. Wear 258, 83–91.

Ubhayaratne, I., Pereira, M.P., Xiang, Y., Rolfe, B.F., 2017. Audio signal analysis for tool wear monitoring in sheet metal stamping. Mech. Syst. Signal Process. 85, 809–826.

Ubhayaratne, I., Xiang, Y., Pereira, M., Rolfe, B., 2015. An audio signal based model for condition monitoring of sheet metal stamping process, in: 2015 IEEE 10th Conference on Industrial Electronics and Applications (ICIEA). IEEE, pp. 1267–1272.

van der Heide, E., Huis in ‘t Veld, A.J., Schipper, D.J., 2001. The effect of lubricant selection on galling in a model wear test. Wear, 13th International Conference on Wear of Materials 251, 973–979.

Van Rensselar, J., 2017. Silicone and dry-film lubricants. Tribol. Lubr. Technol. 73, 30–32,34,36.

Varjoranta, T., Hirvonen, J., Anttila, A., 1981. Measuring the wear of nitrogen-implanted steel. Thin Solid Films 75, 241–245.

Vermeiden, M., Hobleke, H., 2003. Functionality and characterisation of textured sheet steel products, in: Blunt, L., Jiang, X. (Eds.), . Kogan Page Science, Oxford, pp. 249–305.

Vermeulen, M., Hobleke, H., 2003. 10 – Functionality and characterisation of textured sheet steel products, in: Advanced Techniques for Assessment Surface Topography. pp. 249–305.

Voss, B.M., Pereira, M.P., Doolan, M.C., 2014. Automated identification of tool wear in sheet metal stamping, in: IDDRG 2014 Conference. Paris, France, pp. 399–404.

Voss, B.M., Pereira, M.P., Rolfe, B.F., Doolan, M.C., 2017. A new methodology for measuring galling wear severity in high strength steels. Wear 390–391, 334–345.

Voss, B.M., Pereira, M.P., Rolfe, B.F., Doolan, M.C., 2017. Using stamping punch force variation for the identification of changes in lubrication and wear mechanism. J. Phys. Conf. Ser. 896, 12028.

Wagener, H.-W., 1997. New developments in sheet metal forming: sheet materials, tools and machinery. J. Mater. Process. Technol. 72, 342–357.

Wang, C., Chen, J., Xia, Z.C., Ren, F., 2013. Die wear prediction by defining three-stage coefficient K for AHSS sheet metal forming process. Int. J. Adv. Manuf. Technol. 69, 797–803.

Wei, L., Fwa, T.F., Zhe, Z., 2005. Wavelet analysis and interpretation of road roughness. J. Transp. Eng. 131, 120–130.

Westeneng, A., 2001. Modelling of contact and friction in deep drawing processes. University of Twente.

Williams, J.A., 1999. Wear modelling: analytical, computational and mapping: a continuum mechanics approach. Wear 225–229, 1–17.

Wilson, W.R.D., 1997. Tribology in cold metal forming. J. Manuf. Sci. Eng. 119, 695.

Wilson, W.R.D., 1991. Friction models for metal forming in the boundary lubrication regime. J. Eng. Mater. Technol. 113, 60.

Wilson, W.R.D., 1978. Friction and lubrication in sheet metal forming, in: Koistinen, D.P., Wang, N. (Eds.), Mechanics of Sheet Metal Forming. Springer US, Boston, MA, pp. 157–177.

Woodall, W.H., Spitzner, D.J., Montgomery, D.C., Gupta, S., 2004. Using control charts to monitor process and product quality profiles. J. Qual. Technol. 36, 309–320.

Xu, Y., Ge, M., 2004. Hidden Markov model-based process monitoring system. J. Intell. Manuf. 15, 337–350.

Yost, F.G., 1983. Two profilometric measurements of wear. Wear 92, 135–142.

Zhang, G.C., Ge, M., Tong, H., Xu, Y., Du, R., 2002. Bispectral analysis for on-line monitoring of stamping operation. Eng. Appl. Artif. Intell. 15, 97–104.

Zhou, S., Jin, J. (Judy), 2005. Automatic feature selection for unsupervised clustering of cycle-based signals in manufacturing processes. IIE Trans. 37, 569–584.

APPENDIX A

A. Wavelet functions

Haar wavelet (shorthand: **Haar**).

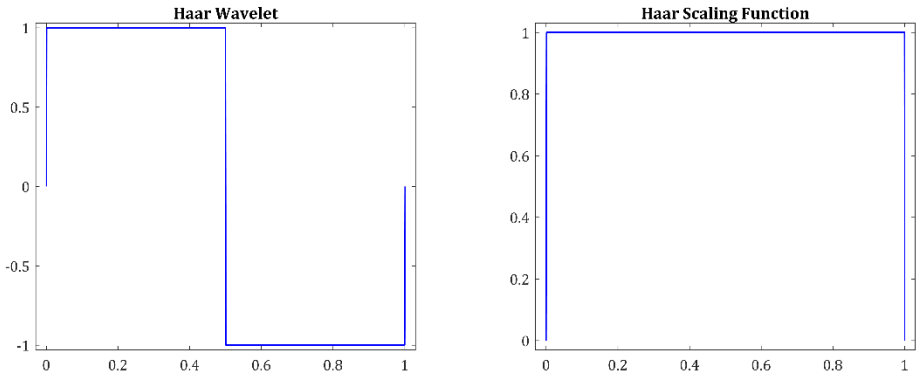

Figure A.1: Haar wavelet and scaling functions.

Daubechies 2 (shorthand: **db2**).

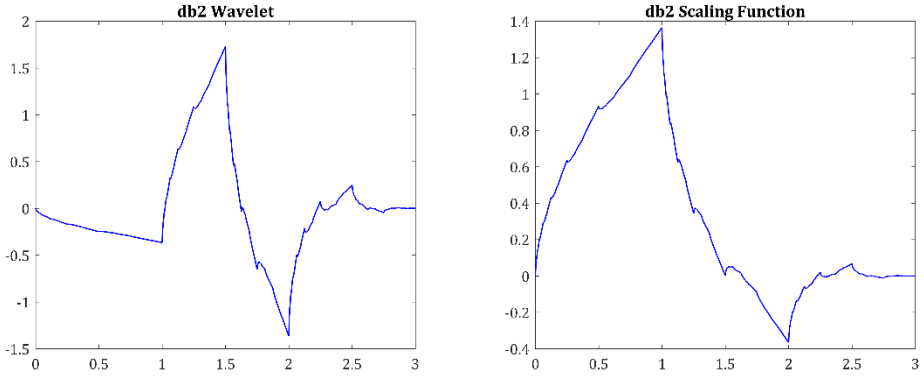

Figure A.2: Daubechies 2 wavelet and scaling functions.

Fejer-Korovkin filter 4 (shorthand: **fk4**).

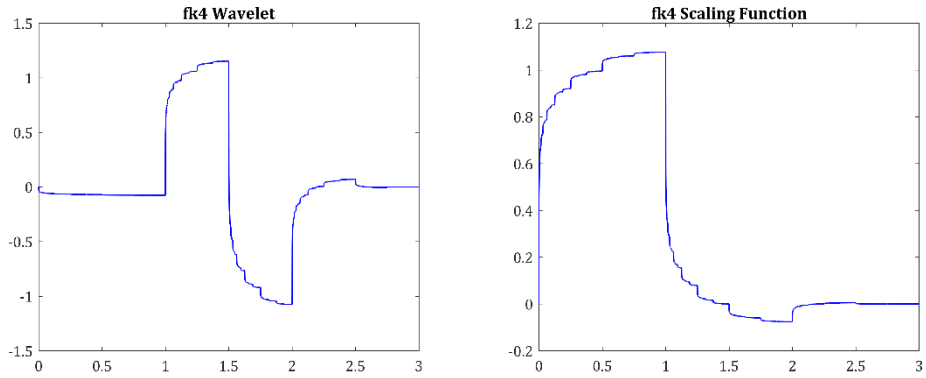

Figure A.3: Fejer-Korovkin filter 4 wavelet and scaling functions.

Biorthogonal 2.2 (shorthand: **bior2.2**).

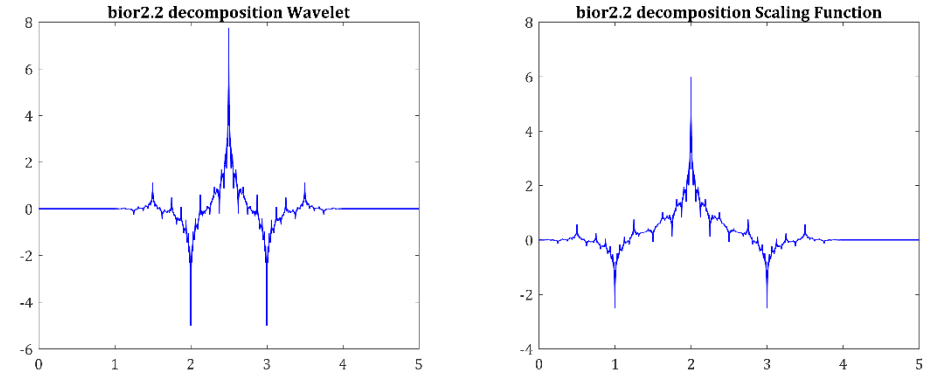

Figure A.4: Biorthogonal 2.2 wavelet and scaling functions.

Biorthogonal 3.1 (Shorthand: **Bior3.1**).

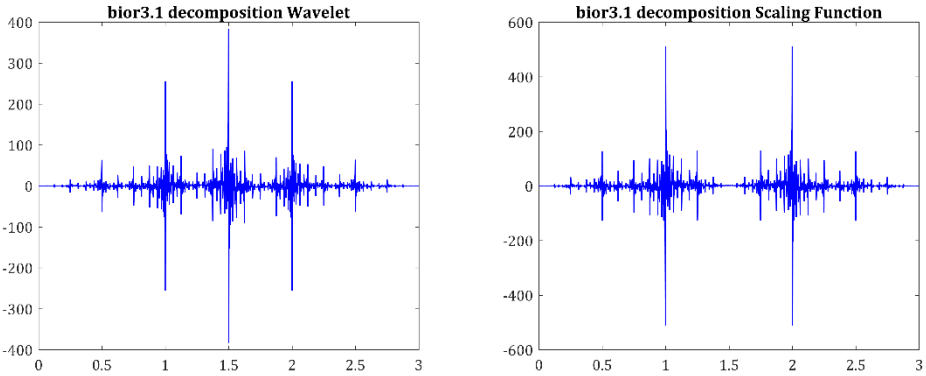

Figure A.5: Biorthogonal 3.1 decomposition wavelet and scaling functions.

Reverse Biorthogonal 1.3 (shorthand: **Rbio1.3**).

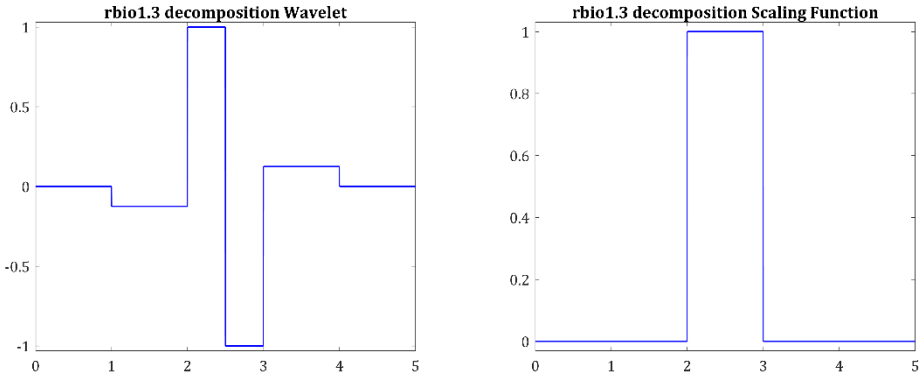

Figure A.6: Reverse biorthogonal 3.1 decomposition wavelet and scaling functions.

Reverse Biorthogonal 2.2 (shorthand: **Rbio2.2**).

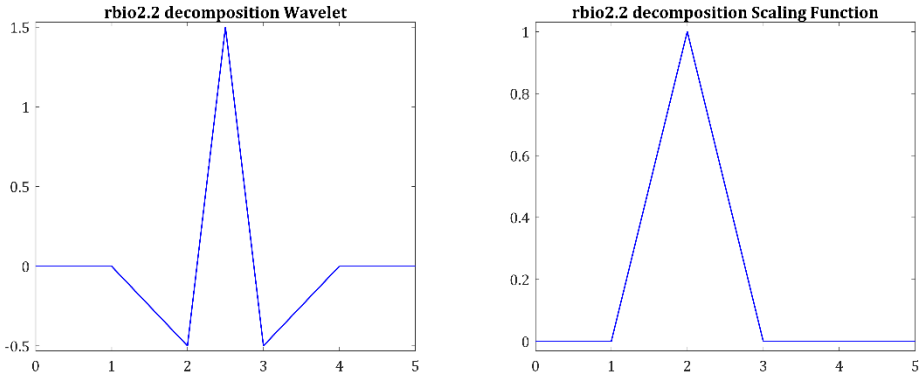

Figure A.7: Reverse biorthogonal 2.2 decomposition wavelet and scaling functions.

Reverse Biorthogonal 3.1 (shorthand: **Rbio3.1**).

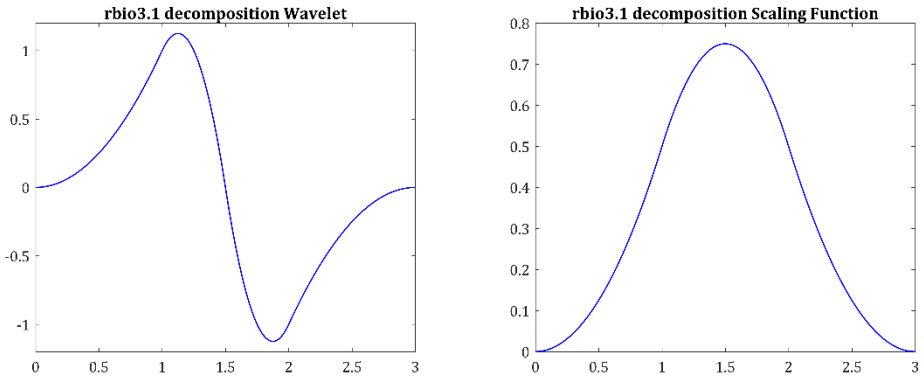

Figure A.8: Reverse biorthogonal 3.1 decomposition wavelet and scaling functions.